University of Exeter
Department of Mathematics

Neural dynamics of perceptual competition

Farzaneh Darki

October 2021

Supervised by Dr James Rankin

Submitted by Farzaneh Darki, to the University of Exeter as a thesis for the degree of Doctor of Philosophy in Mathematics, October 2021.

This thesis is available for Library use on the understanding that it is copyright material and that no quotation from the thesis may be published without proper acknowledgement.

I certify that all material in this thesis which is not my own work has been identified and that no material has previously been submitted and approved for the award of a degree by this or any other University.

(signature) ....

Declaration

Chapter 3 represents the work that is published in *The Journal of Mathematical Neuroscience.* Chapter 4 is also published in *Attention, Perception, & Psychophysics.* For the both papers, I was the lead author, wrote the first drafts and carried out all editing for subsequent drafts. I have implemented and carried out all numerical analysis and simulations in the first paper (Chapter 3). I have also performed the experiments and analysed the data in the second paper (Chapter 4). The manuscript of Chapter 5 is in preparation for submission.

Farzaneh Darki

Abstract

This research aims to understand the neural dynamics and mechanisms underlying perceptual bistability. In perceptual rivalry, ambiguous sensory information leads to dynamic changes in the perceptual interpretation of fixed stimuli. This phenomenon occurs when participants receive sensory stimuli that support two or more distinct interpretations; this results in spontaneous alternations between possible perceptual interpretations. Perceptual rivalry has been widely studied across different sensory modalities including vision, audition, and to a limited extent, in the tactile domain. Common features of perceptual rivalry across various ambiguous visual and auditory paradigms characterise the randomness of switching times and their dependence on input strength manipulations (Levelt's propositions).

Binocular rivalry occurs when the two eyes are presented with incompatible stimuli and perception alternates between these two stimuli. This phenomenon has been investigated in two types of experiments: 1) Traditional experiments where the stimulus is fixed, 2) Eye-swap experiments in which stimulus periodically swaps between eyes many times per second (Logothetis et al. 1996). In spite of the rapid swapping between eyes, perception can be stable for many seconds with specific stimulus parameter configurations. Wilson introduced a two-stage, hierarchical model to explain both types of experiments (Wilson 2003). Wilson's model and other rivalry models have been only studied with bifurcation analysis for fixed inputs and different dynamical behaviours that can occur with periodic forcing have yet to be explored. Here I report 1) a more complete description of the complex dynamics in the unforced Wilson model, 2) a bifurcation analysis with periodic forcing. Previously, bifurcation analysis of the Wilson model with fixed inputs has revealed three main types of dynamical behaviours: Winner-take-all (WTA), Rivalry oscillations (RIV), Simultaneous activity (SIM). The results presented here reveal richer dynamics including mixed-mode oscillations (MMOs) and period-doubling cascade which corresponds to low amplitude WTA (LAWTA) oscillations. On the other hand, studying rivalry models with numerical continuation shows that periodic forcing with high frequency (e.g. 18 Hz, known as flicker) modulates the three main types of behaviours that occur with fixed inputs by the forcing frequency (WTA-Mod, RIV-Mod, SIM-Mod). However, the dynamical behaviour will be different with low frequency periodic forcing (around 1.5Hz, so-called swap), and in addition to WTA-Mod and SIM-Mod, cycle skipping and multi-cycle skipping behaviour exist, which can also lead to chaotic dynamics. This research provides a framework for either assessing binocular rivalry models for consistency checks against empirical results, or for better understanding neural dynamics and the mechanisms necessary to implement a minimal binocular rivalry model.

At present it remains unclear whether the general characteristics of perceptual rivalry are preserved with tactile stimuli. I introduce a simple tactile stimulus capable of generating perceptual rivalry and explores whether general features of perceptual rivalry from other modalities extend to the tactile domain. In these experiments, vibrotactile stimuli consisted of anti-phase sequences of high and low intensity high frequency pulses, each followed by a silent interval, delivered to the right and left index fingers. Participants perceived the stimulus as either one simultaneous pattern of vibration on both hands (SIM), or patterns of vibration that jumped from one hand to the other hand, giving a sensation of apparent movement (AM). For long stimulus presentations, perception switches back and forth between these two percepts. Furthermore, my results confirm that Levelt's proposition II extends to tactile bistability, and that the stochastic characteristics of irregular perceptual alternations agree with non-tactile modalities. An analysis of correlations between subsequent perceptual phases reveals a significant positive correlation at lag 1 (as found in visual bistability), and a negative correlation for lag 2 (in contrast with visual bistability).

In this study, a mathematical model of tactile rivalry is developed that focuses on accurately reproducing the dynamics of the perceptual alternations. The model of tactile rivalry presented here consists of two processing stages; first stage for producing perceptual alternations; and a second stage for encoding the percept types (SIM and AM). Putative neural populations of the first stage could be located early in the somatosensory pathway at brainstem nuclei, and the neural populations of the second stage could be located within area 3b of the primary somatosensory cortex, based on excitatory and lagged inhibitory components of their receptive fields. The powerful combination of bifurcation analysis along with optimisation tools have been used to tune certain features of the model, resulting in a good qualitative and quantitative match to my experimental data. As well as capturing the dynamical characteristics specific to the perceptual interpretations in tactile rivalry, the model presented here is able to produce the general characteristics of perceptual rivalry including Levelt's proposition, short-tailed skewness of reversal time distributions and a scaling property of this distribution's first three moments.

This thesis is dedicated to my parents, Fereshteh and Younes who are far away but always send their endless love and encourage me to go on every adventure, especially this one.

To my forever friend and kind husband, Naser who have always been there for me. Anything good that has come to my life has been because of your support, guidance, and love.

And to my siblings Fahimeh, Ali, and Faezeh who have always been my source of strength, inspiration, and happiness.

Contents

Contents

List of Tables

List of Figures

Nomenclature and Abbreviations

Acronyms and abbreviations

B&S	Blanks and Swap.
EEG	Electroencephalogram.
F&S	Flicker and Swaps.
fMRI	Functional Magnetic Resonance Imaging.
H	High intensity.
HL	Horizontal Left.
HR	Horizontal Right.
L	Low intensity.
Mod	Modulated.
VL	Vertical Left.
VR	Vertical Right.

Dynamical states

AM	Apparent movement.
LAWTA	Low Amplitude Winner-take-all.
MMOs	Mixed-mode Oscillations.
RIV	Rivalry Oscillations.
SIM	Simultaneous Activity.
WTA	Winner-take-all.

Bifurcations

BP	Branch Point.
H	Hopf Bifurcation.
L	Fold Bifurcation.
PD	Period-doubling.
PF	Pitchfork Bifurcation.
T	Torus Bifurcation.

1. Introduction to perceptual competition

In this chapter, I will explain perceptual bistability phenomenon and the fundamental experiments that have remained as a benchmark for theorists and experimentalists. Later in the chapter, physiological basis of sensory processing across visual and tactile domains are reviewed, which will be helpful for understanding the architecture of models presented in Chapter 3 and Chapter 5. I will finish this chapter by reviewing some of well-known computational models for binocular rivalry, which dynamical analysis of these model have been performed in Chapter 2 and Chapter 3.

1.1. Bistability experiments

Multistable perception is the spontaneous alternation between two or more perceptual states that occurs when sensory information is ambiguous. In some special instances, the brain struggles to reconcile competing inputs, and the competition between neural representations resolves slowly over time, resulting in a bistable perceptual experience (Leopold and Logothetis 1999; Sterzer et al. 2009). Binocular rivalry is an example of such a perceptual phenomenon. In the experiments of binocular rivalry, the corresponding retinal locations in the two eyes are presented with incompatible images. During binocular rivalry, a stable visual perception gives way to perceptual alternations in which the dominant percept switches between the two monocular images. Therefore, binocular rivalry provides a unique opportunity to investigate how the brain deals with competing inputs and to study intrinsic neural dynamics (Blake and Logothetis 2002).

Levelt's propositions continue to be considered as a benchmark for modellers and experimentalists since their publication in 1965. They highlight the key properties by which perception during binocular rivalry depends on characteristics of the stimuli like image contrast. The original propositions are as follows: (Levelt 1965)

I. Increasing stimulus strength for one eye will increase the perceptual predominance of that eye's stimulus.

II. Increasing stimulus strength for one eye will not affect the average perceptual dominance duration of that eye's stimulus. Instead, it will reduce the average perceptual dominance duration of the other eye's stimulus.

III. Increasing stimulus strength for one eye will increase the perceptual alternation rate.

IV. Increasing stimulus strength in both eyes while keeping it equal between eyes will increase the perceptual alternation rate.

These are one of the hallmarks that models aim to reproduce (Shpiro et al. 2007). Recently original Levelt's propositions have been modified to be compatible with current knowledge of binocular rivalry. These four modified propositions are as follows:

I. Increasing stimulus strength for one eye will increase the perceptual predominance of that eye's stimulus.

II. Increasing the difference in stimulus strength between the two eyes will primarily act to increase the average perceptual dominance duration of the stronger stimulus.

III. Increasing the difference in stimulus strength between the two eyes will reduce the perceptual alternation rate.

IV. Increasing stimulus strength in both eyes while keeping it equal between eyes will generally increase the perceptual alternation rate, but this effect may reverse at near-threshold stimulus strengths (Brascamp et al. 2015).

1.2. The physiological basis of sensory perception

In this section, I will outline the advances that have been made in understanding the initial operations that occur on visual and tactile input to the brain. Although the basic senses (somatic sensation, vision, audition, and chemical senses) are very different from one another, a few fundamental rules govern the way nervous system deals with each of these diverse modalities. Here, I will begin with how highly specialized nerve cells (receptors) convert the energy associate with mechanical sources and light into neural signals (afferent sensory signals), and then I will describe how these afferent signals convey information about the stimulus to the brain (sensory pathway).

1.2.1. Visual perception

Visual processing pathways

The neural circuitry of the retina transforms a fluctuating pattern of light into a pattern of neural activity in retinal ganglion cells, which is then transmitted along the optic nerve to the brain. The majority of retinal ganglion cells project to the lateral geniculate nuclei (LGN) of the thalamus (see Figure 1.1). LGN cells are arranged in layers, and each layer of LGN cells contains a retinotopic map of half of the visual field, those in the right LGN having maps of the left side of the visual field and those in the left LGN maps of the right side, because the optic nerves cross over completely at the optic chiasm to run to the opposite sides of the brain (Bruce et al. 2003). The axons of LGN cells in turn form the optic radiations (see Figure 1.1) and project to the visual cortex.

The primary visual cortex is that portion of the occipital lobe receiving input from the LGN. It is sometimes referred to as area V1, in recognition of its being the first in a
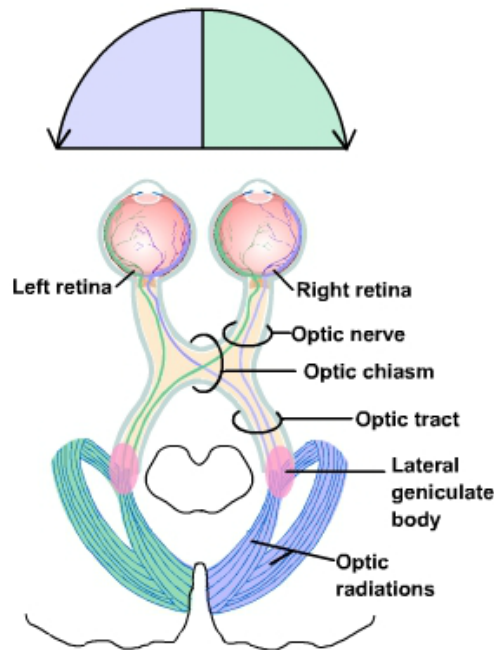
Figure 1.1. The main route for visual information to the brain is the projections from retina via LGN to the visual cortex (geniculocortical pathway). The left and right sides of visual field are shown with blue and green, respectively. Adapted from (Dragoi and Tsuchitani 2016)

hierarchy of cortical visual areas. From visual area V1, neural information is distributed over a number of pathways to higher visual areas of the brain. Receptive fields in these higher visual areas are significantly larger than those found in V1. This means a stimulus may appear anywhere within a relatively large regions of visual space and still activate a given neuron. The flow of information within this complex network is not unidirectional. Every cortical region receiving input from another region also sends feedback connections back to that other region. In addition, these visual areas are directly interlinked, with the neural operations carried out in one set of areas influencing the operations carried out within the others (Gegenfurtner et al. 1996).

Ocular dominance

A fundamental feature of human vision is that, despite having two eyes, we normally see only one representation of the world around us. This phenomenon requires a seamless combination of two completely separate neural signals. Where in the brain does this happen? It might be expected that a harmonious integration of left and right would be constructed at the thalamus which is the very first processing stage and both signals are present in proximity there; however, it has long been known that this is not the case and that the answer is somewhere in the visual cortex (Smith 2015).

Ocular dominance columns or ocular dominance stripes are regions of neurons in the visual cortex that respond to the stimulation from either the left or right eye. The information from the two eyes is distributed in separate layers of each (left and right) LGN, with individual neurons receiving input from either one eye or the other. This ocular segregation is retained in layer 4 of V1, the cortical layer receiving input from LGN. The left and
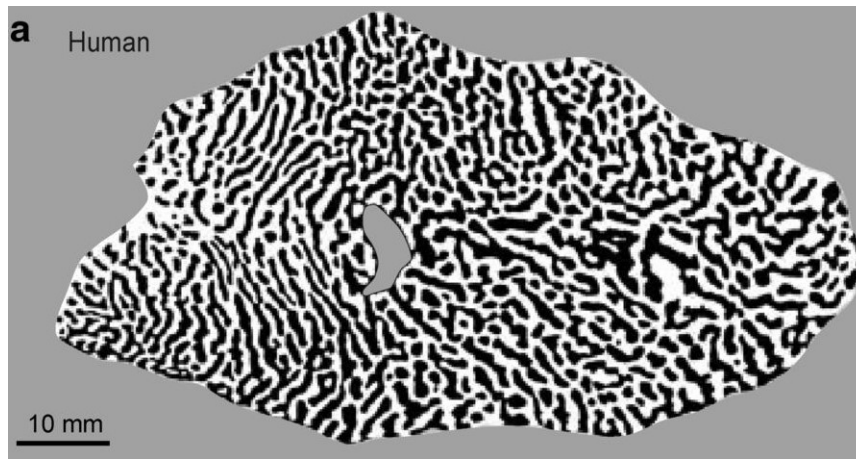
Figure 1.2. The interdigitated stripes of neurons innervated by the right and left eyes appear as alternating black and white bands. Adapted from (Najafian et al. 2019)

right eye neurons are segregated into snakelike stripes, which can easily be visualized by injecting specially labelled dye into area V1 (Figure 1.2) (Horton and Hocking 1996). Neurons in layer 4 of V1, in turn, send signals to other cortical layers immediately above them, and at this stage, monocular (one eye) segregation gives way to binocular (two eyes) integration. Within area V1, and outside layer 4, individual neurons are mostly innervated from both eyes. The variation in the activation strength produced by the two eyes is called ocular dominance. Any neuron that can be excited through both eyes, regardless of its ocular dominance, is called a binocular neuron. Only a small fraction of V1 neurons are monocular, meaning that the neuron can only be activated by stimulation of one eye or the other but not both. The bulk of these monocular neurons reside in layer 4.

Orientation map

One of the most striking characteristics of cortical neurons is their orientation selectivity. In contrast to retinal and geniculate cells which have circular-shape receptive fields, most cortical neurons are tuned to some specific orientation of an edge or a contour (Blake and Sekuler 2006). This means any particular neuron will respond only if the orientation of an edge or line falls somewhere within a narrow range. Each cortical neuron has a preferred orientation, one to which it is maximally responsive. If a line tilts a little away from this optimum, the neuron's response is markedly decreased; if the line tilts even more, the neuron no longer responds at all.

These orientation-selective neurons are not randomly arranged; they are grouped in a very orderly design within the cortex. Figure 1.3 shows schematically how orientation is systematically mapped within a slab of cortical tissue. The visual cortex appears to be composed of columns of neurons, within each column consisting of a stack of neurons all preferring the same orientation and exhibiting the same ocular dominance. The aggregation of adjacent columns (a region where each possible orientation is represented) is collectively known as a hypercolumn. Each hypercolumn contains tens of thousands neurons whose receptive fields all overlap on the same retinal territory.
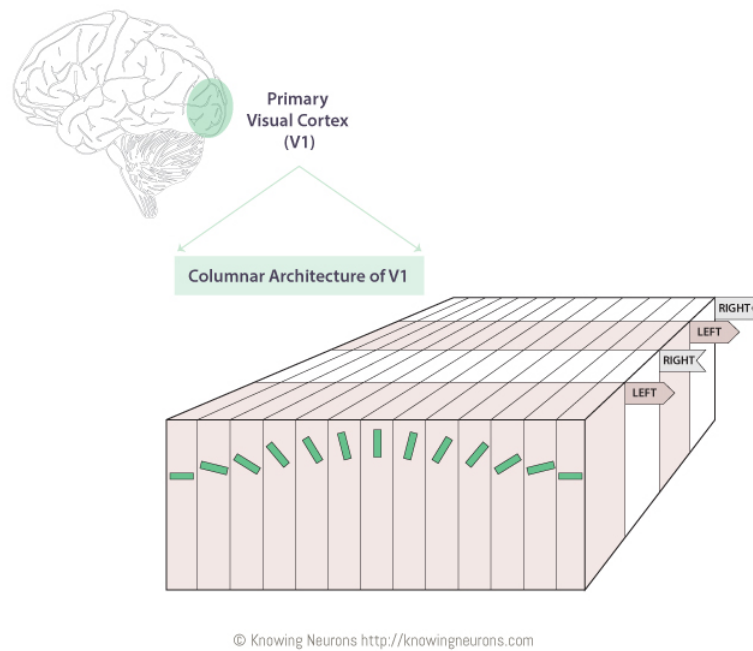
Figure 1.3. The visual cortex is composed of columns consisting of a stack of neurons all preferring the same orientation and exhibiting the same ocular dominance. Adapted from https://knowingneurons.com

1.2.2. Tactile perception

The somatic sensory system has two major components: a subsystem for the detection of mechanical stimuli (such as light touch, vibration, pressure, and cutaneous tension), and a subsystem for the detection of painful stimuli and temperature. This section focuses on the mechanosensory subsystem. The skin on a human hand contains thousands of mechanoreceptors. These receptors are sensitive to mechanical pressure or deformation of the skin. Each individual afferent fiber signals when a particular region of the skin has been touched. Similar to visual neuron's receptive field (the area of retina within which light affects activity of the neuron), the area of skin within which stimuli can influence a fiber's activity constitutes that fiber's receptive field.

Mechanosensory processing of external stimuli is initiated by the activation of a diverse population of cutaneous and subcutaneous mechanoreceptors at the body surface that relays information to the central nervous system for interpretation and ultimately action. Additional receptors located in muscles, joints, and other deep structures monitor mechanical forces generated by the musculoskeletal system and are called proprioceptors. Mechanosensory information is carried to the brain by several ascending pathways that run in parallel through the spinal cord, brainstem, and thalamus to reach the primary somatic sensory cortex in the postcentral gyrus of the parietal lobe. The primary somatosensory cortex projects in turn to higher-order association cortices in the parietal lobe, and back to the subcortical structures involved in mechanosensory information processing.
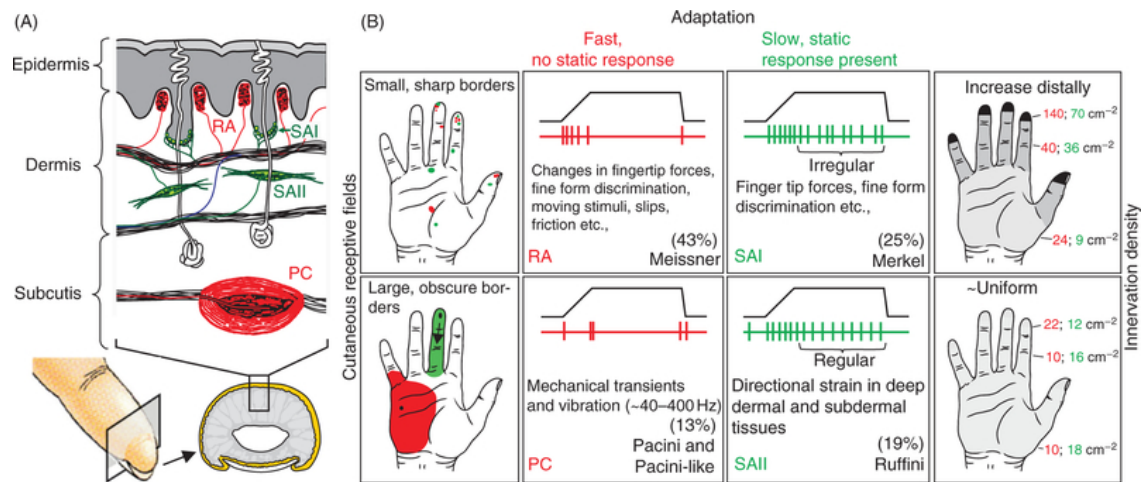
Figure 1.4. The four classes of cutaneous afferents of the glabrous skin. **(A)** Morphology of the different mechanoreceptors and their respective locations in the skin. **(B)** Adaptation properties and receptive field (RF) size of the four classes of cutaneous afferents. Adapted from (Delhaye et al. 2011)

Somatosensory periphery

Fibers carrying touch information from the human palm and fingertips are categorized into four classes, each exhibiting different response properties (SA-type I, SA-type II, RA-type I, RA-type II). These four categories are defined on the basis of the sharpness of the boundaries of each fiber's receptive field and on the fiber's pattern of activity over time. Differences in spatial and temporal response properties enable each class of fibers to signal something unique about sources of stimulation within their receptive fields.

These four classes can be split into two categories according to their responses to skin indentations: slowly adapting afferents (SA) produce a sustained response to a static indentation of the skin, one that declines (adapts) slowly over time, whereas rapidly adapting afferents (RA) respond only at the onset and offset of the indentation Figure 1.4. Each of these classes can be further distinguished based on the size of their receptive fields: mechanoreceptors innervated by type I afferents lie close to the surface of the skin and have small and clearly defined receptive fields (punctuate), whereas mechanoreceptors innervated by type II afferents are deeper in the skin and have large receptive fields with ill-defined boundaries (diffuse). Receptive fields of type II afferents sometimes cover a whole finger or the greater part of the palm.

The four different classes of afferents innervate different types of mechanoreceptors. Each of these four types may deliver a distinct message to the central nervous system, because each is best at signalling the presence of a particular kind of tactile stimulation. This widely accepted view is commonly referred to as the "four-channel" model of mechanoreception.

Somatosensory pathways

Afferent touch fibers enter the dorsal, or back, side of the spinal cord Figure 1.5E. Inside the spinal cord, these afferent fibers make synaptic contact with neurons that travel
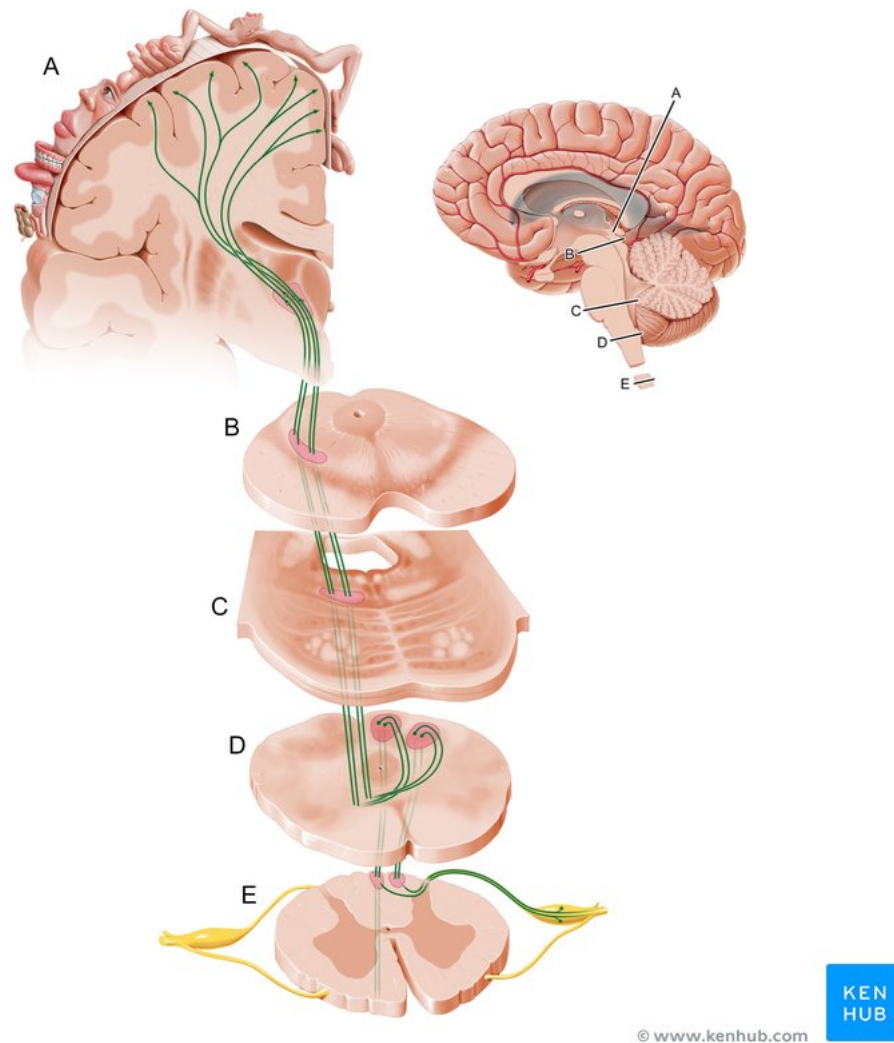
Figure 1.5. Diagram of the ascending lemniscal somatosensory pathway. **(A) Cerebral cortex and thalamus.** Thalamic neurons send axons to the parietal lobe of the somatosensory cortex. Note somatotopic representation of body parts outlining cortical surface (see Figure 1.6 for more details). Inside the spinal cord, afferent fibers make synaptic contact with neurons that travel upward to the brain, carrying input to different regions in the brainstem: **(B) Midbrain. (C) Pons. (D) Medulla. (E) Spinal cord.** Adapted from https://www.kenhub.com

upward to the brain, carrying input to particular regions in the brainstem (including Midbrain, Pods, Medulla Figure 1.5B-D). These neurons comprise the so-called lemniscal pathway Figure 1.5A-E. Axons in the lemniscal pathway project to nuclei in the brainstem. After synapsing, fibers in this pathway cross over the midline Figure 1.5D, projecting to thalamic nuclei on the opposite side of the brain Figure 1.5A. At the level of the thalamus, neurons receiving inputs from the superficial and deeper receptors in the skin are segregated. Thalamic neurons send axons to the parietal lobe of the somatosensory cortex, an area of the cerebral cortex largely devoted to sensory analysis of touch information Figure 1.5A.

Somatosensory Cortex

The somatosensory cortex consists of several neighbouring, functionally distinct areas whose interconnections are complex and only partially understood. Consider, for exam-
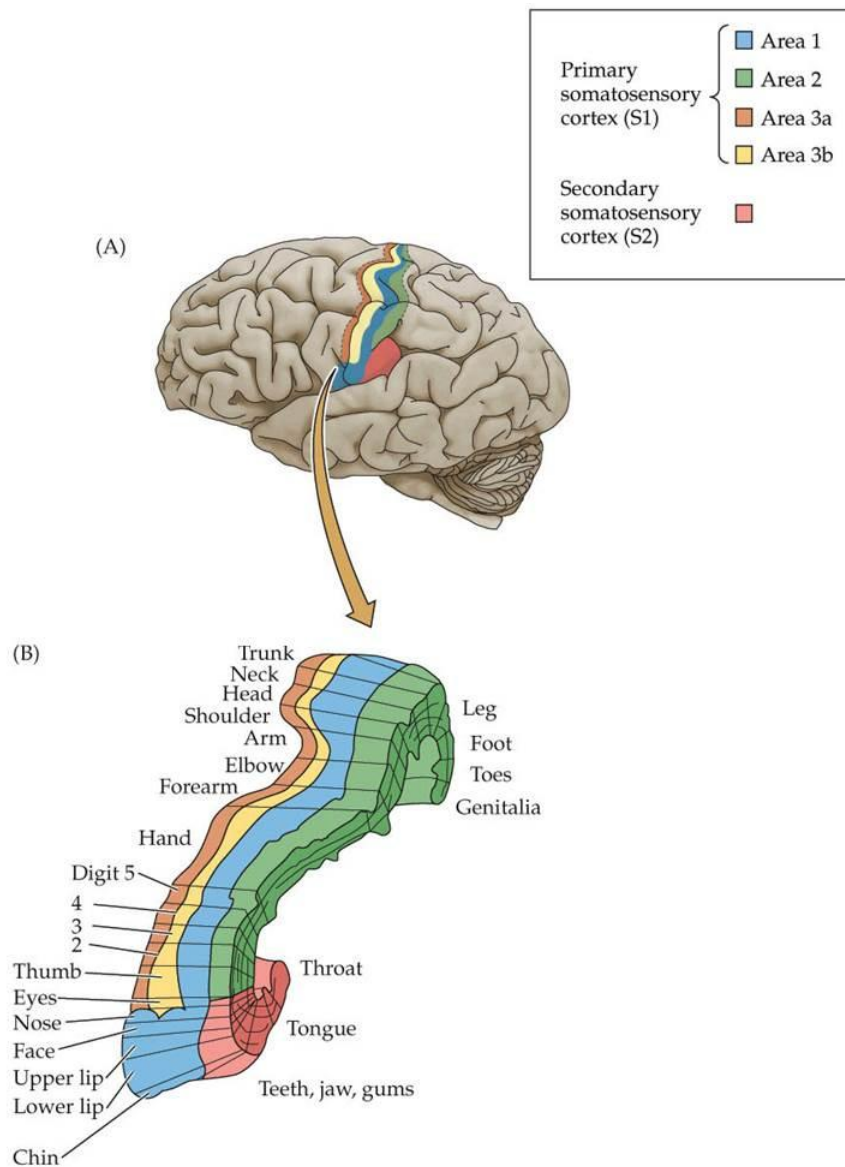
Figure 1.6. **(A)** Organization of somatosensory cortex. **(B)** Different regions of the somatosensory cortex process tactile information from different parts of the body, with these regions forming a map of the body surface on the cortical surface. Adapted from https://www.chegg.com

ple, the two major areas, the so-called first and second somatosensory areas, S1 and S2. Although both receive touch information from the thalamus, S2 also receives input from S1.

In each hemisphere of the cerebral cortex, S1 receives information arising from the contralateral side of the body and face. This is because of the crossover within the lemniscal pathway (see Figure 1.5D). Thus, S1 neurons in the left hemisphere have their receptive fields on the right side of the body, and vice versa. Generally, neighbouring areas of the body are represented within neighbouring regions of the cortex. The body, in other words, is mapped topographically onto somatosensory cortex Figure 1.6B. Our fingers provide the most detailed information about the quality and location of tactile stimulation. For example, the fingertip can distinguish points separately when they are 2 or 3 mm apart, while the arm senses two points separately only when they are 35 to 40 mm apart.

The most anterior (forward) of S1's four strips is known as area 3a, the most posterior (rear) strip is known as area 2, areas 3b and 1 lay in between Figure 1.6. Actually, the four strips, or maps, can be grouped into two sets: neurons in Areas 3b and 1 (the middle strips) respond most vigorously when sites on the skin are touched lightly. They receive inputs, via the thalamus, primarily from the most superficial skin receptors that innervate the RA-type I and SA-type I fibers. Neurons in Areas 3a and 2 (the most anterior and most posterior strips) respond poorly, if at all, to light touch on the skin. Instead, they respond strongly either when particular joints are moved — such as the joints of the fingers — or when other structures deep beneath the skin's surface, for example, tendons and muscles, are stimulated. These areas receive inputs, again via the thalamus, primarily from the more deeply situated skin receptors that innervate the RA-type II and SA-type II fibers.

1.3. Neural competition models

Due to fascinating nonlinear dynamics of perceptual competition, powerful tools such as mathematical modelling have been utilized that are able to capture temporal characteristics of perceptual rivalry with a specific set of model parameters. So several models of perceptual rivalry were developed to either describe neural competition more precisely over a wider range of stimulus parameter, or change the common understanding of this phenomenon by introducing a new structure or dynamics (Lehky 1988; Blake 1989; Laing and Chow 2002; Shpiro et al. 2007; Wilson 2007; Curtu et al. 2008; Salinas 2003; Freeman 2005).

In models of binocular rivalry (Brascamp et al. 2013; Laing and Chow 2002; Li et al. 2017; Wilson 2003) competition takes place as a result of reciprocal inhibition between two monocular patterns presented to two different eyes. In addition of reciprocal inhibition, there must exist a slow process which either decreases the activity of the dominate group of neurons and thus allow the other group to be released from suppression and become dominant (Shpiro et al. 2009) (release mechanism), or increases the activity of the suppressed group of neurons which instead forces its competitor into the suppressed state (escape mechanism). Spike-frequency adaptation and synaptic depression are two candidates for the slow processes necessary for maintenance of rivalry in neural models. Synaptic depression acts by decreasing the effective synaptic connectivity, directly reducing the amount of negative feedback (if in the inhibitory connection) in the system (Shpiro et al. 2007). The second type of slow process is spike-frequency adaptation, which acts by reducing the excitability of active neurons in the network, opposing the positive feedback and external input.

1.3.1. Laing & Chow model

Several models of binocular rivalry have been proposed so far. One of these models was presented by Laing and Chow (LC Model) (Laing and Chow 2002). Most of the models (Blake 1989; Lehky 1988) that have been presented up until this point, were neural networks or rate models and it was not possible to compare model's results with neuro-

physiological recordings quantitatively. The Laing and Chow Model was a biologically plausible model and focused on the specific biophysical mechanisms underlying binocular rivalry and multistable perception.

This model consists of both excitatory and inhibitory populations of Hodgkin-Huxley spiking neurons. These neurons are orientation selective and connected locally to other neurons with similar preferred orientation (with a periodic feature space, see Figure 1.7A). It is also notable that this model is supposed to mimic the binocular rivalry at higher cortical layers after primary visual cortex. Thus, the input of the orientation selective neurons contains information from both eyes together. For slow processes, they include both spike-frequency adaptation and synaptic depression. One interesting point is that synaptic depression could not alone generate rivalry. Spike-frequency adaptation is able to produce rivalry alternations; however, it limits the dominance duration to the order of time constant of adaptation current (around 80 ms). Both of them together can generate robust alternations.

Figure 1.7B shows a raster plot of the firing events of the excitatory neurons in the network given two stimuli centered at neurons whose preferred orientations differ by 90 degrees. At every moment in time, the activity is localized into a bump that is centered at either of the two locations of maximum external input. A bump in one of these locations is thought to represent a perception of bars of the corresponding orientation. They also present a reduced population rate model derived from the spiking neuronal network (Laing and Chow 2002). The reduced model can be represented by mean-field dimensionless equations:

$$
\begin{cases}
\dot{u}_1 = -u_1 + f\left(\alpha u_1 g_1 - \beta u_2 g_2 - a_1 + I_1\right), \\
\tau_a \dot{a}_1 = -a_1 + \Phi_a f\left(\alpha u_1 g_1 - \beta u_2 g_2 - a_1 + I_1\right), \\
\tau_d \dot{g}_1 = 1 - g_1 - g_1 \Phi_d f\left(\alpha u_1 g_1 - \beta u_2 g_2 - a_1 + I_1\right), \\
\dot{u}_2 = -u_2 + f\left(\alpha u_2 g_2 - \beta u_1 g_1 - a_2 + I_2\right), \\
\tau_a \dot{a}_2 = -a_2 + \Phi_a f\left(\alpha u_2 g_2 - \beta u_1 g_1 - a_2 + I_2\right), \\
\tau_d \dot{g}_2 = 1 - g_2 - g_2 \Phi_d f\left(\alpha u_2 g_2 - \beta u_1 g_1 - a_2 + I_2\right).
\end{cases}
\tag{1.1}
$$

Here u_i represents the averaged activity of population i $(i = 1, 2)$, normalized so that its maximum value is 1; a_i is the population adaptation variable, with time scale τ_a; and g_i is the synaptic depression variable, with time scale τ_d. I_i is external stimulus, α and β are constants that define strength of recurrent excitation and cross-inhibition, respectively. Φ_a and Φ_d are scaling constants for gain function of spike-frequency adaptation and synaptic depression, respectively. The gain function f is a Heaviside step function, $f(x) = \begin{cases} 1, & x \geq \theta \\ 0, & x < \theta \end{cases}$, where θ is a threshold.

Time histories from simulations of the reduced model (for the case when synaptic depression is off) is shown in Figure 1.7C. Parameter values are $\alpha = 0.2$, $\beta = 0.4$, $\Phi_a = 0.4$, $\tau_a = 20$, $I_1 = 0.43$, $I_2 = 0.5$. One population becomes active only when its adaptation has worn off by a sufficient amount. For the parameters shown, population 1 switches on when $a_1 = I_1 - \beta = 0.03$ and population 2 switches on when $a_2 = I_2 - \beta = 0.1$.
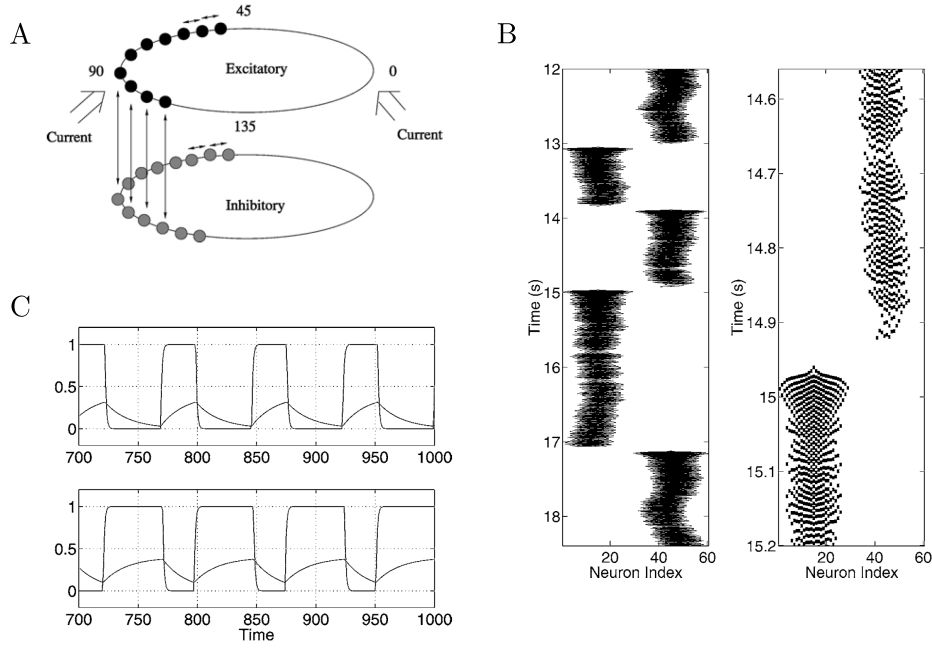
Figure 1.7. **(A)** Two coupled networks of binocular, orientation-selective neurons. The neurons are labelled with their preferred orientation in degrees. Current is injected to two groups of neurons whose preferred orientations differ by 90 degrees. **(B)** Activity in the excitatory population as a function of time. The current stimuli are centered at neurons 15 and 45. The right panel shows detail of the left panel. **(C)** Solution of the reduced model in Equation 1.1. Parameter values are $\alpha = 0.2$, $\beta = 0.4$, $\Phi_a = 0.4$, $\tau_a = 20$, $I_1 = 0.43$, $I_2 = 0.5$, $g_1 = g_2 = 1$. The top plot is u_1 and a_1, the bottom is u_2 and a_2. Adapted from (Laing and Chow 2002)

1.3.2. Shpiro models

To investigate the role of slow processes in the system's behaviour separately, Shpiro et al. modified the LC model to include only one of the slow processes, spike-frequency adaptation or synaptic depression (Shpiro et al. 2007). In addition, they also omitted the recurrent excitation term in the gain function inputs. The model which only includes the spike-frequency adaptation (AdaptationLC model) described by:

$$
\begin{cases}
\dot{u}_1 = -u_1 + f\left(-\beta u_2 - ga_1 + I_1\right), \\
\tau_a \dot{a}_1 = -a_1 + u_1, \\
\dot{u}_2 = -u_2 + f\left(-\beta u_1 - ga_2 + I_2\right), \\
\tau_a \dot{a}_2 = -a_2 + u_2.
\end{cases}
\tag{1.2}
$$

Where I_i is the input to the population i $(i = 1, 2)$, $u_i(t)$ is the firing rate of the population i, $a_i(t)$ is the adaptation variable, β is cross-inhibition strength and g is the strength of the adaptation. The gain function f is sigmoid function,

$$
f(x) = \frac{1}{1 + e^{-k(x-\theta)}}
\tag{1.3}
$$

Where k defines the slope and θ defines the threshold.

The model which only includes the synaptic depression (Depression-LC model) described
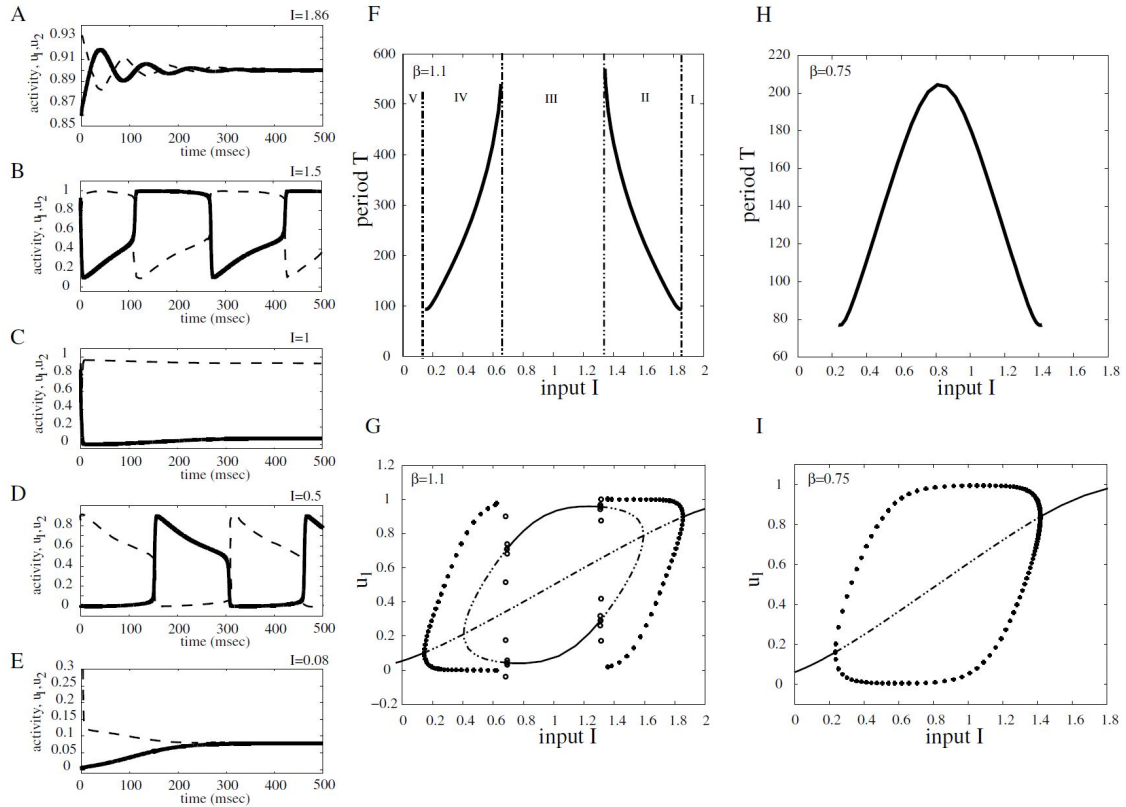
Figure 1.8. Bifurcation diagrams and examples of activity time courses for neuronal competition model in Equation 1.2 with parameter values $g = 0.5$, $\tau = 100$, $r = 10$, $\theta = 0.2$, and $\beta = 1.1$ (panels A–G), respectively, $\beta = 0.75$ (panels H–I). Time courses of u_1, u_2 corresponding to panel F for different values of I: **(A)** $I = 1.86$, **(B)** $I = 1.5$, **(C)** $I = 1$, **(D)** $I = 0.5$, and **(E)** $I = 0.08$. Bifurcation diagrams of period T of the network oscillation versus input strength I (panels F and H). Bifurcation diagram of population activity u_1 versus I (panels G and I). Adapted from (Curtu et al. 2008)

by:

$$
\begin{cases}
\dot{u}_1 = -u_1 + f\left(-\beta u_2 g_2 + I_1\right), \\
\tau_d \dot{g}_1 = 1 - g_1 - \gamma u_1 g_1, \\
\dot{u}_2 = -u_2 + f\left(-\beta u_1 g_1 + I_2\right), \\
\tau_d \dot{g}_2 = 1 - g_2 - \gamma u_2 g_2.
\end{cases}
\tag{1.4}
$$

Where $g_i(t)$ is the synaptic depression variable. The gain function again is a sigmoid.

The system in Equation 1.2 exhibits five possible types of behaviour: for large values of I (region I in Figure 1.8F) both populations are active at identically high levels (Figure 1.8A); the time courses of u_1 and u_2 tend to a stable steady state larger than u_0. As I decreases (region II, Figure 1.8F) the system starts oscillating with u_1 and u_2 alternatively on and off (Figure 1.8B); in this region the period of oscillation decreases with increasing input strength (escape mechanisms). At intermediate values of I a winner-take-all kind of behaviour is observed (region III, Figure 1.8F); depending on the choice of initial conditions, one of the two populations is active indefinitely, while the other one remains inactive (Figure 1.8C). Decreasing I even more (region IV, Figure 1.8F) the neuronal model becomes oscillatory again (Figure 1.8D) with u_1 and u_2 competing for the active state; however, for this range of parameter the oscillation period T increases with input value I (release mechanisms, an opposite behaviour to that observed in region II). Last,

for small values of stimulus strength (region V, Figure 1.8F) both populations remain inactive at identically low level firing rates (Figure 1.8E); the time courses of u_1 and u_2 tend to a stable steady state less than u_0.

1.3.3. Wilson model

Spike-rate equations for the Wilson model (Wilson 2003) are given by:

$$
\begin{aligned}
\tau \dot{E}_1 &= -E_1 + \frac{100(J_1(t) - gI_2)_+^2}{(10 + H_1)^2 + (J_1(t) - gI_2)_+^2}, \\
\tau_H \dot{H}_1 &= -H_1 + hE_1, \\
\tau_I \dot{I}_1 &= -I_1 + E_1, \\
\tau \dot{E}_2 &= -E_2 + \frac{100(J_2(t) - gI_1)_+^2}{(10 + H_2)^2 + (J_2(t) - gI_1)_+^2}, \\
\tau_H \dot{H}_2 &= -H_2 + hE_2, \\
\tau_I \dot{I}_2 &= -I_2 + E_2.
\end{aligned}
\tag{1.5}
$$

Here J_i is the input to populations i ($i = 1, 2$), E_i is the firing rate of the excitatory population i, H_i is the adaptation variable, and I_i is the inhibitory firing rate. The asymptotic firing rate, the second term on the right-hand side of the first and fourth expressions in (1), is determined by a Naka–Rushton function for positive values of its argument $(J - gI)_+$, where $(J - gI)_+ = J - gI$ if $J >= gI$ and $(J - gI)_+ = 0$ if $J < gI$ (Naka and Rushton 1966). Parameters g and h are inhibition and adaptation strength, respectively.

1.3.4. Conclusion

We went through different approaches in neural competition modelling. With a broad look at these models, it seems that reciprocal inhibition and a slow negative feedback processes are considered as the underlying mechanism for rivalry. However, the actual mechanism that gives rise to binocular rivalry is still not entirely understood (Brascamp et al. 2015).

In addition to slow processes, noise also considered as the underlying mechanism for alternating perception (Shpiro et al. 2009). We can distinguish between two approaches in competition modelling: first, adaptation-driven models and second, noise-driven models. Adaptation-driven models, also called oscillator models, such as Laing and Chow 2002 (Laing and Chow 2002), Wilson 2003 (Wilson 2003), can generate oscillation even in the absence of noise, but the oscillations are exactly periodic. As observed in experiments (Levelt 1965; Logothetis et al. 1996; Cao et al. 2014), there is some variability in dominance duration times which are characterized by an e.g. log-normal distribution. Adding noise to adaptation-driven models captures this property. On the other hand, there are noise-driven attractor models such as Salinas 2003 (Salinas 2003), Freeman 2005 (Freeman 2005), that argue noise is an essential mechanism for generating oscillations. In this

regime of modelling, adaptation processes even if they exist, are not strong enough to produce alternation without noise.

In the computational models that have been presented so far, the stochastic nature of dominance durations modelled with additive noise using an Ornstein-Uhlenbeck process. However, the results of (Cao et al. 2014) and (Cao et al. 2016) showed that the distributions of dominance durations must have a scaling property that cannot be captured with additive noise. The stochastic process that they suggested for maintaining this scaling property requires many equations and does not describe the phenomena biologically. One line for future research is to focus on the introduction of a noise process to the previous computational models like the Laing model (Laing and Chow 2002) which can produce current stochasticity of dominant time durations preserving the scaling property.

The dynamical characteristics that are common between neural competition models had been investigated in (Shpiro et al. 2007). For this aim they selected the Laing and Chow model (Laing and Chow 2002) (firing-rate version), Wilson model (with one stage) and two variations of the Laing and Chow model, which they called adaptation-LC model and depression-LC model. Although these models posed different features in the implementation of cross-inhibition, slow processes and gain function, all of them showed common qualitative characteristics for neural competition, some of which were reported for the first time in (Shpiro et al. 2007). Bifurcation analysis of these models over a wider range of input strength revealed that there is a lower range of stimulus strength in which, despite Levelt's proposition IV, dominance duration increases with increasing stimulus strength. It seems that additional experimental tests of Levelt's proposition IV are needed to describe perceptual rivalry more specifically.

1.4. Dissertation outline

In Chapter 2, I investigate a model of neural competition (Adaptation-LC model) analytically to describe different dynamical behaviours of the system that appear depending on the input strength. These analytical investigations help us to understand the underlying mechanisms of perceptual alternations in competition models, in order to refine the mechanisms in a way to be consistent with Levelt's propositions. In Chapter 3, I have done deeper dynamical analysis of a widely used binocular rivalry model (Wilson 2003) with fixed and periodic stimuli. In Chapter 4, I have presented a new, simple form of tactile rivalry and explored generalisations with respect to perceptual rivalry in other sensory modalities. Chapter 5 includes dynamical analysis of a model for vibrotactile rivalry with periodic stimuli and slow-fast timescale separation. Chapter 6 concludes the thesis with a discussion of each chapter, links between them and future work.

2. Piecewise linear analysis of Adaptation-LC model

2.1. Introduction

For conventional models of binocular rivalry (Laing and Chow 2002; Wilson 2003), Levelt's proposition IV is valid only within a limited range of stimulus strength (Shpiro et al. 2007). These differences between experimental reports and theory have important implications, either predicting new possible dynamics in binocular rivalry or, if future experiments do not confirm them, pointing to necessity for other types of models (Curtu et al. 2008). Meanwhile it is important to understand the sources or mechanisms that lead to the non-monotonic dependence of oscillation period on stimulus strength for these conventional competition models. Here, a mathematical model of neural competition (Adaptation-LC model, see subsection 1.3.2 for model description) (Laing and Chow 2002; Shpiro et al. 2007) is considered with the aim to describe different dynamical behaviours of the system that appear depending on the input strength and the relative values of system's parameters such as cross-inhibition β and synaptic depression g.

In the following sections, I will consider some simplifying assumptions such as, linearising the sigmoid function and turning off the adaptation process. Firstly, the sigmoid function was estimated with Heaviside function and found different dynamical behaviours over different ranges of input strength. Secondly, the nonlinearity was considered as a piecewise linear function, I found the equilibria existing over different ranges of input strength and their stability, and also showed when the system has limit cycle and oscillatory behaviours. Further study extends this analysis for the full model with sigmoidal nonlinearity (see (Curtu et al. 2008)). These analytical investigations help us to understand the underlying mechanisms of perceptual alternations in competition models, in order to refine the mechanisms in a way to be consistent with Levelt's propositions.

2.2. Methods and Results

2.2.1. Heaviside nonlinearity and adaptation OFF

For the simplest case, I consider the Heaviside function as an approximation of the sigmoid function (see Figure 2.1). At this time, I suppose that spike-frequency adaptation process is off ($g = 0$ in Equation 1.2) and the two units u_1 and u_2 interact only through reciprocal
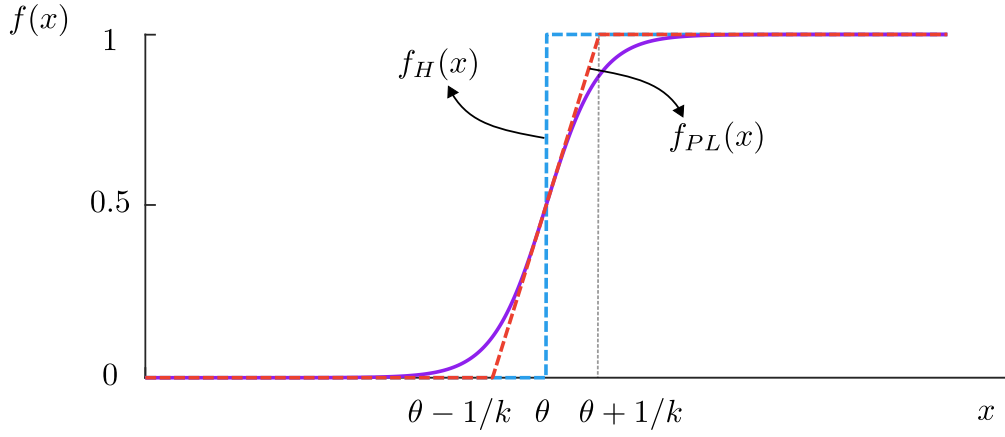
Figure 2.1. The sigmoid function (purple solid curve) have been estimated with Heaviside function $f_H(x)$ (dashed blue curved), and also with piecewise linear function $f_{PL}(x)$ (dashed red curved)

inhibition. The system's equations will be as follows:

$$\begin{cases} \dot{u}_1 = -u_1 + f_H\left(-\beta u_2 + I\right) = F(u_1, u_2, I), \\ \dot{u}_2 = -u_2 + f_H\left(-\beta u_1 + I\right) = G(u_1, u_2, I), \end{cases} \tag{2.1}$$

$$f_H(x) = \begin{cases} 1, & x \geq \theta, \\ 0, & x < \theta. \end{cases} \tag{2.2}$$

In order to find the steady states of the model I consider:

$$\begin{cases} u_1{}^* = f_H\left(-\beta u_2{}^* + I\right), \\ u_2{}^* = f_H\left(-\beta u_1{}^* + I\right). \end{cases} \tag{2.3}$$

As f_H is a Heaviside function, $u_1{}^*$ and $u_2{}^*$ can either be 0 or 1. So, there are three parameter regimes with different solutions:

$$1) \quad u_1{}^* = u_2{}^* = 0 \quad \text{for} \quad I < \theta, \tag{2.4}$$

$$2) \quad \begin{cases} u_1{}^* = 0 \text{ and } u_2{}^* = 1 \\ \qquad \text{coexisting with} \qquad \text{for} \quad \theta \leq I < \beta + \theta, \\ u_1{}^* = 1 \text{ and } u_2{}^* = 0 \end{cases} \tag{2.5}$$

$$3) \quad u_1{}^* = u_2{}^* = 1 \quad \text{for} \quad \theta + \beta \leq I. \tag{2.6}$$

In order to check stability of the system, the Jacobian matrix A is examined at the equilibrium points. As the slope of f_H is always 0 (or undefined at the threshold), the Jacobian matrix A evaluated at equilibrium will be as follows:

$$A|_* = \begin{bmatrix} \frac{\partial F}{\partial u_1} & \frac{\partial F}{\partial u_2} \\ \frac{\partial G}{\partial u_1} & \frac{\partial G}{\partial u_2} \end{bmatrix} \Big|_* = \begin{bmatrix} -1 & 0 \\ 0 & -1 \end{bmatrix}. \tag{2.7}$$

A

B

C
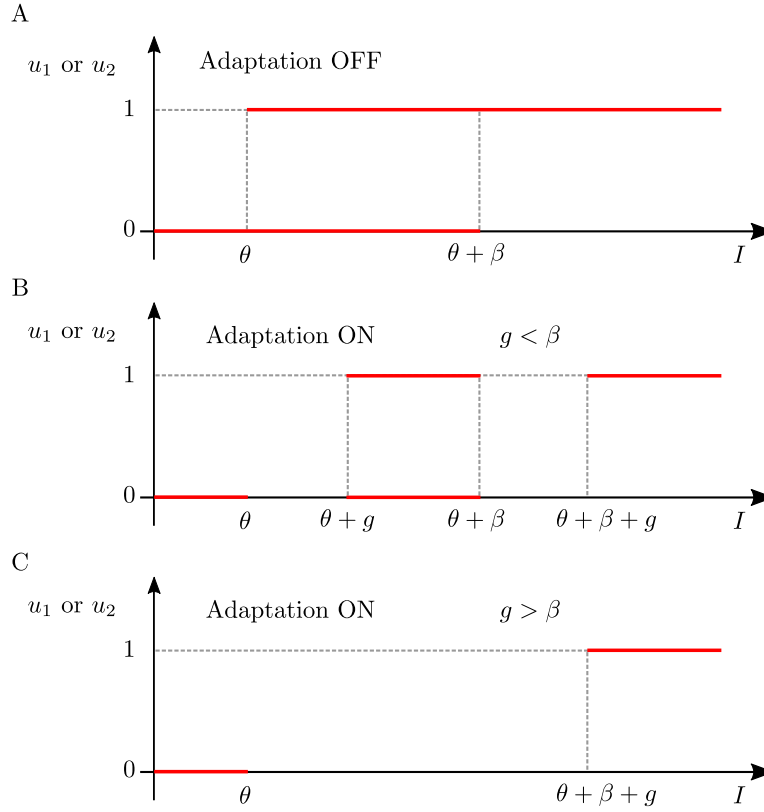
Figure 2.2. **(A)** The bifurcation diagram varying input strength I when f_H is a Heaviside function and adaptation is OFF, **(B)** adaptation is ON, for $g < \beta$, **(C)** adaptation is ON, for $g > \beta$

This means both eigenvalues are negative for any steady state solutions. So, all steady states are stable. The bifurcation diagram with respect to input strength I is shown in Figure 2.2A.

2.2.2. Heaviside nonlinearity and adaptation ON

For the next step, the adaptation process is turned on and the model's steady states are investigated. At equilibrium point we have $\begin{cases} a_1 = u_1 \\ a_2 = u_2 \end{cases}$ and again by considering f_H as a Heaviside function, there are 3 parameter regimes with different solutions as:

$$1) \quad u_1 = u_2 = 0 \ \text{ for } \ I < \theta, \tag{2.8}$$

$$2) \quad \begin{cases} u_1 = 0 \text{ and } u_2 = 1 \\ \quad \text{coexisting with} \quad \text{ for } \quad g < \beta, \quad \theta + g \leq I < \theta + \beta, \\ u_1 = 1 \text{ and } u_2 = 0 \end{cases} \tag{2.9}$$

$$3) \quad u_1 = u_2 = 1 \ \text{ for } \ \theta + \beta + g < I. \tag{2.10}$$

The second solution only exists when $g < \beta$. The bifurcation diagrams are shown in Figure 2.2B and Figure 2.2C. Note that there are ranges for parameter I where the model has no equilibria. This happens as very simple approximation for the sigmoid function

39
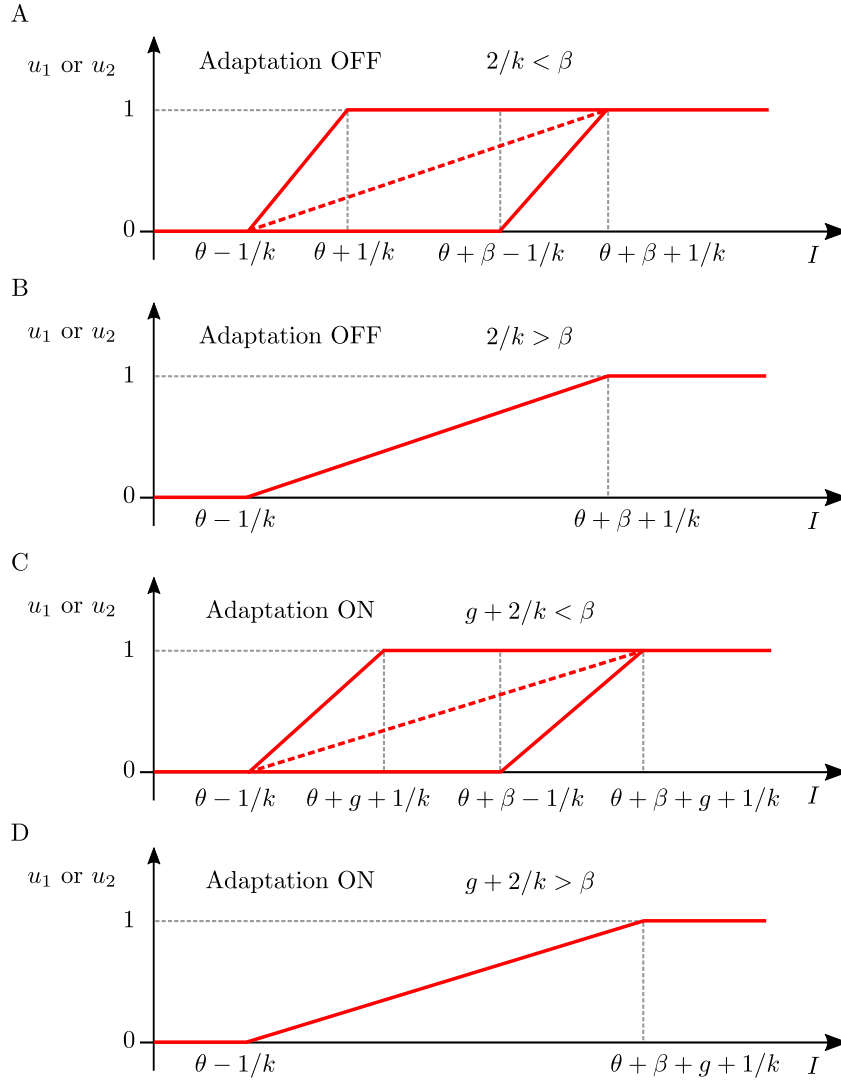
Figure 2.3. **(A)** Bifurcation diagram varying input strength I when f_{PL} is a piecewise linear function and adaptation is OFF, for $\frac{2}{k} < \beta$. **(B)** Bifurcation diagram varying input strength I when f_{PL} is a piecewise linear function and adaptation is OFF, for $\frac{2}{k} > \beta$. **(C)** Bifurcation diagram varying input strength I when f_{PL} is a piecewise linear function and adaptation is ON, for $g + \frac{2}{k} < \beta$. **(D)** Bifurcation diagram varying input strength I when f_{PL} is a piecewise linear function and adaptation is ON, for $g + \frac{2}{k} > \beta$

(with a discontinuity) has been considered. I expect oscillatory steady states in these regions. I will investigate this in subsection 2.2.5.

2.2.3. Piece-wise linear approximation for nonlinearity and adaptation OFF

Now I make the approximation of sigmoid function more accurately and suppose f_{PL} to be a piecewise linear function as described below (see Figure 2.1):

$$f_{PL}(x) = \begin{cases} 0 , & x \leq \theta - \frac{1}{k} \\ \frac{k}{2}(x - \theta) + \frac{1}{2} , & \theta - \frac{1}{k} < x < \theta + \frac{1}{k} \\ 1 , & \theta + \frac{1}{k} \leq x. \end{cases} \tag{2.11}$$

At first, the adaptation process is turned off. Considering three segments of the function

f_{PL}, we will have six different cases:

$$1) \quad u_1 = u_2 = 0 \quad \text{for} \quad I \leq \theta - \frac{1}{k} \tag{2.12}$$

$$2) \quad \begin{cases} u_1 = 0 \text{ and } 0 < u_2 < 1 \\ \qquad \text{coexisting with} \\ u_2 = 0 \text{ and } 0 < u_1 < 1 \end{cases} \quad \text{for} \quad \frac{2}{k} < \beta, \quad \theta - \frac{1}{k} < I < \theta + \frac{1}{k} \tag{2.13}$$

$$3) \quad 0 < u_1 < 1 \quad \text{and} \quad 0 < u_2 < 1 \quad \text{for} \quad \theta - \frac{1}{k} < I < \theta + \beta + \frac{1}{k} \tag{2.14}$$

$$4) \quad \begin{cases} u_1 = 0 \text{ and } u_2 = 1 \\ \qquad \text{coexisting with} \\ u_1 = 1 \text{ and } u_2 = 0 \end{cases} \quad \text{for} \quad \frac{2}{k} < \beta, \quad \theta + \frac{1}{k} \leq I \leq \theta + \beta - \frac{1}{k} \tag{2.15}$$

$$5) \quad \begin{cases} u_1 = 1 \text{ and } 0 < u_2 < 1 \\ \qquad \text{coexisting with} \\ u_2 = 1 \text{ and } 0 < u_1 < 1 \end{cases} \quad \text{for} \quad \frac{2}{k} < \beta \quad \theta + \beta - \frac{1}{k} < I < \theta + \beta + \frac{1}{k} \tag{2.16}$$

$$6) \quad u_1 = u_2 = 1 \quad \text{for} \quad \beta + \theta + \frac{1}{k} \leq I \tag{2.17}$$

The second, fourth and fifth solutions only exist when $\frac{2}{k} < \beta$. The bifurcation diagrams depending this condition are shown in Figure 2.3A and Figure 2.3B. For the stability check, only at the third solution, matrix A can have eigenvalues different from -1.

$$A|_* = \begin{bmatrix} \frac{\partial F}{\partial u_1} & \frac{\partial F}{\partial u_2} \\ \frac{\partial G}{\partial u_1} & \frac{\partial G}{\partial u_2} \end{bmatrix}\Big|_* = \begin{bmatrix} -1 & -\frac{\beta k}{2} \\ -\frac{\beta k}{2} & -1 \end{bmatrix} \tag{2.18}$$

Which has eigenvalues $\lambda_1 = \frac{\beta k}{2} - 1$, $\lambda_2 = -\frac{\beta k}{2} - 1$. One of these eigenvalues can be positive if $\frac{2}{k} < \beta$. So, the middle branch in Figure 2.3A is a unstable equilibrium.

2.2.4. Piece-wise linear estimate for nonlinearity and adaptation ON

At this step, the adaptation process is turned on and model's steady states are investigated. At equilibrium point we have $a_1 = u_1, a_2 = u_2$, and again by considering the three pieces

of function f_{PL}, we can have six different cases:

$$1) \quad u_1 = u_2 = 0 \quad \text{for} \quad I \leq \theta - \frac{1}{k} \tag{2.19}$$

$$2) \begin{cases} u_1 = 0 \text{ and } 0 < u_2 < 1 \\ \quad \text{coexisting with} \\ u_2 = 0 \text{ and } 0 < u_1 < 1 \end{cases} \text{for} \quad g + \frac{2}{k} < \beta , \quad \theta - \frac{1}{k} < I < \theta + g + \frac{1}{k} \tag{2.20}$$

$$3) \quad 0 < u_2 < 1 \quad \text{and} \quad 0 < u_1 < 1 \quad \text{for} \quad \theta - \frac{1}{k} < I < \theta + \beta + g + \frac{1}{k} \tag{2.21}$$

$$4) \begin{cases} u_1 = 0 \text{ and } u_2 = 1 \\ \quad \text{coexisting with} \\ u_1 = 1 \text{ and } u_2 = 0 \end{cases} \text{for} \quad g + \frac{2}{k} < \beta , \quad \theta + g + \frac{1}{k} \leq I \leq \theta + \beta - \frac{1}{k} \tag{2.22}$$

$$5) \begin{cases} u_1 = 1 \text{ and } 0 < u_2 < 1 \\ \quad \text{coexisting with} \\ u_2 = 1 \text{ and } 0 < u_1 < 1 \end{cases} \text{for } g + \frac{2}{k} < \beta , \quad \theta + \beta - \frac{1}{k} < I < \theta + \beta + g + \frac{1}{k} \tag{2.23}$$

$$6) \quad u_1 = u_2 = 1 \quad \text{for} \quad \theta + \beta + g + \frac{1}{k} \leq I \tag{2.24}$$

The second, fourth and fifth solutions only exist when $g + \frac{2}{k} < \beta$. The bifurcation diagrams depending this condition are shown in Figure 2.3C and Figure 2.3D.

2.2.5. Periodic solutions with Heaviside nonlinearity and adaptation ON

So far, the equilibria of the system have been found. For completing analysis of the system, I need to look for periodic solutions as well. For finding periodic solutions, the adaptation process needs to be on. For simplicity, the nonlinearity f_H is considered to be a Heaviside function. The adaptation dynamics is much slower than the average firing rate dynamics. So, in our analysis we can suppose that u_1 and u_2 have reached their steady states, however, a_1 and a_2 still evolve with time. Knowing that f_H is a Heaviside function, u_1 and u_2 must be either 0 or 1, and a_1 and a_2 have their own slow dynamics which can change the states of u_1 and u_2 from 0 to 1 and vice versa. By this mechanism, oscillatory behaviour can exist in this system for some range of model parameters.

When each of u_1 and u_2 is equal to 0 or 1, then the corresponding adaptation variable a_1 and a_2 evolves slowly with dynamics:

$$\tau_a \dot{a}_i = -a_i + u_i \quad i = 1, 2. \tag{2.25}$$

When u_i is equal to one, then the solution of Equation 2.25 is:

$$a_i(t) = 1 + (a_i(t_0) - 1)e^{-(t-t_0)/\tau_a} \quad , \quad u_i = 1, \tag{2.26}$$

where $a_i(0)$ is the initial value of a_i. And when u_i is equal to 0, the solution of Equation 2.25 is:

$$a_i(t) = a_i(t_0)e^{-(t-t_0)/\tau_a} \quad , \quad u_i = 0. \tag{2.27}$$
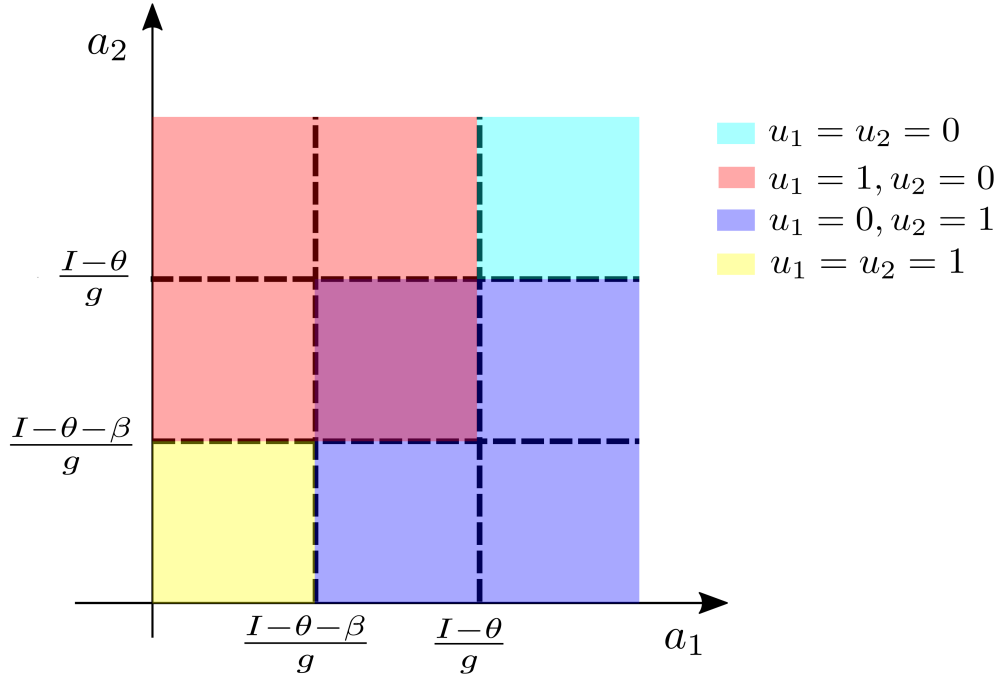
Figure 2.4. 2D bifurcation diagram varying variables a_1 and a_2 which considered here as the bifurcation parameters, when f_H is a Heaviside function

As a_1 and a_2 evolve slowly, we can consider them as fixed parameters when analyse the steady state values of u_1 and u_2. I want to assess different values of a_1 and a_2, as parameters of the system, which correspond to different steady states of u_1 and u_2. Here input strength is considered as a fixed parameter and the role of varying a_1 and a_2 is investigated in u_1 and u_2 steady states. Remembering f_H is a Heaviside function, we will have 4 different cases:

$$1) \quad u_1 = u_2 = 0 \quad \text{for} \quad \begin{cases} a_1 > \frac{I-\theta}{g} \\ a_2 > \frac{I-\theta}{g} \end{cases} \tag{2.28}$$

$$2) \quad \begin{cases} u_1 = 0 \\ u_2 = 1 \end{cases} \quad \text{for} \quad \begin{cases} a_1 > \frac{I-\theta-\beta}{g} \\ a_2 < \frac{I-\theta}{g} \end{cases} \tag{2.29}$$

$$3) \quad \begin{cases} u_1 = 1 \\ u_2 = 0 \end{cases} \quad \text{for} \quad \begin{cases} a_1 < \frac{I-\theta}{g} \\ a_2 > \frac{I-\theta-\beta}{g} \end{cases} \tag{2.30}$$

$$4) \quad u_1 = u_2 = 0 \quad \text{for} \quad \begin{cases} a_1 < \frac{I-\theta-\beta}{g} \\ a_2 < \frac{I-\theta-\beta}{g} \end{cases} \tag{2.31}$$

The summary of these cases has shown in Figure 2.4. This figure can be considered as a 2D bifurcation diagram varying a_1 and a_2 as bifurcation parameters. As Figure 2.4 shows, two threshold lines in a_1-a_2 plan exist which when crossed over the steady states of u_1 and u_2 will switch from 0 to 1 and vice versa.

We call the line $a_i = \frac{I-\theta-\beta}{g}$ low threshold and the line $a_i = \frac{I-\theta}{g}$ high threshold. As Figure 2.4 shows, if a_1 and a_2 are greater than high threshold, the steady states of both u_1 and u_2 are 1. If a_1 and a_2 are both less than low threshold, the steady states of both
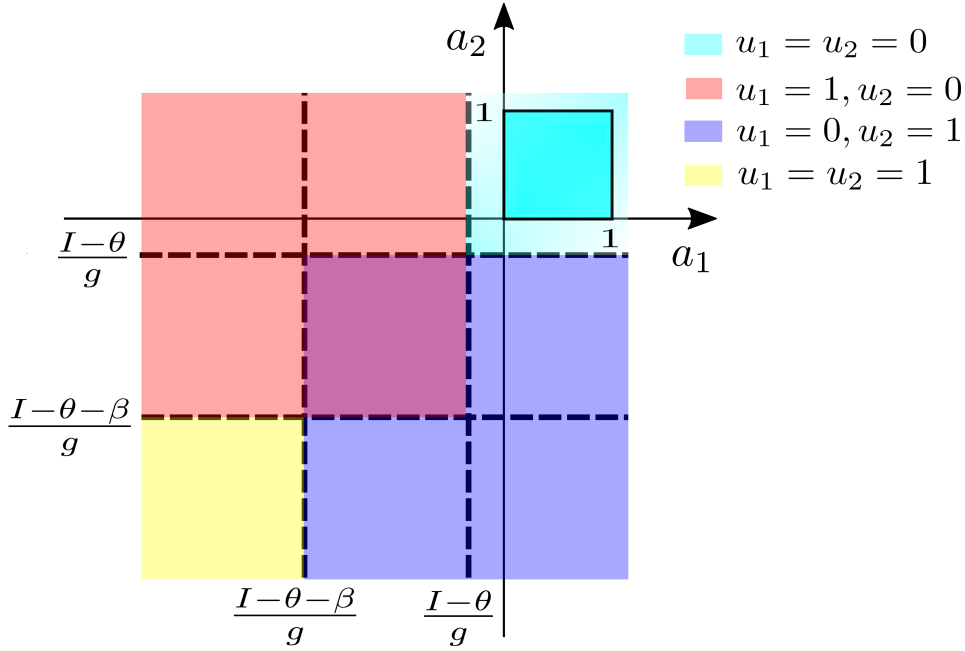
Figure 2.5. 2D bifurcation diagram according to a_1 and a_2, if $I < \theta$

u_1 and u_2 are 1. If one of the a_1 and a_2 is less than high threshold and the other one is greater than low threshold, we have rivalry with one of variables u_1 and u_2 is equal to 1 and the other one is equal to 0. If both of variables a_1 and a_2 are between the high and low thresholds, we have winner-take-all case in which two steady states coexist.

For different range of input strength, depending if $\beta < g$ or $\beta > g$, one or both of the threshold lines can go beyond the valid range for a_1 and a_2 . If none of the thresholds is present in the a_1-a_2 plane, we cannot have oscillatory behaviour. If one of the threshold lines is presented, we will have oscillatory dynamics. If both threshold lines are presented, we may have only one of two possible types of oscillations depending on the input strength. In what follows, these cases will be discussed in more details.

I) If $I < \theta$, both threshold lines go beyond the a_1-a_2 plane from the negative sides as shown in Figure 2.5. So, for all values of a_1 and a_2, the system only has simultaneously inactive responses.

II) If $I > \theta + \beta + g$, both threshold lines go beyond the valid range of a_1 and a_2 (are always less than one), and for the valid range of a_1 and a_2, as Figure 2.6 shows, the system only has simultaneously active responses.

III) If $\theta + g < I < \theta + \beta$, and $\beta > g$, the high threshold go beyond the valid range from the positive side and low threshold go beyond valid range from the negative side. As Figure 2.7 shows, the system operates in a winner-take-all regime.

IV) If $\theta + \beta < I < \theta + \beta + g$, and $\beta > g$, and also if $\theta + g < I < \theta + \beta + g$, and $\beta < g$, only the low threshold is in the valid range Figure 2.8.

V) If $\theta < I < \theta + \beta$, and $\theta < g$, and also if $\theta < I < \theta + g$, and $\theta > g$, only the high thresh-
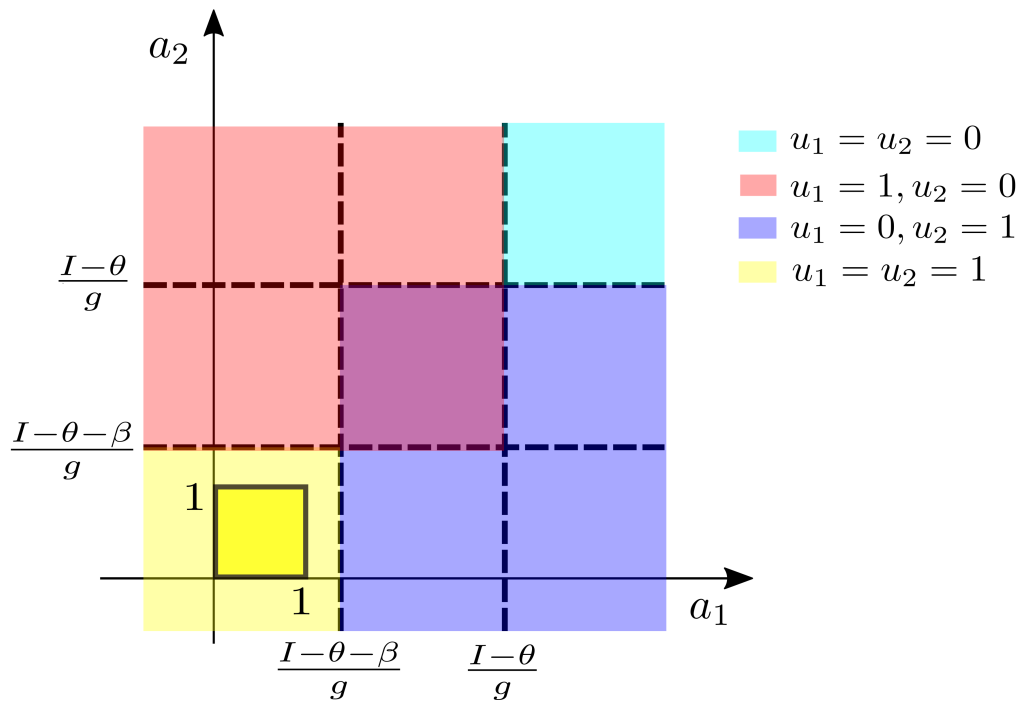
Figure 2.6. 2D bifurcation diagram according to a_1 and a_2, if $I > \theta + \beta + g$
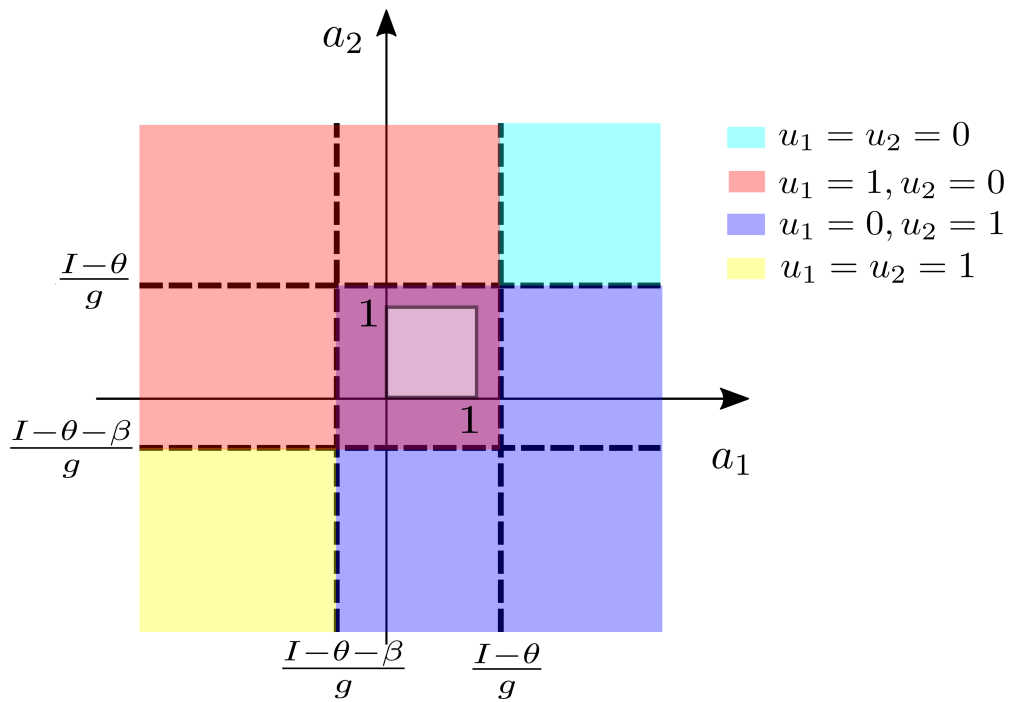
Figure 2.7. 2D bifurcation diagram varying a_1 and a_2, if $\theta + g < I < \theta + \beta$ and $\beta > g$
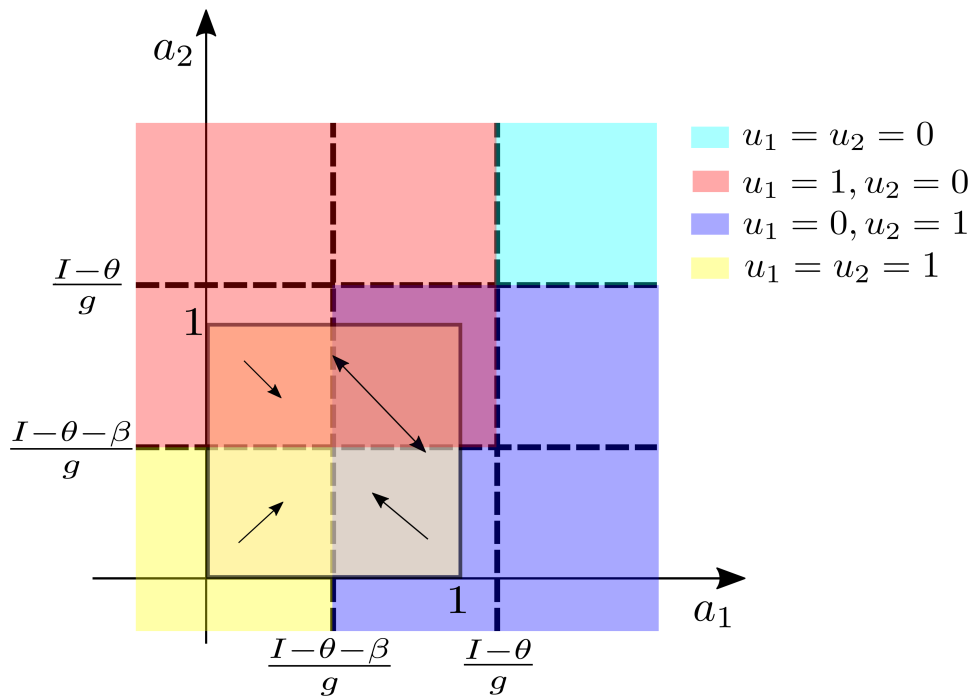
Figure 2.8. 2D bifurcation diagram according to a_1 and a_2, if $\theta + \beta < I < \theta + \beta + g$, and $\beta > g$, and also if $\theta + g < I < \theta + \beta + g$, and $\beta < g$
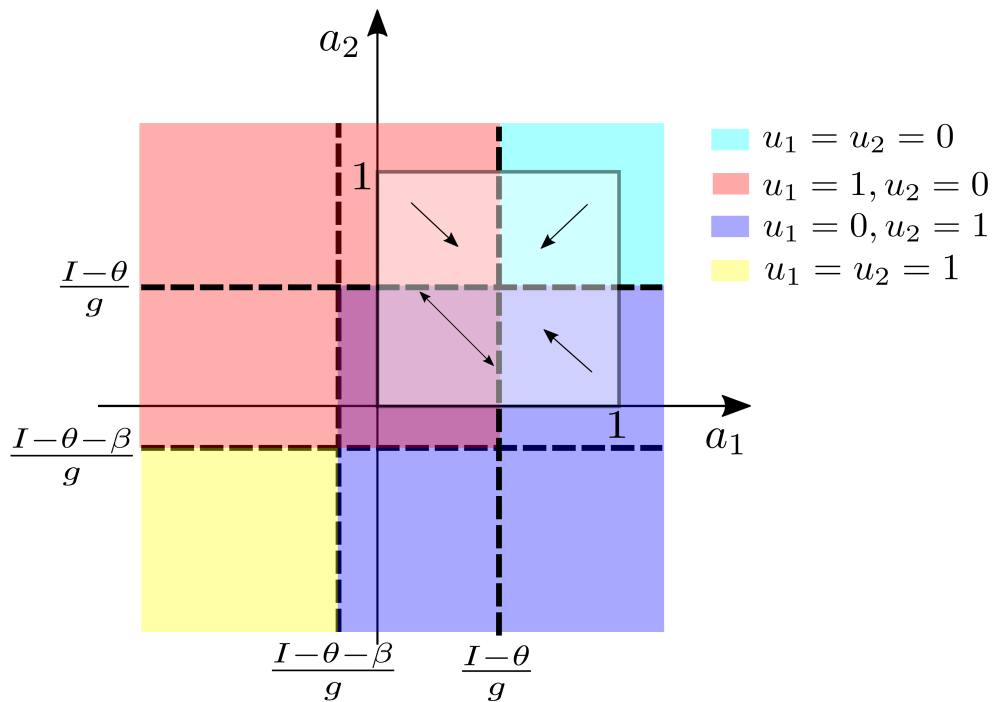
Figure 2.9. 2D bifurcation diagram according to a_1 and a_2, if $\theta < I < \theta + \beta$, and $\theta < g$, and also if $\theta < I < \theta + g$, and $\theta > g$

46
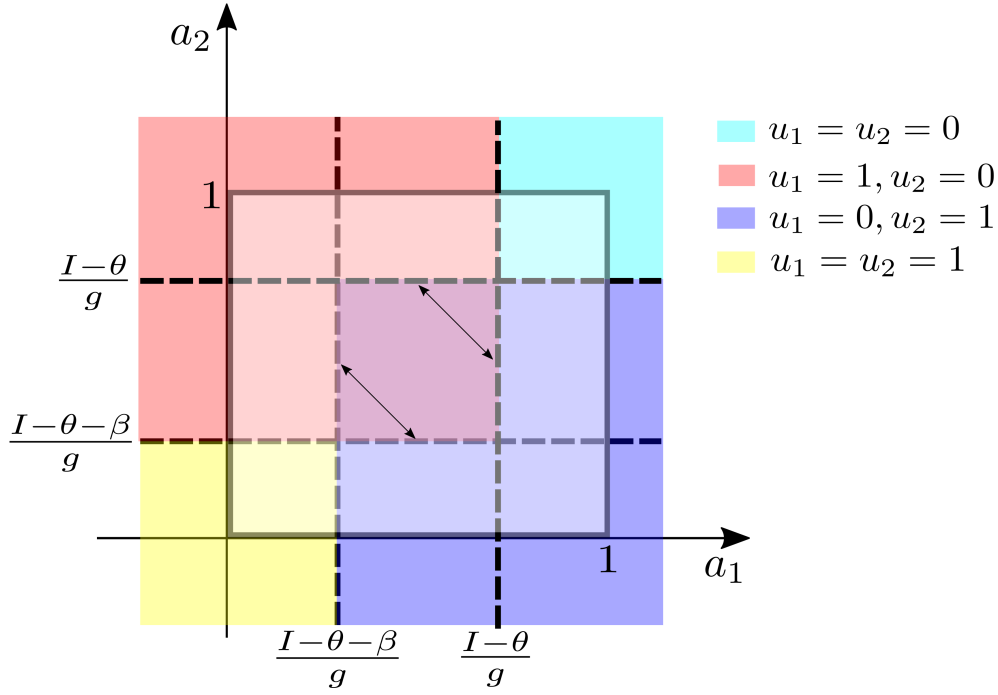
Figure 2.10. 2D bifurcation diagram according to a_1 and a_2, if $\theta + \beta < I < \theta + g$, and $\beta < g$

old is in the valid range Figure 2.9.

VI) If $\theta + g < I < \theta + \beta$, and $\beta < g$, both threshold lines exist in a_1 and a_2 valid range Figure 2.10.

Oscillations may exist in the system for cases IV, V and VI. Figure 2.8, Figure 2.9, and Figure 2.10 also show vector fields. The direction of a_1 and a_2 trajectories depend on the state of u_1 and u_2. If u_i is equal to 0, a_i moves toward 0 and if u_i is equal to 1, a_i moves toward 1. The direction of these trajectories may suddenly change if they cross over the low threshold from the right side or above and also cross over the high threshold from left side and beneath. As a_1 and a_2 evolve continuously, oscillations may exist if we have at least one of threshold lines within the valid range for a_1 and a_2.

If the low threshold line only exists, the oscillation of a_1 and a_2 are limited to the low threshold and a fixed value greater than the low threshold (Figure 2.8). The higher limitation is equal to $1 - \frac{I - \theta - \beta}{g}$ and period of these oscillations is equal to $2\tau \ln(\frac{g}{I - \theta - \beta} - 1)$.

If the high threshold line only exists, the oscillation of a_1 and a_2 are limited to $1 - \frac{I - \theta}{g}$ and the high threshold (Figure 2.9). Period of these oscillations is equal to $2\tau \ln(\frac{I - \theta}{g - I - \theta})$.

If both of the threshold lines are present in the valid range (Figure 2.10), the oscillations are either limited to the low threshold (similar to case IV), or to the high threshold (similar to case V). The first case happens if $\theta + g/2 < I < \theta + (\beta + g)/2$ and the second case happens if $\theta + (\beta + g)/2 < I < \theta + \beta + g/2$.

2.3. Discussion

In this models, five distinct regimes of behaviour was observed in different ranges of stimulus strength. At very low stimulus strengths the system goes into fusion with both populations simultaneously active at a low level (SIM). Over a range of weak stimulus strengths the period of oscillations increases with increasing input (increasing RIV branch). For intermediate values of the stimulus strength, a winner-take-all regime is present (WTA). Another oscillatory regime exists for larger inputs, with the period of oscillations decreasing as input increases (decreasing RIV branch). For very strong stimuli alternation is terminated and both populations are highly and identically active (SIM). Thus period depends non-monotonically on stimulus strength with a winner-take-all behaviour that separates the two oscillatory regimes.

These types of perceptual rivalry models are typically just investigated numerically with a smooth firing rate function. Here, with the Heaviside nonlinearity and the adaptation process, I showed analytically that periodic solution exists for some range of stimulus strength. I also found expressions for the period of these oscillations which shows non-monotonic dependence of the oscillation period on stimulus strength which means Levelt's proposition IV is valid only within a limited range of stimulus strength (Seely and Chow 2011). In another case, when a piece-wise nonlinearity function was considered, the model does not have any periodic solution (but there is bistablity region). Thus perceptual alternations can only occur through introduction of noise. In another study by Curtu et al. (2008) some analysis with a Heaviside function has been done (but not with a piece-wise linear function).

The presence of the winner-take-all and increasing-RIV regimes is common to all mutual-inhibition models (Shpiro et al. 2007; Laing and Chow 2002; Wilson 2003), however, this can be controlled by the strength of inhibition between two neuronal populations. The strength of inhibition β affects whether there will be an increasing-RIV regime. It has been shown in Shpiro et al. (2007) that there is a rather narrow range of β values where models show a monotonic behaviour, that is, a decreasing period of oscillations as stimulus strength is increased from zero to large values.

In this chapter, the existence of multiple modes of behaviour was investigated over ranges of stimulus intensity. More generally, other model parameters, such as the strength of inhibition may be varied, and other modes of behaviour are expected to occur. In Chapter 3, this is pursued in a related model, where an in depth numerical analysis reveals some previously unreported behaviour.

3. Methods to assess binocular rivalry with periodic stimuli

3.1. Introduction

In bistable perception, our perceptual experience evolves dynamically with fixed sensory inputs, thus providing a window into the intrinsic neural computations underlying the dynamics of sensory processing. Binocular rivalry is one example from a broad range of bistable or multistable perceptually ambiguous stimuli. It occurs when the two eyes are presented with incompatible monocular patterns (exclusively to one eye). Even though the patterns are fixed, perceptual awareness alternates every 1-5 s between two perceptual interpretations consistent with only one monocular pattern (Blake and Logothetis 2002). In other words, one of the monocular patterns is suppressed totally and the other one is dominant (thus winning the rivalry). This phenomenon has been investigated in a wide range of experimental approaches: human behavioural studies (Logothetis et al. 1996; Wilke et al. 2003), primate physiological experiments (Logothetis and Schall 1989; Leopold and Logothetis 1996), fMRI (functional magnetic resonance imaging) studies (Polonsky et al. 2000; Tong and Engel 2001), and EEG (electroencephalogram) recordings in humans (Zhang et al. 2011). Despite a long tradition of binocular rivalry research there are still questions about the neuro-computational basis and the underlying mechanisms of this phenomena. In addition to experimental investigations, powerful tools such as mathematical modelling and bifurcation analysis have been utilized to explain this phenomenon (Laing and Chow 2002; Shpiro et al. 2007; Curtu et al. 2008), but many interesting questions remain.

There are contradictory ideas about whether rivalry takes place between neural populations associated with each eye or associated with stimulus features (Logothetis et al. 1996; Lee and Blake 1999). The complex hierarchical architecture of visual cortical areas makes it difficult to associate object perception to a particular locus in cortex. The locus of visual perception and the level at which binocular rivalry is resolved are unknown. Previously, primary visual cortex (V1) had been considered as the locus of rivalry alternations and the phenomena known as interocular eye rivalry (Sengpiel et al. 1995a;b; Li et al. 2005). According to this traditional interpretation, perceptual rivalry occurs as a result of competition between monocular driven neurons in primary visual cortex (V1) (eye-based rivalry). On the contrary, there are some studies which show correlation between perception during rivalry and activity in feature-selective higher cortical areas whose inputs are pooled from both eyes (supporting stimulus rivalry) (Logothetis and Schall 1989; Leopold and Logothetis 1996). In order to resolve this dispute, Logothetis et al. introduced a new stimulus paradigm, so-called Flicker and Swap (F&S) in which monocular stimuli were

swapped between two eyes at 1.5 Hz (eye-swapping). The stimuli were flickered on and off at 18 Hz in order to reduce the subject's awareness of the swap times (Logothetis et al. 1996). The notion of eye rivalry predicts that a subject's perception must follow the stimulus as it switches between the eyes. However, F&S experiments, similar to traditional experiments, showed that each period of perceptual dominance lasts on average around 2 seconds and spans over six to seven stimulus swaps (Logothetis et al. 1996). It can be concluded from the F&S experiment that rivalry cannot be the result of suppressing one eye completely (and dominance of the other eye). These results suggest that the stimulus rivalry hypothesis is a more accurate interpretation of rivalry than eye rivalry notion.

For decades, the common empirical paradigm for studying binocular rivalry has been through stimulation of each eye with fixed stimuli (always on) (Levelt 1965; Cao et al. 2014). Several computational models of binocular rivalry have been proposed that were able to capture temporal characteristics of traditional rivalry (eye-based) with a specific set of model parameters (Lehky 1988; Blake 1989; Laing and Chow 2002; Shpiro et al. 2007; Wilson 2007; Curtu et al. 2008; Salinas 2003; Freeman 2005). The minimal properties required to implement a model that is compatible with the existing rivalry evidence is reciprocal inhibition between two monocular neural populations and a slow process (spike frequency adaptation or synaptic depression) together with nonlinearity of the spike rate gain function (Wilson 2007). Although these models posed different features in the implementation of reciprocal inhibition, slow processes and gain function, all of them show common qualitative characteristics for neural competition (Shpiro et al. 2007).

Wilson sought to explain the stimulus rivalry with a two-stage model (Wilson 2003). The first stage represents monocular neurons in primary visual cortex, and the second stage represents binocular neurons in later (higher) stages of processing (Figure 3.1A). The Wilson model can account for maintained perceptual dominance across eye swaps with F&S stimuli (Wilson 2003). However, this model predicts that monocular neural activities are not modulated during stimulus rivalry, which is contradicted by experimental evidence (Brascamp et al. 2013). Whilst a later paper from Wilson (Wilson 2007) suggested these could be accounted for by descending connections to the monocular layer, Brascamp et al. claimed that it is possible to have stimulus rivalry without binocular contributions (Brascamp et al. 2013). The Li et al. model (Li et al. 2017) similar to the Wilson model (Wilson 2003) included a second stage to explain stimulus rivalry; however, unlike the Wilson model this second layer is responsible for attentional modulation rather than another layer of rivalry. Attentional modulation provides feedback to monocular layers, and thus stimulus rivalry can be seen in the first layer. Li et al. (Li et al. 2017) also note that stimulus rivalry can occur without flicker in experiments if there are blank intervals before swaps times (van Boxtel et al. 2008; Denison and Silver 2012), which was not captured by the Wilson model.

Traditional rivalry with a fixed stimulus in each eye was studied with the Wilson model (Wilson 2003). Earlier work presented a bifurcation analysis of the Wilson model with fixed inputs and identified parameter regions with different dynamical behaviour (Shpiro et al. 2007). However, we found that a richer bifurcation structure exists at the crucial transition from winner-take-all to rivalry. Thus, a bifurcation analysis for fixed inputs that

investigates all bifurcations occurring between different dynamical states is required. Furthermore, Wilson's model and other rivalry models have been only studied using bifurcation analysis for fixed inputs, whilst the different dynamical behaviour that can occur with periodically forced inputs have only been investigated at isolated parameter values with direct simulations (time histories) (Wilson 2003) (although see (Vattikuti et al. 2016)). In general, sensitivity to model parameters with periodic inputs has not been studied so far. To fully explain F&S experiments, we need to understand the bifurcations that distinguish different states such as perception following the stimulus swaps and perception being stable for many seconds. Thus, a complete bifurcation analysis of the model with fixed and periodic inputs with careful attention to complex dynamics phenomena is required.

We aim to properly explain and understand the dynamics of binocular rivalry and how they change with different kinds of inputs (traditional, flickering, swapping, and F&S stimuli). Here we focus on the Wilson model and we were successful in building a framework to study rivalry models with, not only fixed input, but also with periodic forcing. For a thorough dynamical analysis, we analyse the Wilson model with periodic input using numerical continuation tools. This allows us to investigate different dynamical regimes and boundaries between them (bifurcations), as computed for multiple parameters. The approach presented here is applicable to a range of models for bistable perception with periodically varying stimuli.

3.2. Methods

Here we focus on the two-stage, hierarchical Wilson model which can explain both traditional and F&S experiments (Wilson 2003). The first stage represents monocular neurons in primary visual cortex, and the second stage represents binocular neurons in higher cortical areas (Figure 3.1A). These neurons self-adapt, as modelled by spike-frequency adaptation, and there is mutual inhibition between monocular neurons representing different eyes and grating orientations. We split the first level into two isolated subunits:

1) competition between neurons representing the horizontal grating in the left eye (HL) and the vertical grating in the right eye (VR).

2) competition between neurons representing the vertical grating in the left eye (VL) and the horizontal grating in the right eye (HR).

Spike-rate equations for the first isolated subunit in the first stage of the Wilson model (Wil-
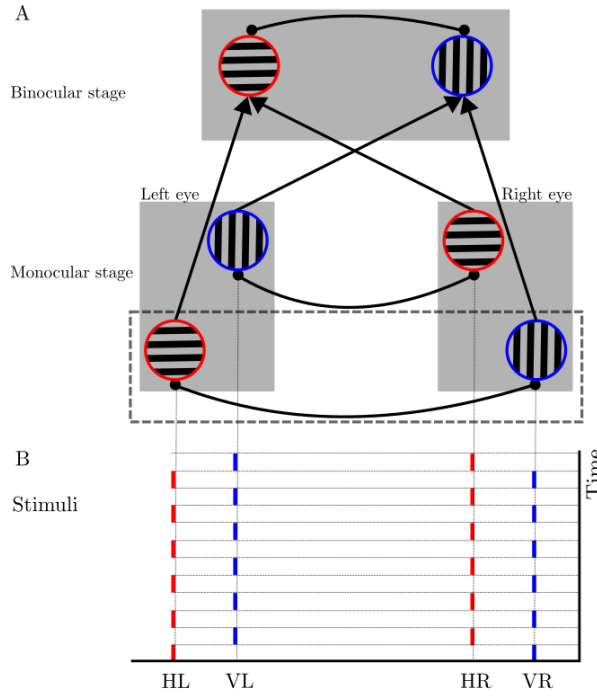
Figure 3.1. **Two stage Wilson neural network model.** (**A**) The first stage comprises monocular left and right neurons selective to orthogonal gratings. Reciprocal inhibition between different eyes and grating orientations are represented by heavy lines with filled circles at the ends. The second stage represents binocular neurons in higher cortical layers that receive summation of left and right monocular neurons with the same grating orientation. (Wilson 2003). The isolated units at the first stage that we analyse are marked with the dashed box. (**B**) Horizontal (H) and vertical (V) stimuli swapped between the left (L) and the right (R) eyes (no flicker). At a specific time, one eye receives horizontal stimuli and the other receives vertical stimuli, each stimulates their own corresponding population at the first stage.

son 2003) are given by:

$$
\begin{aligned}
\tau \dot{E}_{HL} &= -E_{HL} + \frac{100(J_{HL}(t) - gI_{VR})_+^2}{(10 + H_{HL})^2 + (J_{HL}(t) - gI_{VR})_+^2}, \\
\tau_H \dot{H}_{HL} &= -H_{HL} + hE_{HL}, \\
\tau_I \dot{I}_{HL} &= -I_{HL} + E_{HL}, \\
\tau \dot{E}_{VR} &= -E_{VR} + \frac{100(J_{VR}(t) - gI_{HL})_+^2}{(10 + H_{VR})^2 + (J_{VR}(t) - gI_{HL})_+^2}, \\
\tau_H \dot{H}_{VR} &= -H_{VR} + hE_{VR}, \\
\tau_I \dot{I}_{VR} &= -I_{VR} + E_{VR}.
\end{aligned}
\tag{3.1}
$$

Here J_{HL} and J_{VR} are inputs to populations representing horizontal grating in the left eye and vertical grating in the right eye, respectively. E_i is the firing rate of the excitatory population i ($i = HL, VR$), H_i is the adaptation variable, and I_i is the inhibitory firing rate. The asymptotic firing rate, the second term on the right-hand side of the first and fourth expressions in (1), is determined by a Naka–Rushton function for positive values of its argument $(J - gI)_+$, where $(J - gI)_+ = J - gI$ if $J >= gI$ and $(J - gI)_+ = 0$ if $J < gI$ (Naka and Rushton 1966). The following values of the parameters are used: $\tau = 20\,\text{ms}$, $\tau_H = 900\,\text{ms}$, $\tau_I = 11\,\text{ms}$, as in the original paper (Wilson 2003). The values of inhibition strength g and adaptation strength h are varied as part of the bifurcation analysis.

Here we only consider one of the isolated subunits in the first stage (marked by a dashed box in Figure 3.1A). By this simplification, we will only have two populations of neurons which correspond to the monocular neurons sensitive to horizontal stimuli in the left eye (HL) and vertical stimuli in the right eye (VR). For the traditional experiment, we will not lose generality since each eye only receives horizontal or vertical stimuli and one of the subunits always has no inputs. For the periodically forced cases, both subunits have their own inputs (Figure 3.1B). However, because of symmetry and feed-forward nature of network we can carry out our analysis without the other subunit at monocular layer. We only investigate one of the subunits, which is further justified and considered along with the implications of our results for full model in the discussion.

Stimuli for different cases: traditional rivalry, swap only, flicker only, F&S, and B&S are shown in Figure 3.2. In order to produce periodic forcing stimuli, we add two ODEs to the main equations in Equation 3.1, which describe a nonlinear oscillator,

$$\begin{aligned}
\dot{x}_s &= x_s + (2\pi f_s)y_s - x_s(x_s^2 + y_s^2), \\
\dot{y}_s &= -(2\pi f_s)x_s + y_s - y_s(x_s^2 + y_s^2),
\end{aligned} \tag{3.2}$$

with solutions: $x_s(t) = \sin(2\pi f_s t)$, $y_s(t) = \cos(2\pi f_s t)$, where f_s is the frequency of oscillations. In order to build a smooth square waveform (a square wave that is differentiable, i.e. with smooth transitions between 0 and 1) using the sinusoidal waveforms $(x_s(t))$, we will apply a steep sigmoid function,

$$x(t) = \frac{1}{1 + e^{-kx_s(t)}}, \tag{3.3}$$

with $k = 10$. Thus our desirable periodic forcing for swap only $(f_s = 1.5\,Hz)$ and flicker only $(f_s = 18\,Hz)$ cases can be applied by replacing $J_{HL}(t) = J_{VR}(t) = x(t)$ in Equation 1.1. For F&S stimuli, we have two forcing terms with different frequencies. Considering that the flickering frequency is an integer multiple of swap frequency $(f_f = 12f_s)$, we first build the lower frequency forcing (x_s) using equations Equation 1.2, and the higher frequency forcing (x_f) can be computed by:

$$x_f(t) = \text{Re}\{[x_s(t) + iy_s(t)]^{12}\}. \tag{3.4}$$

Then the F&S stimuli can be produced from its components:

$$x_{fs}(t) = x_f(t)x_s(t). \tag{3.5}$$

The nonlinear gain function that appears in the right-hand side of the original Wilson model is a discontinuous function in its first derivative due to the rectification operation $(J - gI)_+$. Numerical continuation routines require smooth systems of equations. In order to solve this problem we have used a steep sigmoid function to smooth out the transition at zero. So instead of $(J - gI)_+$ terms in Equation 1.1, we substitute $R(J - gI)$ as:

$$R(x) = \frac{x}{1 + e^{-k(x-\theta)}}. \tag{3.6}$$
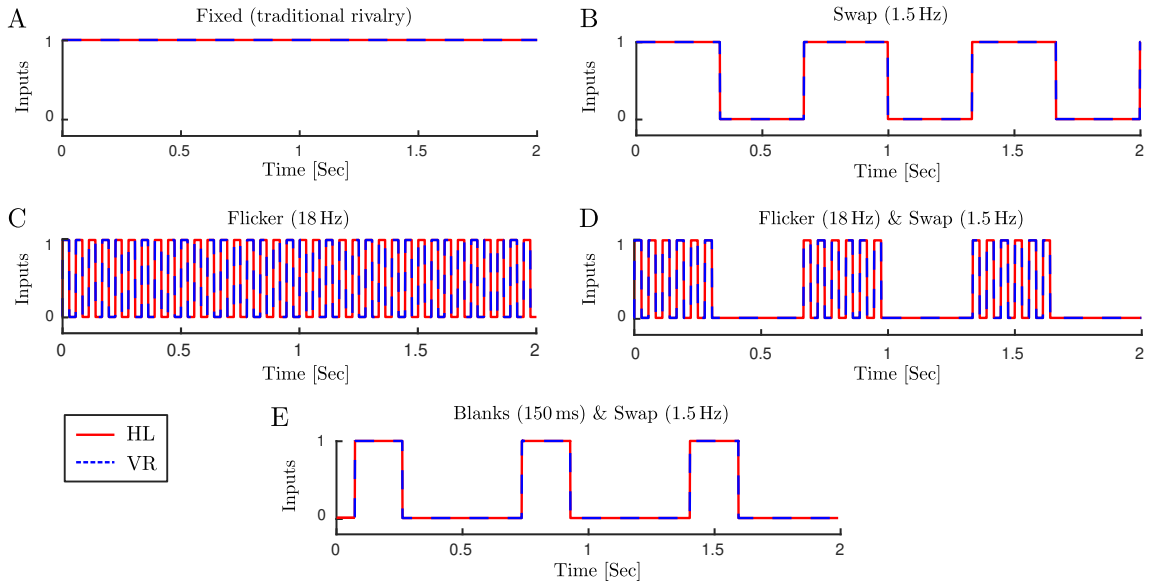
Figure 3.2. **Stimuli for different input cases.** Stimuli for monocular populations selective to the horizontal grating in the left eye (HL) and vertical gratings in the right eye (VR) are shown with red solid and blue dashed lines respectively. (A) Fixed inputs for traditional rivalry. (B) Periodic 1.5 Hz square waves for swap only experiment. (C) Periodic 18 Hz square waves for flicker only experiment. (D) Periodic 1.5 Hz square waves modulated with 18 Hz on/off switches for the F&S experiment. (E) Periodic 1.5 Hz square waves with blank intervals (150 ms duration) inserted before swaps for the B&S experiment.

Where $k = 30$ defines the slope and $\theta = 0.05$ defines the threshold. This becomes particularly important when we want to follow the locus of torus bifurcations (T) in parameter plane. Further difficulties in following the locus of torus bifurcations were resolved by introducing a small parameter ($\epsilon = 0.001$) to break the $HL \leftrightarrow VR$ symmetry in the first ODE in Equation 1.1,

$$\tau \dot{E}_{HL} = -E_{HL} + \frac{100(J_{HL}(t) - gI_{VR})_+^2}{(10 + H_{HL} + \epsilon)^2 + (J_{HL}(t) - gI_{VR})_+^2}. \tag{3.7}$$

This removed a potential degeneracy in the torus bifurcation defining system that allowed for the computations to be completed. The numerical integration of the initial value problems were carried out in `MATLAB` using a fourth-order Runge-Kutta method with time step 0.1 ms. Numerical continuation was performed with the package `AUTO07p`, by and large using relatively standard constants, but notably increasing the mesh size (`NTST`) for the computation of periodic orbits in the forced cases and when the period became large (Doedel et al. 2007). Source code for the model is available in the GitHub repository farzaneh-darki/Darki2020-methods: https://github.com/farzaneh-darki/Darki2020-methods.

3.3. Results

3.3.1. Bifurcation analysis of traditional rivalry with fixed inputs.

Previously, three main types of dynamical behaviours were found in many models of rivalry with fixed inputs (including the Wilson model): Winner-take-all (WTA), Rivalry oscillations (RIV), Simultaneous activity (SIM). The bifurcation diagram with fixed inhi-

bition strength $g = 1.5$, and varying adaptation strength h, is presented in Figure 3.3A. A trivial symmetric equilibrium always exists, which is stable for large values of adaptation strength and corresponds to simultaneous activity (SIM) (Figure 3.3C). This equilibrium loses its stability with decreasing adaptation strength and a stable limit cycle emerges from a supercritical Hopf bifurcation (H). These relaxation oscillations correspond to rivalry (RIV). For h increasing from zero on the symmetric unstable branch, a pair of unstable fixed point branches emerge at a pitchfork bifurcation (PF) with the $E_1 = E_2$ symmetry broken. The complementary branches undergo fold bifurcations (L) nearby but remain unstable. These two unstable fixed point branches go through two supercritical Hopf bifurcations and become stable. These two stable equilibria create a bistable parameter range known as winner-take-all (WTA), which exists for small h. The qualitative transformation of the system from RIV to WTA remains unclear and must involve as yet undetermined bifurcations at changes in stability on the RIV branch (Figure 3.3B, green curve). Existence of multiple fixed points in the intermediate region of adaptation strength h separating WTA and RIV states is similar to the WTA bistability bifurcation structure in a two-dimensional dynamical system for visual perception (You et al. 2011). However, here we found the WTA branch becomes unstable at a Hopf bifurcation and the other remaining fixed points which appear and disappear through pitchfork and fold bifurcations are unstable (which is possible in a six-dimensional ODEs).

In this study, a more complete numerical bifurcation analysis has been carried out to find other stable solutions in the small parameter gap between the WTA and RIV (Figure 3.3B). As seen in Figure 3.4A, a pair of stable limit cycles emerge from two supercritical Hopf bifurcations (on upper and lower WTA branches) as adaptation strength is increased. These low-amplitude oscillations move around the top-most and bottom-most of the 5 equilibrium branches existing between PF and L. We call this dynamical behaviour low-amplitude-winner-take-all (LAWTA) since there is bistability like WTA behaviour; however, the stable states are oscillatory solutions with very small amplitude around asymmetric unstable equilibria (Figure 3.4A). By further increasing adaptation strength, a cascade of period-doubling bifurcations emerges from the LAWTA branch (Figure 3.4C). For example, one period of the original limit cycle emerging from a supercritical Hopf bifurcation looks like a sinusoidal signal with one peak and one trough. After the first period-doubling bifurcation (PD), one period of oscillations will have two peaks and two troughs with tiny differences between the peak and trough amplitudes. As seen in Figure 3.5, even after three PD bifurcations, the difference in amplitude between the 8 peaks remains small.

On the other side, the limit cycle emerging from the supercritical Hopf bifurcation (green branch labelled RIV in Figure 3.3A-B) becomes unstable as adaptation strength decreases; however, the continuation software does not detect any bifurcation where the stability changes. This appears to be a global bifurcation which is not detectable by local analysis. We will refer to this putative global bifurcation at the change in stability at the RIV branch as the global bifurcation. Without any specific bifurcation in hand, we cannot follow any emerging stable branch. To tackle this issue we compute the stable periodic solution (assuming one exists, using numerical integration) for a specific value of adaptation strength
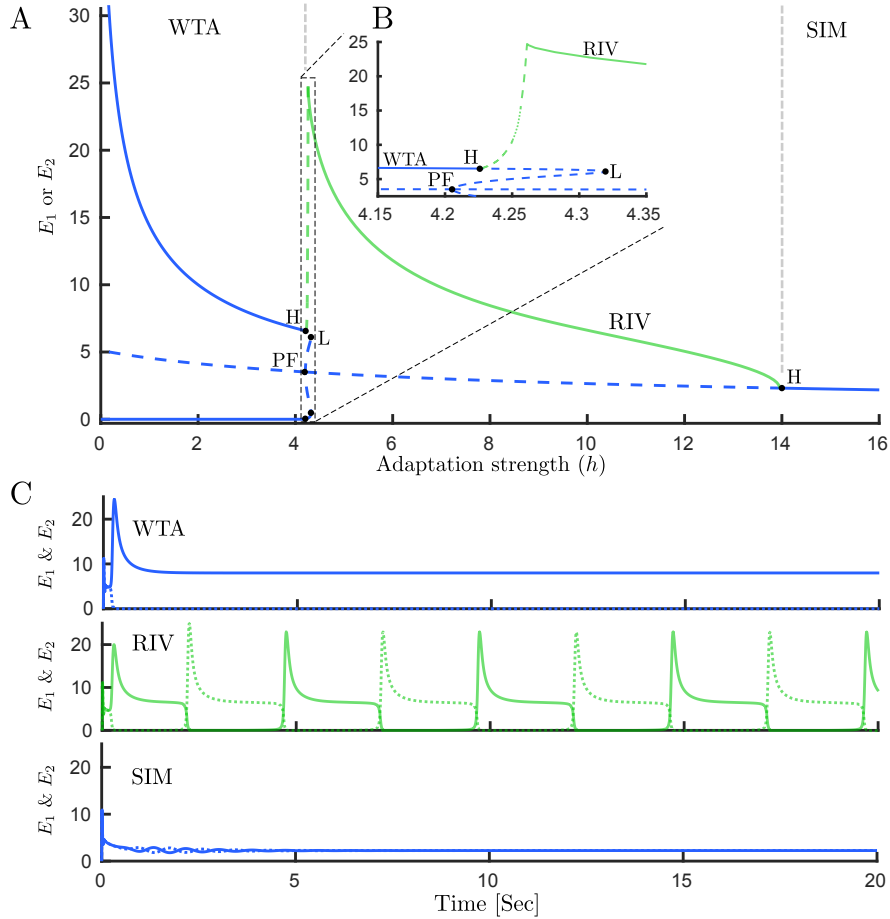
Figure 3.3. **Bifurcation analysis and time histories for traditional rivalry.** (A) Bifurcation diagram for the Wilson model (1) with fixed inputs varying adaptation strength h. Three main types of dynamical behaviours are presented: Winner-take-all (WTA), Rivalry oscillations (RIV), Simultaneous activity (SIM). Blue lines show fixed point branches and the green line shows the maximum of $E_1\&E_2$ on the limit cycle branch. The minimum of RIV branch oscillations is close to zero once away from Hopf bifurcation (not shown). (B) Details of the diagram are shown in a zoomed panel. The period of oscillations on the unstable limit cycle branch shown with green dashed lines increase sharply as we move toward a critical parameter value $h \approx 4.22843$ and continuation fails. The dotted green line shows the assumed location of a branch segment that proved difficult to compute due to the orbits having large period. The sequence of bifurcations that transform the system from WTA to RIV periodic solutions has not been described previously. (C) Time histories associated with each dynamical behaviour: WTA ($h = 1$), RIV ($h = 4.3$), SIM ($h = 15$). Other parameters: $g = 1.5$, $J_{HL} = J_{VR} = 10$.
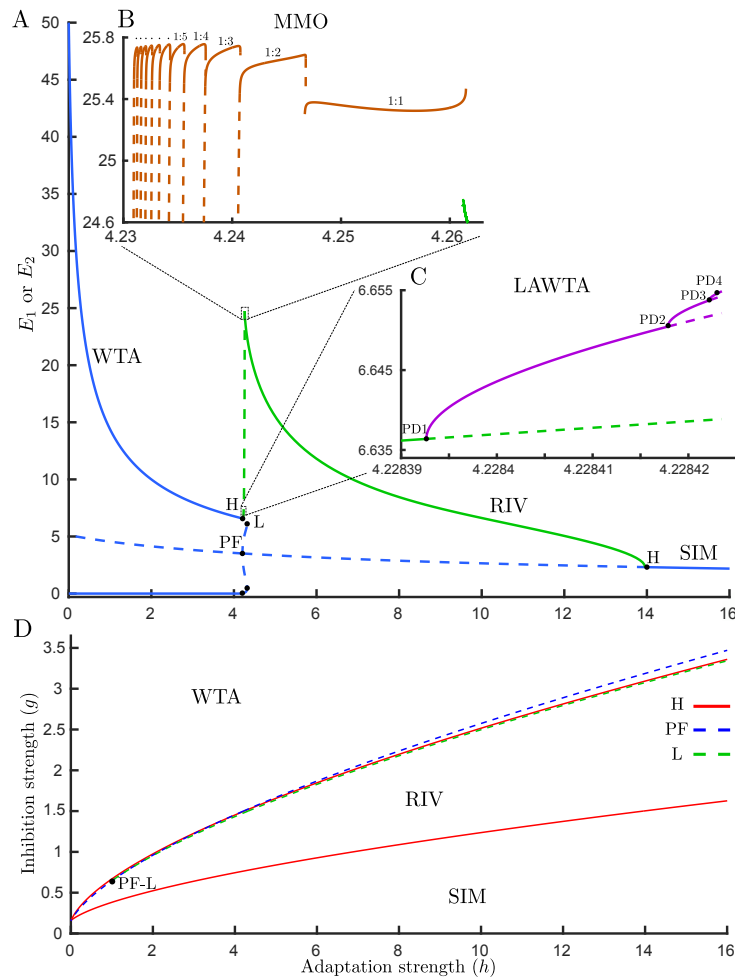
Figure 3.4. **Detailed bifurcation analysis for traditional rivalry.** (A) Bifurcation diagram of the Wilson model (1) with fixed inputs varying adaptation strength h. In addition to WTA, RIV, and SIM, two other regions with different dynamical behaviour are revealed: (B) Mixed-mode oscillations (MMOs) emerging from high amplitude relaxation oscillations (RIV) with discontinuous transitions between segments. Each period of these MMOs has one high and one or more low amplitude oscillations (see figure 6 for time histories). On MMO branches n:m defines n high to m low amplitude oscillations ratio. The number of low amplitude oscillations starts from one and is increased by one as we move down the bifurcation parameter. (C) Low amplitude winner-take-all (LAWTA) oscillations emerge from supercritical Hopf bifurcation on the WTA branch and by further increasing the bifurcation parameter, a cascade of period-doubling bifurcations emerges. Panels B and C show the maximum of $E_1 \& E_2$ on the limit cycle branches. The minimum of MMOs is close to zero. (D) Boundaries of different dynamical behaviours are shown in parameter space (h, g). The region with the periodic solution (RIV) is confined by Hopf bifurcation (red solid line) from beneath and by fold bifurcation (L, green dashed line) from above. Other parameters: $g = 1.5$, $J_{HL} = J_{VR} = 10$.
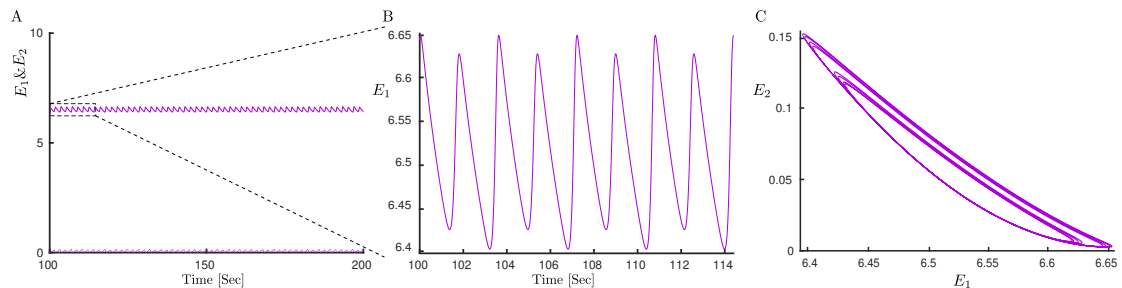
Figure 3.5. **LAWTA oscillations time histories for traditional rivalry.** (A) Time history of LAWTA oscillatory activity for two neural populations (solid and dashed lines correspondingly). (B) One period of LAWTA after PD3 in figure 4C. LAWTA has 8 different high and low peaks. (C) Limit cycle in $E_1 - E_2$ plane. Parameters: $h = 4.22842214$, $g = 1.5$, $J_{HL} = J_{VR} = 10$.

(in a range between last PD and the change in stability on the RIV branch) and then follow any periodic solution branch using numerical continuation. On the right side of the global bifurcation, time simulations show relaxation oscillations that reach high amplitude rapidly before relaxing to baseline (Figure 3.6B). However, on the left side of the change in stability (close to the global bifurcation), we observe that in addition to high amplitude oscillations, one low amplitude oscillations appears (Figure 3.6C). By further decreasing adaptation strength, there is always one high amplitude oscillation, but the number of low amplitude oscillations increase (Figure 3.6C-F). The period of these oscillations increase sharply as we move toward a critical parameter value $h \approx 4.22843$ (Figure 3.6A). This complex behaviour is known as mixed-mode oscillations (MMOs) since it is a mixture of low and high amplitude oscillations. Using the approach described above we could complete stable branches on the left side of global bifurcation (Figure 3.4B). Interestingly, stable solutions occur through a series of discrete branches. The discontinuous transitions from one branch segment to the next are similar to the spike adding mechanism from (Nowacki et al. 2012). The bifurcation structure here appears similar to the canard induced MMOs identified in a spiking neuron model (Ermentrout and Wechselberger 2009). The sharp increase in amplitude of the limit cycle branch over a short parameter range emerging near the critical value of h (Figure 3.6 caption) suggests the complex behaviour in this region is also associated with canards. Bifurcation analysis of another simple rivalry model with 4 ODEs and different nonlinearity revealed a similar structure for MMOs through the interaction of canards and a singular Hopf point (Curtu and Rubin 2011). Whilst, there are some similarities with the MMOs found in the present study, a more rigorous approach would be needed to say whether these MMOs are canard-induced, Hopf-induced, or result from an interaction of both mechanisms. The global bifurcation and the transitions between MMO branches remain to be determined. The behaviours reported here are confined to a narrow region of the (g, h) parameter plane near the left-hand locus of Hopf bifurcation (Figure 3.4D).

Here, a more complete analysis has revealed MMOs emerge from high amplitude RIV oscillations (Figure 3.4B) and a cascade of period-doubling bifurcations emerge from LAWTA oscillations (Figure 3.4C) which have not been reported before in the Wilson model. This analysis describes the mechanism of state transition from WTA to RIV which was not clear before. Whilst MMOs have been reported in another model of rivalry (Curtu and Rubin 2011; Curtu 2010), the appearance of a stable PD cascade has revealed richer dynamics in the Wilson model which may also play a part in the mechanisms that lead to appearance and disappearance of limit cycles associated with MMOs. An interesting avenue of investigation will be to understand how the low-amplitude PD cascade (Figure 3.4C) interacts with periodic forcing. This provides the context to fully understand the periodically forced case.
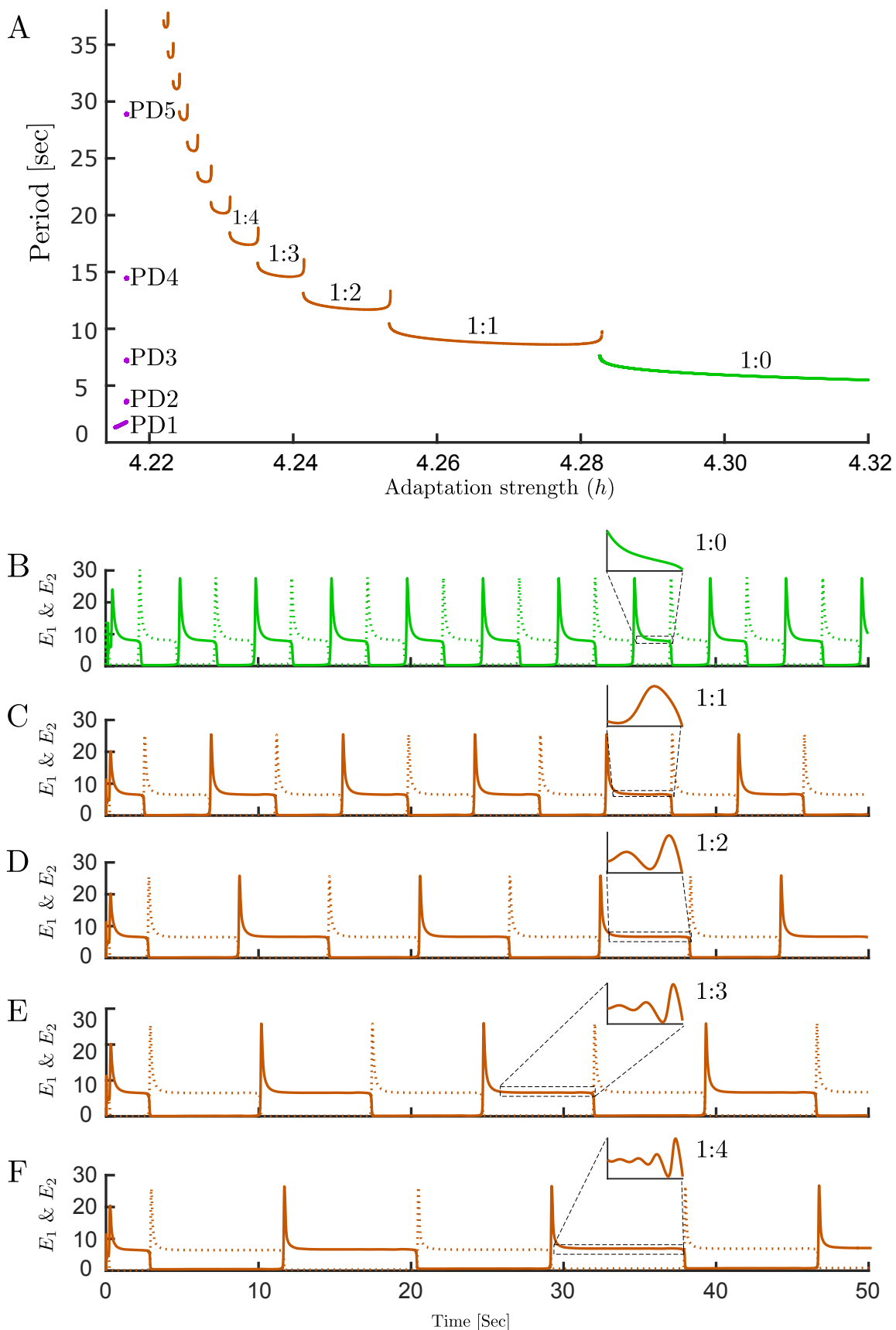
Figure 3.6. **Periods of oscillatory states and MMOs time histories for traditional rivalry.** (A) Periods of oscillations for three types of oscillatory dynamics: LAWTA (purple), MMOs (brown) and rivalry oscillations (green). The period of oscillations increase sharply as we move toward a critical parameter value $h \approx 4.22843$ from either side. (B)-(F) Time histories associate with different branch segments of MMOs with different adaptation strength in each panel. Number of low amplitude oscillations increases as adaptation strength is decreased: (B) RIV ($h = 4.3$) (C) One ($h = 4.26$) (D) two ($h = 4.243$) (E) three ($h = 4.24$) (F) four ($h = 4.237$) low amplitude oscillations in one period. On MMOs branches n:m defines n high to m low amplitude oscillations ratio. Other parameters: $g = 1.5$, $J_{HL} = J_{VR} = 10$.

3.3.2. Bifurcation analysis of binocular rivalry with periodic forcing.

Flicker (18 Hz) only

Bifurcation analysis with the flickering stimulus shows that periodic forcing with high frequency (e.g. 18 Hz) modulates the three main types of behaviours that occur with fixed inputs. Instead of WTA and SIM fixed point branches in traditional rivalry with fixed stimulus (Figure 3.3A), modulated WTA (WTA-Mod) and modulated SIM (SIM-Mod) periodic solution branches are found with the flickering stimulus (Figure 3.7A). Subsequently, the SIM-Mod branch undergoes a torus bifurcation (T) giving rise to a torus branch with periodic oscillations corresponding to modulated slow rivalry alternations (RIV-Mod). Following the torus bifurcation in the (g, h) parameter plane defines the boundary of rivalry oscillations (Figure 3.7B). The locus of a pitchfork bifurcation (BP) remains close to the left-hand torus curve (Figure 3.7B, not shown). It appears that the MMO branches and PD cascade identified for fixed inputs disappear with the introduction of flicker. This analysis found evidence that slow rivalry alternations RIV-Mod can exist at parameter values adjacent to regions where stimulus-induced oscillations exist (SIM-Mod). Time histories of these dynamical behaviours are shown in (Figure 3.7C). These results are consistent with experiments: Flicker stimuli do not differ from the traditional rivalry case (Lee and Blake 1999).

Swap (1.5 Hz) only

The dynamical behaviour with low frequency periodic forcing (around 1.5 Hz, so-called swap) is different, and in addition to WTA-Mod behaviour (for small values of adaptation strength) and SIM-Mod (for large values of adaptation strength), cycle skipping occurs through a PD bifurcation on the SIM-Mod branch (Figure 3.8A). Cycle skipping refers to the response of each competing population to every other stimulus onset. This means two populations respond in turn to stimulus cycles and while one has high activity during a cycle the other one stays inactive (Figure 3.9A). We note that the period of the period-doubled solution is 1.333 s and is plausibly the result of a resonance with the fixed-input limit-cycle, which has a period > 2 s, for larger values of h (Shpiro et al. 2007). SIM-Mod and cycle skipping have been reported in a simpler model of rivalry (Jayasuriya and Kilpatrick 2012) and via direct simulations of the Wilson model in (Li et al. 2017).

As seen in (Figure 3.8B-C), the cycle skipping branch loses stability at a fold bifurcation (L) for decreasing h. For h increasing, branching off from the PD point on the WTA-mod branch leads to a cascade of PD bifurcations (Figure 3.8D). In order to find the possible stable periodic branches between the last PD and the fold bifurcation, we compute the stable periodic solution (assuming it exists) using numerical integration for a specific value of adaptation strength, and then start continuation from this solution. With this approach, we found a family of discontinuous branches, which correspond to multi-cycle skipping (Figure 3.8C). On these branches, the number of stimulus cycles between switches of activity from one population to the other is variable and increases by one as the bifurcation parameter decreases (Figure 3.9A-E). Here we found a small region of bistability between the one cycle skipping and two cycle skipping behaviours (at around $h = 0.05$
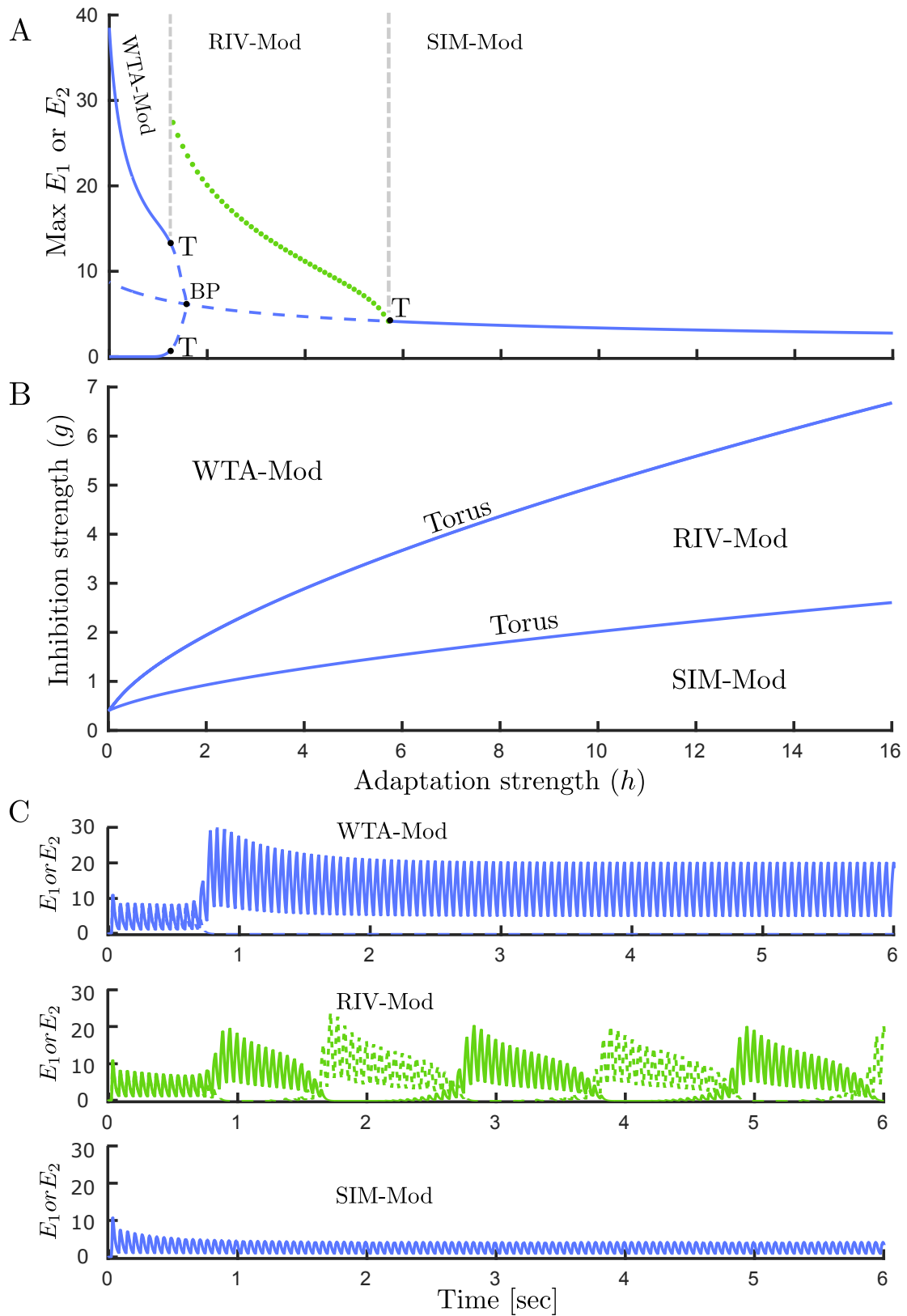
Figure 3.7. **Bifurcation analysis and time histories for flicker only case.** (A) Bifurcation diagram for the Wilson model (1) with high frequency periodic forcing (flicker; 18Hz) varying adaptation strength h, $g = 1.5$. Three main types of dynamical behaviours are modulated by forcing frequency: 1) Modulated WTA (WTA-Mod), 2) Modulated rivalry (RIV-Mod), 3) Modulated SIM (SIM-Mod). RIV-Mod branch which occurs through supercritical torus bifurcation (T), is associated with slow rivalry alternations. Solid curve: stable limit cycle, dashed curve: unstable limit cycle, filled circles: attracting torus. (B) Boundaries of different dynamical behaviour with high frequency periodic forcing (flicker 18Hz) are shown in parameter space (h, g). The region with RIV-Mod solution is confined by torus bifurcation. (C) Firing activity of each competing population E_1 (solid lines) and E_2 (dashed lines) with high frequency periodic forcing; flicker 18Hz and different adaptation strength h: WTA-Mod regime with $h = 0.5$, RIV-Mod regime with $h = 2$, SIM-Mod regime with $h = 6$. Other parameters: $[J_{HL}]_{max} = [J_{VR}]_{max} = 10$.
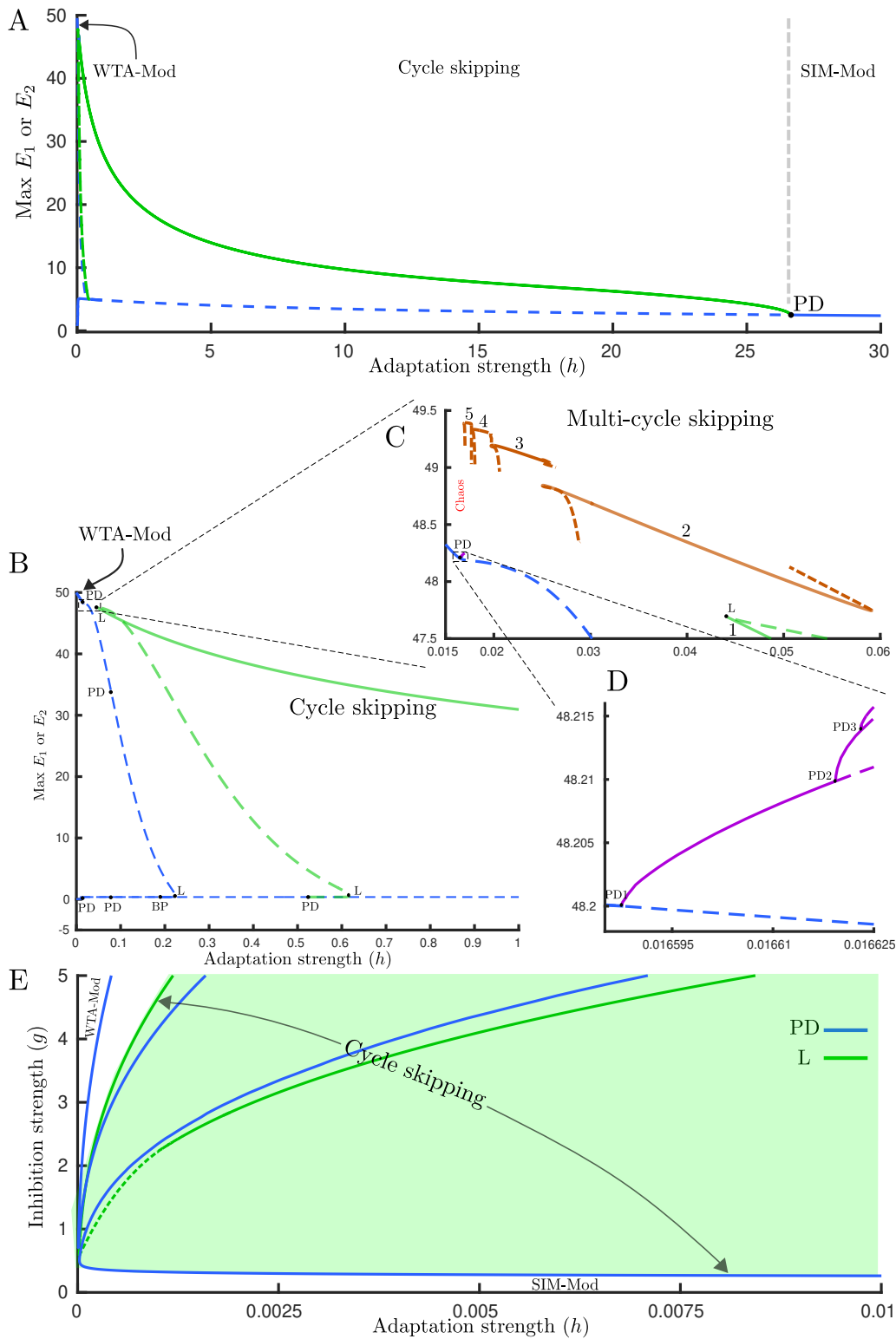
Figure 3.8. **Bifurcation analysis for swap only case.** (A) Bifurcation diagram for the Wilson model (1) with low frequency periodic forcing (swap; 1.5Hz) varying adaptation strength h, $g = 1.5$. Dynamical behaviour for large values of adaptation strength is modulated SIM (SIM-Mod). Cycle skipping behaviour appears through period-doubling bifurcation (PD) in which every population only responds to every other stimulus onset in turn. There also exists a pair of stable limit cycles for very small values of adaptation strength which corresponds to modulated WTA (WTA-Mod). Solid curve: stable limit cycle, dashed curve: unstable limit cycle. (B) Detailed bifurcation diagram for the Wilson model with low frequency periodic forcing (swap; 1.5Hz) varying adaptation strength h, $g = 25$. (C) Multi-cycle skipping occurs through discontinuous branches. The number of cycles skipped between switches increases by one as we move left from each branch segment to the next. (D) A cascade of period-doubling bifurcations which leads to chaos. In panels C and D, the ordinate shows maximum of E_1&E_2. (E) Boundaries of different dynamical behaviours with low frequency periodic forcing (swap 1.5Hz) are shown in parameter space (h, g). The region with the cycle skipping solution is confined by period-doubling (PD) bifurcations from beneath and by fold bifurcation from above (marked with arrows). Other parameters: $[J_{HL}]_{max} = [J_{VR}]_{max} = 10$.
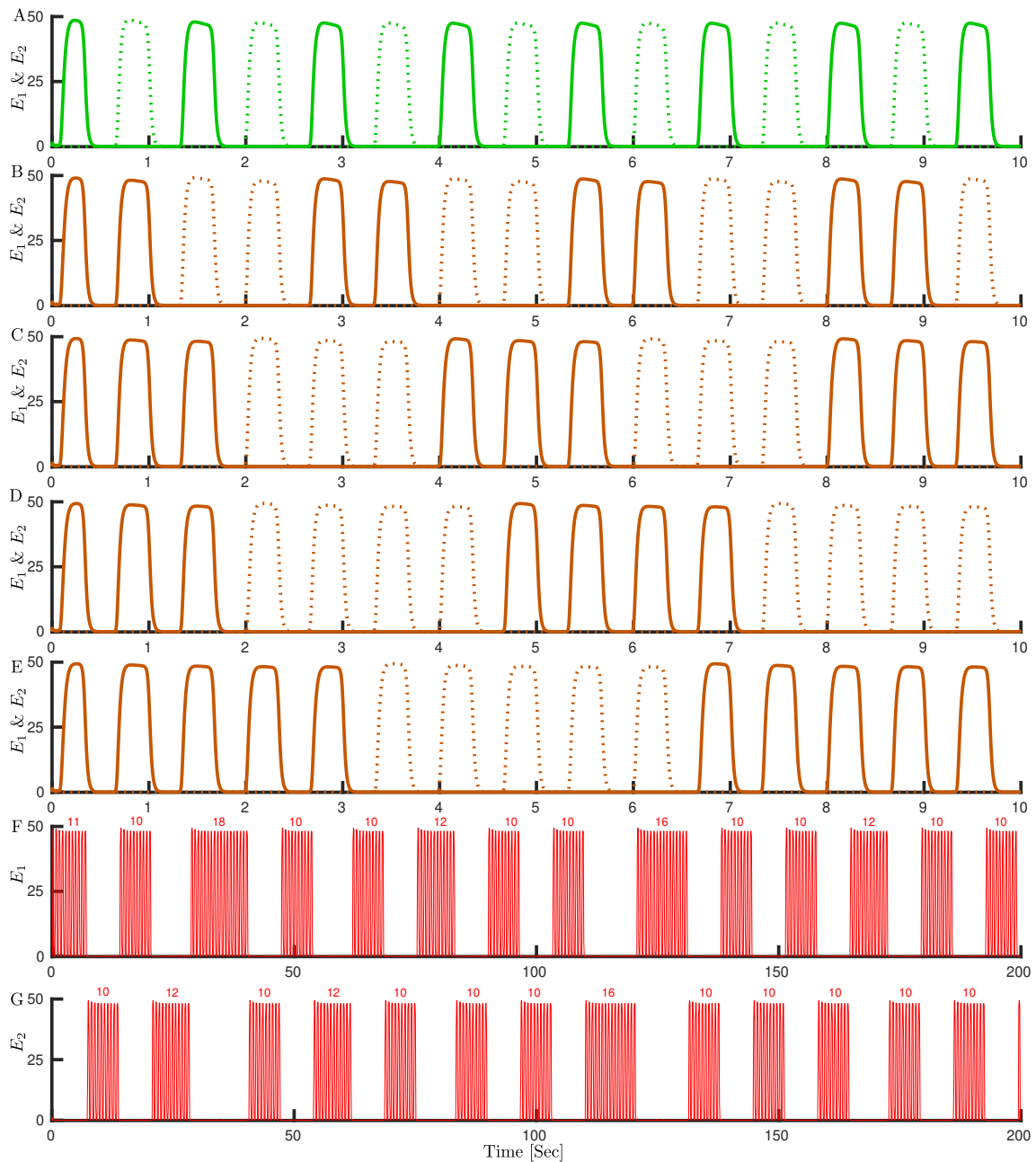
Figure 3.9. **Cycle skipping, multi-cycle skiping and chaos time histories for Swap only case.** Firing activity of each competing population E_1 (solid lines) and E_2 (dashed lines) with low frequency periodic forcing; swap 1.5Hz and different adaptation strength h. (A) Cycle skipping regime with $h = 1$. (B-E) Multi-cycle skipping regime with variable number of cycles to respond and skip between switches. (B) $h = 0.03$, (C) $h = 0.02$, (D) $h = 0.0185$, (E) $h = 0.017$. Chaotic firing activity of (F) E_1 and (G) E_2 with irregular number of cycles to respond or skip between switches, $h = 0.01663$. Other parameters: $g = 25$, $[J_{HL}]_{max} = [J_{VR}]_{max} = 10$.

in Figure 3.8C). Therefore, in the full hierarchical model it would be possible to find an asymmetric solution where the HL-VR units at the first stage behave differently. However, as explained in the discussion the model normally operates close to the SIM-Mod region, which is far away from the cycle skipping region with bistability in the parameter space.

Another interesting behaviour is the appearance of a chaotic attractor in a parameter range between the PD cascade and multi-cycle skipping family branches (Figure 3.8C). Figure 3.9F-G represents chaotic firing activity for each population in a 200 s simulation. The number of cycles between switches does not show any regular or repeating pattern.

Flicker (18 Hz) & (1.5 Hz) Swap

The bifurcation structure with both high frequency flicker and low frequency swap appears to be analogous to bifurcation structure with swap only case (Figure 3.10A–B). However, the right-hand PD bifurcation point in the transition from cycle skipping to SIM-Mod moves down in adaptation strength. This is shown in a direct comparison of two-parameter bifurcation diagrams for the F&S and swap only cases in (Figure 3.11A). In fact, with the same values of adaptation strength that we might expect cycle skipping from swap only case, with F&S stimulus we can get SIM-mod, which turns out to be critical for obtaining slow alternations, see discussion.

Blanks (150 ms) & (1.5 Hz) Swap

Our result shows that the effect of blank insertion before swap times, similar to the effect of adding flicker to swap stimuli, moves the PD bifurcation point down the bifurcation parameter (Figure 3.11B), but to a much lesser extent than the introduction of flicker, compare Figure 3.11A and B.

3.4. Discussion

3.4.1. Summary

Earlier work with models of bistable perception has identified parameter ranges with winner-take-all dynamics (WTA), rivalry oscillations (RIV) and simultaneous activity (SIM) (Shpiro et al. 2009; Seely and Chow 2011). Such regimes are known for the Wilson model as input strength is increased (Shpiro et al. 2007). Our results show that the Wilson model with fixed inputs is capable of generating complex dynamical behaviours such as MMOs and LAWTA oscillations, previously not reported. We have also built a framework for studying rivalry models with periodic inputs using numerical continuation. Given symmetry between orientations (0° & 90°) and eyes (L & R), and the feed-forward structure of the hierarchical Wilson model, it is sufficient to study one pair of units in the monocular layer. We found that periodic forcing with high frequency (e.g. 18 Hz, known as flicker) modulates the three main types of behaviours that occur with fixed inputs with forcing frequency (WTA-Mod, RIV-Mod, SIM-Mod). However, the dynamical behaviour changes with low frequency periodic forcing (around 1.5Hz, so-called swap), and in addition to
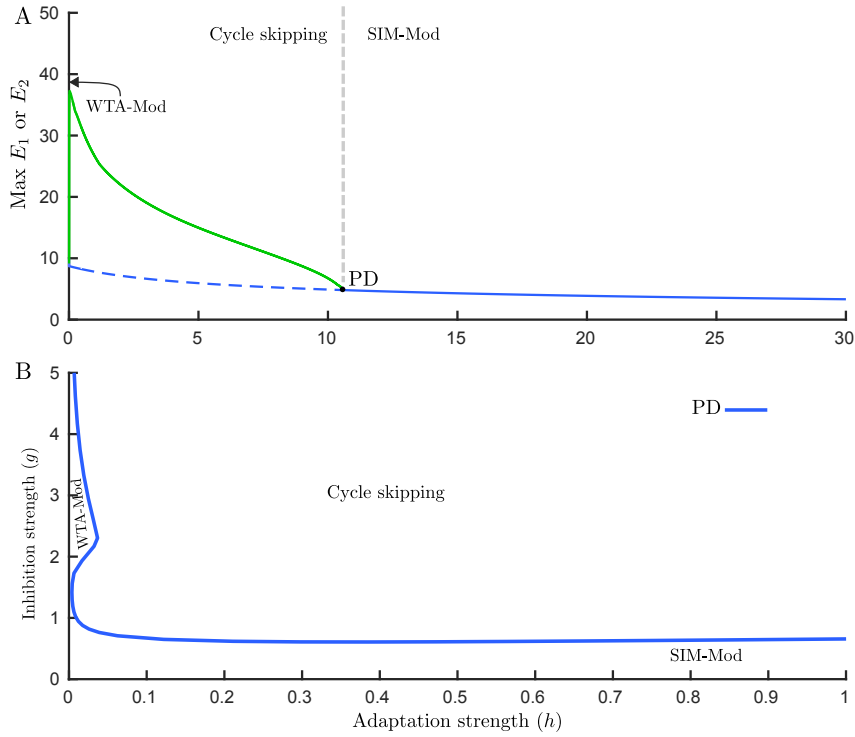
Figure 3.10. **Bifurcation analysis for F&S rivalry. (A)** Bifurcation diagram for the Wilson model (1) with high frequency flickering (18Hz) and low frequency swap (1.5Hz) varying adaptation strength h, $g = 1.5$. Dynamical behaviour for large values of adaptation strength is modulated SIM (SIM-Mod). Cycle skipping behaviour appears through period-doubling bifurcation (PD) in which every population only responds to every other stimulus onset in turn. There also exists a pair of stable limit cycles for very small values of adaptation strength which corresponds to modulated WTA (WTA-Mod), not visible at this scale. Solid curve: stable limit cycle, dashed curve: unstable limit cycle. **(B)** Boundaries of different dynamical behaviours are shown in parameter space (h, g). The region with cycle skipping solution is confined by period-doubling (PD) bifurcations. Other parameters: $[J_{HL}]_{max} = [J_{VR}]_{max} = 10$.
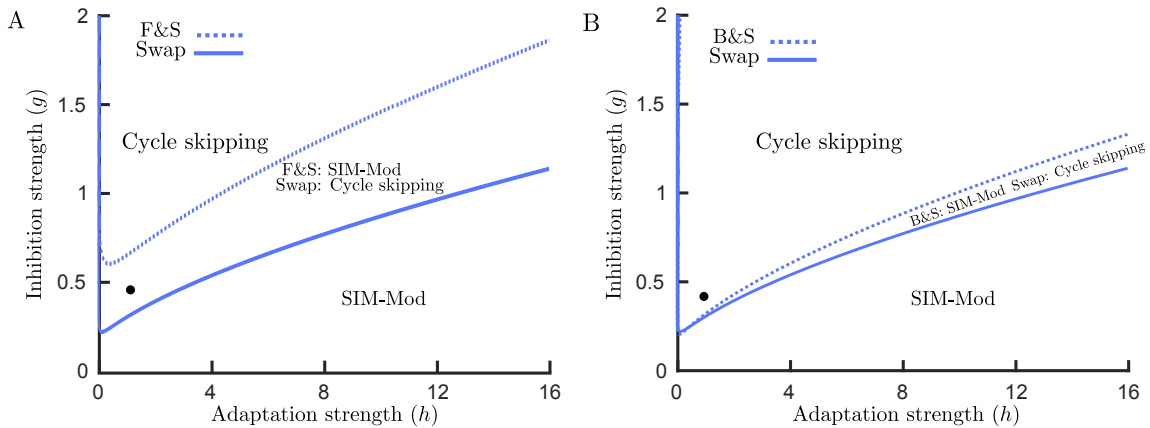
Figure 3.11. **Why does the Wilson model produce slow alternations with the F&S ,but not with Swap only and B&S stimuli?** Two parameter bifurcation diagram for the Wilson model (1) which defines regions with different dynamical behaviours. Blue curves show PD bifurcation and boundary for cycle skipping behaviour. Below this curve the dynamical behaviour is SIM-Mod. The black dot defines the point where the Wilson model operates at. **(A) Comparison of swap and F&S cases.** As seen, for swap only stimuli the monocular layer operates at cycle skipping regime; however, for F&S stimuli it operates at SIM-Mod. The binocular layer for F&S stimuli is effectively stimulated with flickering stimuli and by selecting the current inhibition strength it is possible to get slow rivalry alternations in the second layer. **(B) Comparison of swap and B&S cases.** Inserting blanks (with 150 ms durations) before swap times, like adding flicker, moves the boundary between Cycle skipping and SIM-Mod regions up in the parameter plane (but to a lesser extent) and the likelihood of being in the SIM-Mod region increases.

WTA-Mod and SIM-Mod, cycle skipping and multi-cycle skipping behaviour exist which can lead to chaotic dynamics. Cycle skipping behaviour with swap stimuli (1.5 Hz fast alternations) is not consistent with experiments (Lee and Blake 1999; Blake et al. 1980), where we expect slow rivalry alternation (duration around 2 s). In order to understand the dynamics of the full hierarchical model with periodic forcing, we should consider that the inputs for the second layer of the Wilson model are the responses of populations selective to the same orientation from the first monocular layer (fFigure 3.1A). For example, if the isolated subunits in the first layer are in the SIM-Mod regime (Figure 3.11A), the stimuli for the second layer will look like a fixed stimulus to the second layer (where SIM-Mod occurs in the first layer for the Swap only stimulus) or a flickering stimulus (where SIM-Mod occurs in the first layer for the F&S stimulus). This means the second layer is effectively stimulated with traditional or flickering stimuli and by selecting the current inhibition strength it is possible to get slow rivalry alternations in the second layer. This provides a deeper explanation of how the Wilson model produces slow alternations with the F&S (but not Swap only stimulus).

3.4.2. Rivalry model complexity & comparison with other models

There are other computational models that can capture properties of perceptual dominance durations in both types of experiments (traditional experiments and F&S experiments) (Brascamp et al. 2013; Li et al. 2017). Brascamp's model, with less complexity than Wilson's, has only one layer of monocular units with the extension of inhibition to within-eye and cross-eye iso-orientation connections (Baker et al. 2007; Moradi and Heeger 2009). The model proposed by Brascamp et al. correctly reflects the fluctuations in monocular neurons; however, their model generates slow alternations only when the blank intervals before swaps are short. The Li et al. model (Li et al. 2017) with another layer of attentional modulations (in addition to monocular and binocular layers) is the most sophisticated binocular rivalry model, accounting for a wide range of phenomena but with greatly increased complexity (14 ODEs).

MMOs have already been reported in a simpler rivalry model with 4 ODEs (without an inhibition equation in each subunit) through interactions of singular Hopf and canard (Curtu and Rubin 2011; Curtu 2010). However, the LAWTA regime emerging through a PD cascade has not been reported before. The question arises as to whether there is a distinct mechanism (from say (Curtu and Rubin 2011; Curtu 2010)) specific in the Wilson model that leads to similar MMO dynamics. We found that by assuming instantaneous inhibition dynamics ($\tau_I \to 0$ in Equation 1.1) in the Wilson model, all of the complex behaviours with traditional stimuli still persist (Figure 3.12). Thus any differences to the bifurcation structure across different models are likely due to the differences in the nonlinearity processing inputs to each unit. In the Wilson model the Hopf bifurcation is supercritical (subcritical in (Curtu and Rubin 2011)) and stable branches emerging in a PD cascade appear to terminate (lose stability) at the h-value where MMOs first emerge. The large increase in period and the large excursion in phase space required to jump from the PD branch to the full-amplitude MMO branches at a critical value of h are consistent with a canard mechanism, but more exotic than reported previously. Indeed, further analysis
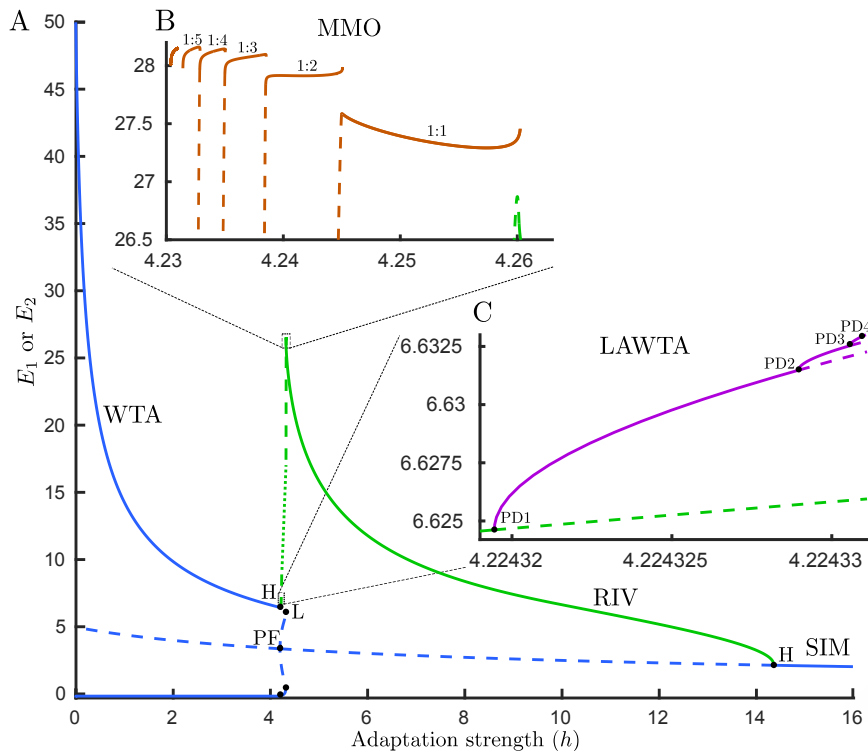
Figure 3.12. (A) Detailed bifurcation diagram of the reduced Wilson model (instantaneous inhibition dynamics, $\tau_I \to 0$ in Equation 1.1) with fixed inputs varying adaptation strength h, $g = 1.5$. The dotted green line shows the assumed location of a branch segment that proved difficult to compute due to the orbits having large period. All complex dynamical behaviours still persist: (B) Mixed-mode oscillations (MMOs) with discontinuous transitions between segments. On MMO branches n:m defines n high to m low amplitude oscillations ratio. The number of low amplitude oscillations starts from one and is increased by one as we move down the bifurcation parameter. (C) Low amplitude winner-take-all (LAWTA) oscillations emerge from Hopf bifurcation on the WTA branch and by further increasing the bifurcation parameter, a cascade of period-doubling bifurcations emerges. Panels B and C show the maximum of $E_1 \& E_2$ on the limit cycle branches.

would be needed to resolve how the PD cascade terminates and the MMO branches emerge through a common mechanism.

3.4.3. Limitations of the Wilson model

As discussed in (Brascamp et al. 2013; Li et al. 2017), the Wilson model is only capable of generating slow perceptual alternations with the F&S stimulus, and it fails to do so with blank intervals inserted before each swap, so-called Blank & Swap (B&S) (van Boxtel et al. 2008; Denison and Silver 2012). Our results show that blank insertion similar to a flickering stimulus moves the boundaries up in adaptation-inhibition strength plane (Figure 3.11B), but to a lesser change than F&S. In order to be in the SIM-Mod area, which as discussed before is necessary for slow rivalry alternations at the second stage, adaptation strength needs to be increased or inhibition strength decreased. On the other hand, the existence of cycle skipping behaviour with swap stimuli leads to perceptual alternation with a frequency half of the swap rate at the second stage (Li et al. 2017), which to our knowledge is not consistent with empirical results (Blake et al. 1980; Lee and Blake 1999). This reported limitation of the Wilson model could simply be avoided if the parameters had been set in a way that the model operated in the SIM-Mod regime. Our

result casts a new light on binocular rivalry with periodic forcing and it is now clear that these two limitations of the Wilson model could be fixed by tuning model parameters.

3.4.4. Implications for experiments

Even though we showed that model parameters can be tuned for consistent behaviour with experimental results, our results also predict apparently spurious dynamical behaviours such as cycle skipping with swap stimuli at the monocular level that has not been reported by experimental work. It is possible that this behaviour (a 1.5 Hz fast alternation) was not distinguishable from 3 Hz fast alternation in perceptual reports. Future empirical studies could investigate the existence of such behaviour at the early stages of visual processing with monocular contributions and at later stages, i.e. higher cortical layers where the activity would propagate.

3.4.5. Future work

Levelt's propositions (Levelt 1965) with traditional rivalry are well known. However, they have not been investigated with F&S stimuli in any of the existing models of rivalry. It has been shown in experiments (Logothetis et al. 1996) that Levelt's proposition II holds with F&S stimuli (whilst to our knowledge Levelt's proposition IV has yet to be investigated). By implementation of these forcing cases with numerical continuation we now have the tools to determine constraints on models such that they are consistent Levelt's propositions with periodic forcing (Wilson 2003).

The PD cascade found in the traditional rivalry case suggests the existence of chaotic dynamics in a small range of parameter between PD cascade and MMOs branches. This could be checked by computing Lyapunov exponents for a continuous-time dynamical system. Note that these low amplitude oscillations (LAWTA) appear to interact with periodic forcing to produce chaotic dynamics at high amplitude (Figure 3.9).

Taking the unforced system and adding periodic inputs we might expect the fine structure from the traditional rivalry case to be washed out. This is true in e.g. the flicker case. However, we find in the swap case that the periodic forcing does interact with the deterministic dynamics to produce a family for cycle skipping branches and chaotic dynamics. Noise plays an important role in rivalry, and this is often considered in models (Shpiro et al. 2009). It remains outside the scope of the current work to explore whether the regions of exotic dynamics found in the traditional case and in the swap case would be washed out by the inclusion of noise. Nevertheless, the introduction of noise to timescale-separated dynamical systems (like the Wilson model) can introduce dynamics not present in the deterministic case, especially local to bifurcations (Berglund and Gentz 2008). Interactions between noise and the dynamics may modify the exotic dynamics reported here in an interesting way, and could expand the parameter regions where these states persist.

Our approach for studying perceptual bistability with periodic stimuli is applicable for a range of other stimuli including auditory streaming (Rankin et al. 2015), motion illusions (Vattikuti et al. 2016), haptic bistability (Carter et al. 2013), and also for studying

stochastic resonance and entrainment phenomena in binocular rivalry (Kim et al. 2006) and in auditory streaming (Byrne et al. 2019).

3.4.6. Conclusions

The main conclusions of this work are drawn together and presented here. First, the results of our study show that the transition from slow rivalry alternation to the WTA regime is much more complicated than previously reported. As shown in Shpiro et al. (Shpiro et al. 2009), the stochastic characteristic of the dominance durations in the presence of noise are best described near this boundary (transition from RIV to WTA). It would be of interest to see how these complex dynamics (MMOs & LAWTA) will interact with noise. Further analysis is needed to check whether these dynamical regimes persist or are modified in the presence of noise.

Second, several competition models have been proposed to describe binocular rivalry with periodic stimuli, however, interpretation of results from these models are based on a specific set of parameters. Here we introduced a method to assess whether the existing models of binocular rivalry are valid or not in a specific parameter regime and, more generally, to find the parameter regions where these models work. This research provides a framework for either assessing binocular rivalry models for consistency with empirical results, or for better understanding neural dynamics and the mechanisms necessary to implement a minimal binocular rivalry model.

4. Perceptual rivalry with vibrotactile stimuli

4.1. Introduction

Multistable perception occurs when sensory information is ambiguous and consistent with two or more perceptual states. In this phenomenon, perception alternates intermittently between two (bistable) or more (multistable) interpretations of the fixed stimulus (Sterzer et al. 2009). Examples of multistable perception are well known in vision such as motion direction with plaids (ambiguous barber poles) (Hupé and Rubin 2003; Wuerger et al. 1996), apparent motion (Meso et al. 2016; Ramachandran and Anstis 1983), the Necker cube (Toppino 2003), and binocular rivalry (Blake 1989), and span across other sensory modalities including audition (Pressnitzer and Hupé 2006) and olfaction (Zhou and Chen 2009). All of these multistable phenomena share common features, such as exclusivity of perceptual interpretations, randomness, inevitability of alternations, independence of perceptual phases (Lathrop 1966; Fox and Herrmann 1967), and Levelt's propositions (Levelt 1965; Leopold and Logothetis 1999). These similar characteristics give rise to the conclusion that perceptual ambiguity must have a common neural basis and is likely resolved at a higher level of cognition that is not specific to individual sensory modalities (Pressnitzer and Hupé 2006; Logothetis et al. 1996; Wolfe 1996). However, a more recent study suggests that perceptual switching arises from a distributed system of similar but independent processes (Denham et al. 2018). As far as we know, these theories have been limited to the visual or auditory domains, and no previous research has investigated the possible outcomes with tactile stimuli.

Many of the early studies of tactile perception were focused on investigating the existence of tactual equivalents of apparent motion illusions. These kind of illusory experiments were generally extensions of known illusions from vision (Lederman and Klatzky 2009). In visual experiments, two spatially separated lights flash on and off in turn and can produce the illusion of movement (also known as phi phenomenon or beta movement). A tactile variant of smooth apparent motion was first produced with stimulation of two vibrotactile bursts of 150 Hz presented sequentially on the skin (Boring 1942; Sherrick and Rogers 1966). Observers typically report that the series of discrete tactile vibrations feel like vibratory stimulation moving across the skin (Burtt 1917; Kirman 1974; Lederman and Jones 2011; Burtt 1917). Various stimulus parameters such as the inter-stimulus onset interval (ISOI) and stimulus duration (from 25 to 400 ms) have been studied to find the optimal ranges for the induction of smooth apparent movement (Sherrick and Rogers 1966). Apparent motion can also happen with a bilateral stimulus delivered to each arm,

however, the movement is less robust than the movement reported when stimulation is delivered to a unilateral limb such as a single thigh or a single arm (Sherrick 1968). These observations from illusory experiments provide insight into mechanisms leading to perceptual alternations (bistability) with tactile stimuli.

Tactile pulses separated in location and time can induce a sensation of movement. For more complicated patterns, where different directions of movement are consistent with pulses, perception can be bistable. The first example of an apparent motion stimulus that leads to perception of motion in different directions is the "apparent motion quartet" stimulus realized in both the visual and tactile domains (Carter et al. 2008). In different studies, pairs of vibrotactile stimuli were attached to the tip of a participant's index finger (Carter et al. 2008), at locations on both index fingers (Conrad et al. 2012), to the thumbs and index fingers (Haladjian et al. 2020), or to both forearms (Liaci et al. 2016). The position of each consecutive stimulus pair alternated between the opposing diagonal corners of an imaginary rectangle which leads to switches between the perception of motion travelling either horizontally or vertically (Figure 4.1A). The proximity of stimulus pairs is the strongest contributor to the direction in which apparent motion is perceived, with motion more likely to be experienced between closer stimulus pairs than more distant ones (Gengerelli 1948).

There are numerous stimulus examples for perceptual ambiguity that show similar properties across sensory modalities and across different paradigms within the same sensory modality. Levelt's propositions have been broadly used to describe perceptual rivalry in the visual (Moreno-Bote et al. 2010; Brascamp et al. 2015) and auditory (Rankin et al. 2015) domains. For example, the generalization of Levelt's proposition II states that increasing the difference between percept strengths increases the mean perceptual dominance of the stronger percepts (Levelt 1965). Despite mean dominance times varying widely in multistable experiment, across different observers and stimulus contrasts (Zhou et al. 2004; Brascamp et al. 2005), the distribution of perceptual phases maintains a constant shape (gamma-like distribution) (Blake et al. 1980; Cao et al. 2016; Denham et al. 2018). Previous studies in vision suggested that the durations of successive perceptual phases are statistically independent (insignificant correlation) (Logothetis et al. 1996; Pressnitzer and Hupé 2006), however, recent studies of binocular rivalry (van Ee 2009; Cao et al. 2021) revealed positive correlations for perceptual phases that were one phase apart (between different percepts). Auditory streaming experiments also show positive correlations for durations separated by one phase and negative correlations for durations that are two phases apart (between same percepts) (Barniv and Nelken 2015). To the best of our knowledge, no previous research has investigated these stochastic properties of perceptual rivalry in tactile modality.

Levelt's propositions and other common characteristics in multistable perception have yet to be explored with tactile stimuli. We hypothesize that Levelt's propositions will extend to tactile rivalry appropriately chosen stimulus parameter manipulations. Here we present a new ambiguous tactile stimulus paradigm, similar to beta motion from vision, presented at only two locations on the skin but still capable of producing tactile bistability during minutes-long trials. Whilst beta motion in vision results from a fixed intensity

Table 4.1. Two-way repeated measure ANOVA of mean duration of **both percept types (AM, SIM)** with respect to intensity difference (ΔI) and percept type for the preliminary experiment. Analysis shows a significant effect of percept and also ΔI on the mean durations.

Source	df_{num}	df_{den}	F	p	$\eta_p{}^2$
(Intercept)	1	35	210.13	$< .001$	
percept	1	35	41.50	$< .001$	$.25 \pm .08$
ΔI	2	70	15.74	$< .001$	$.09 \pm .06$
ΔI:percept	2	70	67.92	$< .001$	$.37 \pm .07$

(contrast) moving dot, the stimulus presented here involves alternating changes in intensity (vibration amplitude) at the locations on each index finger. Two different perceptual interpretations can arise that compete for dominance over time. Because of the simplicity of this tactile stimulus, it is well suited to investigate the mechanisms underlying tactile rivalry. We varied intensity difference (ΔI) asymmetrically during different trials as a control parameter to assess its effect on perceptual durations. We aim to characterise the stochasticity of perceptual alternations by looking at properties of the distribution of switching times. Our results show that general characteristics of bistable perception such as Levelt's proposition II (LVII) and stochastic characteristics like a scaling property hold for the tactile modality. This provides a new avenue to expand studies of the general mechanisms underlying neural competition across multiple sensory modalities.

4.2. Methods

4.2.1. Power analysis

The factors tested in our experiments had not been tested in any earlier studies, so we carried out a preliminary experiment with six participants. For each participant, we had six repetitions at each intensity difference level ($\Delta I = 2, 4, 6\,dB$), resulting in 36 samples for each condition. For calculations of partial η^2, we used the *effectsize* package in R to perform a two-way repeated measures ANOVA. The reported partial η^2 values in Table 4.1 correspond to the following Cohen's measurements of effect size $f(percept) = .58$, $f(\Delta I) = .31$, $f(\Delta I : percept) = .77$.

We used the minimum effect of $\eta^2 = .09$ in the preliminary experiment to estimate the sample size. The correlation between means of SIM and AM perceptual durations is $-.43$. In order to detect an effect of partial $\eta^2 = .09$ with 85% power in a two-way within-subjects ANOVA (5 groups, $\alpha = .05$, non-sphericity correction $= 1$), G*Power (Faul et al.) suggests we would need 14 participants.

4.2.2. Participants

Fifteen volunteers (8 male, mean age 29.07±7.43 SD) were recruited from the University of Exeter. Each gave written informed consent and received minor monetary compensation for participating in a 1-h session. Participants were naive to the purpose of the study and did not self-declare any neurological or sensory disorders. Procedures were in compliance
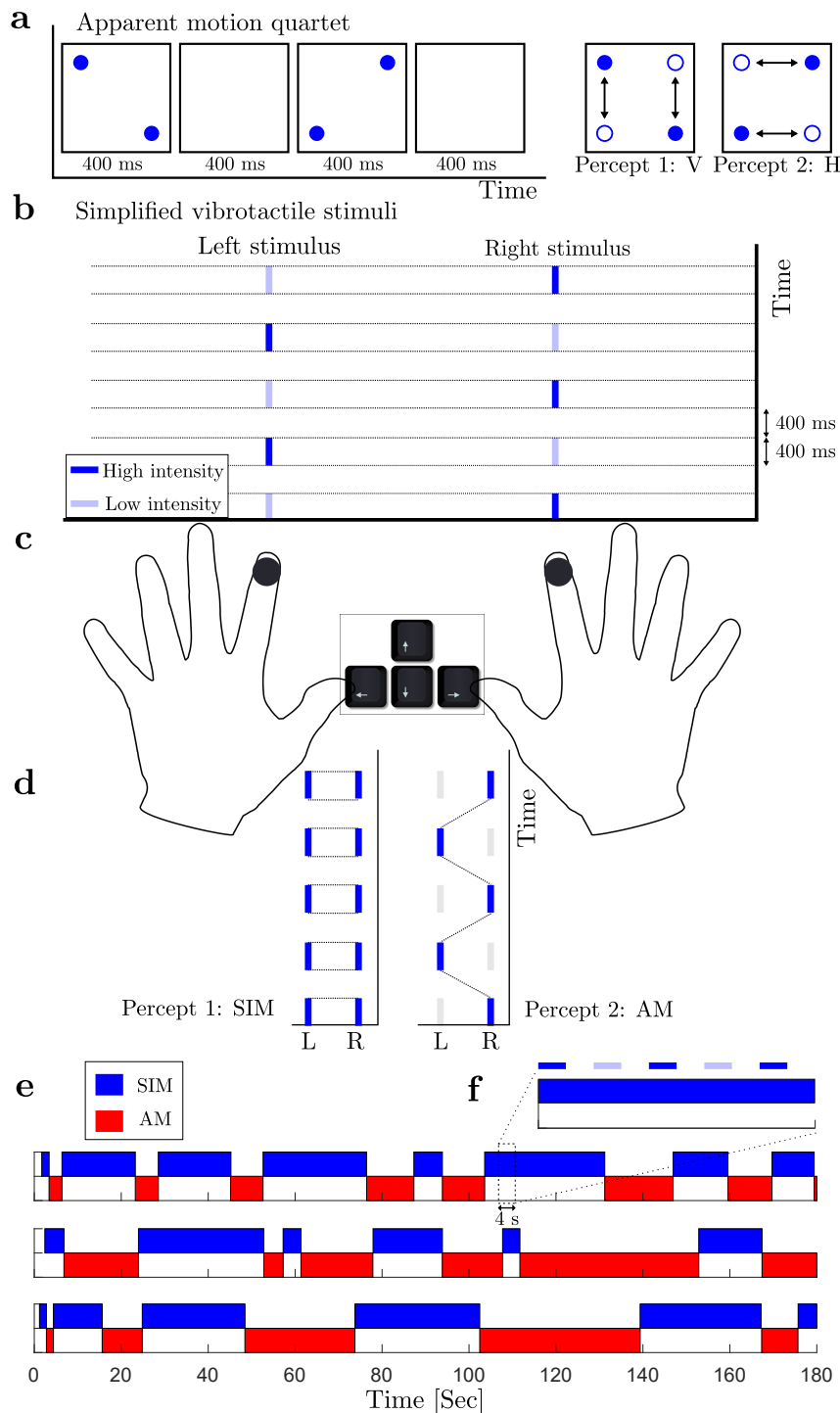
Figure 4.1. (**A**) Apparent motion quartet. The stimulus consists of a cycle of four stimulus frames. Two dots appear at the diagonal corners of an invisible square during stimulus interval, then disappear during the inter-stimulus interval (ISI), reappear at the opposing corners and disappear during the ISI. The stimulus is perceptually ambiguous and can yield either horizontal or vertical motion percepts (indicated by the *black arrows*). For the tactile motion quartet, four stimulus locations on e.g., a subject's fingers are used with similar timing intervals. (**B**) Vibrotactile stimuli. Sequences of high (*darkblue*) and low-intensity (*lightblue*) of $200\,\mathrm{KHz}$ vibrations are delivered to the right and the left index finger. (**C**) Experimental setup. Vibrotactile stimuli are delivered to subject's index fingers. During a trial subject's perception of the stimuli changes and they report it by holding appropriate keys on the keyboard using their thumbs. (**D**) Percept types. When the patterns are played with equal intensity, they can be perceived as one simultaneous vibration (SIM). With a fixed intensity difference ($\Delta I > 0\,dB$) between the high- and low-intensity tactile pulses, perception switches back and forth between two percepts: SIM (perceived as a fixed intensity on each hand, even though the intensity is changing) and AM (perceived as pulses of vibrations jumping from one hand to the other hand). We associate the left arrow key with SIM and the right arrow key with AM. (**E**) Perceptual phases. Perceptual interpretations of the stimuli for three different subjects during 3-min trials at $\Delta I = 2\,dB$. (**F**) Relative scale of the stimuli. A 4-s zoomed panel which shows the relation between the stimulus and the perceptual phases.

73

with guidelines for research with human subjects and approved by University of Exeter Research Ethics Committee.

4.2.3. Experiment design and procedure

Participants sat in an acoustically isolated booth and attended to vibrotactile stimulators attached to their right and left index fingers. We used miniature vibrotactile electromagnetic solenoid-type stimulator (18 mm diameter, Dancer Design tactors, www.dancerdesign .co.uk) driven by a tactile amplifier (Dancer Design Tactamp) to deliver stimuli. Vibrotactile stimuli consisted of sequences of 400 ms high (H) and low (L) intensity 200 Hz vibratory pulses, each followed by a 400 ms silent interval (H-L-H-L for the right hand and L-H-L-H for the left hand, "-" indicates the silent gap) (Figure 4.1B). The intensity of the L stimulus was ΔI below the intensity of the H stimulus on a logarithmic scale (dB). We chose the full-amplitude based on a value where differences in amplitude were noticeable in unambiguous perception. The voltages applied to the tactors for full-amplitude 200 Hz sinusoidal vibration was 3.38 V. To mask any unwanted low-intensity sound emitted by the vibrotactile stimuli, participants listened to pink noise played through noise-isolating headphones at a comfortable listening level. During a trial participants' perception of the stimulus changed over time and they reported their current perceptual interpretation with key presses (sampled at 100 Hz) on a keyboard (Figure 4.1C). Participants perceived the stimulus as either one simultaneous pattern of vibration on both hands (SIM), or patterns of vibration that jumped from one hand to the other hand, giving a sensation of apparent movement (AM) (Figure 4.1D). Subjects were instructed to report their percepts passively and not try to hold one perceptual interpretation over another.

During experimental sessions, 3-min trials were repeated three times in blocks of five trials for a range of intensity differences ($\Delta I = .5, 1, 2, 4, 6 \, dB$) in random order. For a given participant, this resulted in a total of 15 trials (45 min total trial time). The interval between trials was a minimum of 20 s. We used a 5×5 Latin square design with nine randomized and unique grids so that the order of conditions for each participant in a block of trials was counterbalanced within/across participants and repetitions.

4.2.4. Data analysis

In the first stage of our analysis, every trial with average percept durations larger than 150 s (above dashed line in Figure 4.2A) or smaller than 4 s (equivalent to H-L-H-L-H-) were excluded from data set before further analysis (91 trials were excluded from the total of 225 trials). For each of 15 subjects, we take the average percept duration across all repetitions. So, each subject contributes a mean SIM and a mean AM duration averaged across all durations for the three repetitions at each condition. Other measures such as proportion of time with SIM or AM percept, and the frequency of switches are computed in a similar fashion. To see the effect of discarding trials with mean SIM and mean AM durations below 4 s and beyond 150 s compare Figure 4.2 with Figure A.1 in supplementary material (no qualitative change).
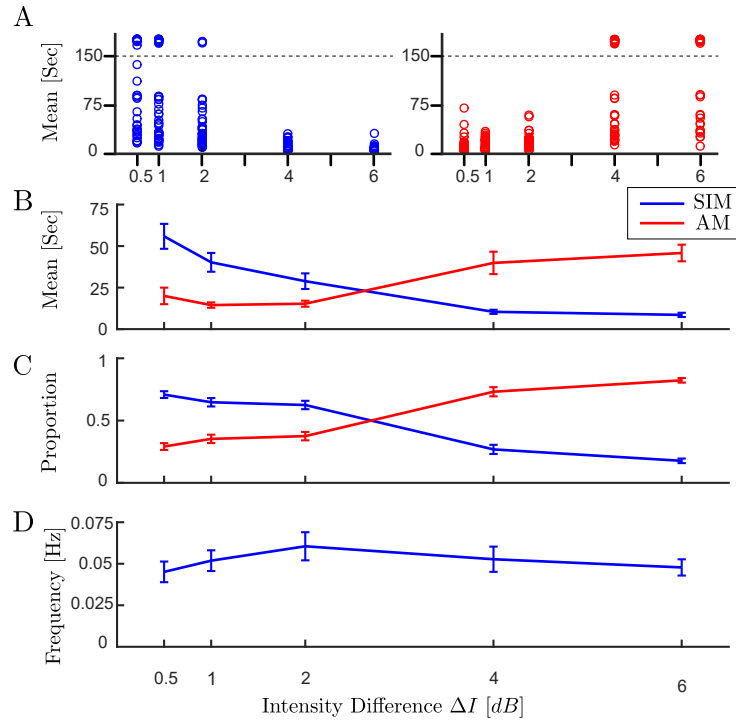
Figure 4.2. (**A**) The distribution of dominance durations at each trial with different experimental conditions (45 observations per experimental condition). All the samples above the dashed line (larger than 150 s), were excluded from the data set before further analysis (for similar analysis without excluding data see Figure A.1 in supplementary materials). It is assumed that durations longer than 150 s are from trials where perception did not alternate. (**B**) Mean dominance duration, (**C**) proportion of dominance for each percept type, (**D**) alternation rate, as a function of intensity difference (ΔI).

In order to establish whether the parameter ΔI had a significant effect on the measures described above, we used repeated measure ANOVA with Bonferroni corrections. As we had discarded some of the trials (due to unacceptably large or small means), we resampled data from mean percept durations at each experimental condition to substitute discarded trials and balance the number of observations across experimental conditions. ANOVA tables and post hoc analyses are reported in full in Table A.1-Table A.7 (supplementary material). A significance level of .05 is used throughout this paper. In ANOVA tables the Greenhouse–Geisser (GG) corrected p-values are reported if a Mauchly sphericity (MS) test reached significance. In post hoc analyses quoted p-values are Bonferroni corrected to account for multiple comparisons. Standard measures of effect size (generalized eta-squared) are quoted for statistically significant results. All statistical analyses were carried out in the statistical package R.

The distributions of normalized percept durations of both types shown in Figure 4.3 were compared with gamma and log-normal distributions using a one-way Kolmogorov–Smirnov (KS) test. The null hypothesis is that the test data are drawn from the standard distribution and a significant result ($p < .05$) indicates that the test data are not drawn from the comparison distribution.

In order to check for a scaling property, we first need to compute central moments. The distribution shape of samples t may be quantified in terms of the mean $\mu_1 \equiv \mathbb{E}[t]$ and the central moments $\mu_2 \equiv \mathbb{E}\left[(t - \mu_1)^2\right]$, $\mu_3 \equiv \mathbb{E}\left[(t - \mu_1)^3\right]$, etc., or, equivalently, in

terms of normalized moments, such as the coefficient of variation $c_v = \mu_2^{1/2}/\mu_1$ and the skewness $\gamma_1 = \mu_3/\mu_2^{3/2}$. A scaling property obtains if central moments are proportional to corresponding powers of the mean or, equivalently, if normalized moments are constant as follows:

$$
\begin{aligned}
\mu_2 &\propto \mu_1{}^2, \\
\mu_3 &\propto \mu_1{}^3.
\end{aligned}
\quad \Leftrightarrow \quad
\begin{aligned}
c_v &= const, \\
\gamma_1 &= const.
\end{aligned}
\tag{4.1}
$$

The normalization of percept durations was used in order to combine data across participants and different experimental conditions (Rankin et al. 2015), whilst accounting for some of the subject variability in experiments (supplementary material Figure A.2). For correlation analysis, durations were normalized to the average value of each percept type separately within each trial and subject, in order to avoid spurious correlation due to inter-subject and inter-trial differences in switching behaviour. Here we used the Pearson correlation that measures the strength and direction of the linear relationship between two variables. Pearson's linear correlation coefficient $Corr$ is defined as:

$$
Corr(x, y) = \frac{\Sigma(x - \mu_x)(y - \mu_y)}{\sqrt{\Sigma(x - \mu_x)^2 \Sigma(y - \mu_y)^2}},
\tag{4.2}
$$

where μ_x and μ_y are the means of variables x and y.

To ensure consistency of our method, we also computed the correlations with a second method (Figure 4.4E–H) based on correlations in single trials without normalization. As correlations may not be reliable as computed for single trials in isolation, we treated each trial as a sample of the correlation and tested whether the mean of the distribution was significantly above or below zero.

The data and materials for all experiments are available in the GitHub repository farzaneh-darki/Darki2021_perceptual: https://github.com/farzaneh-darki/Darki2021_perceptual.

4.3. Results

The experiment with antiphase sequences of high and low intensity tactile stimuli on the right and the left index finger showed irregular perceptual switches between two interpretations for a range of the parameter ΔI. The average percept duration across all participants and trials for both percept types was $17.9\,s \pm 22.7\,s$, which spans on average over 35 periods of the stimuli (Figure 4.1E and F). The average percept duration across all participants for both percept types at $\Delta I = 2\,dB$ was $15.8\,s \pm 19.4\,s$. The fraction of time spent in SIM was .52. For some participants at small or large ΔI values perception may not alternate, these trials were excluded from dataset.

4.3.1. Levelt's proposition II

To establish whether Levelt's proposition II extends to the tactile domain, we chose intensity difference (ΔI) as a control parameter and examined the temporal dynamics of

Table 4.2. Two-way repeated measure ANOVA of mean duration of **both percept types (AM, SIM)** with respect to intensity difference (ΔI) and percept type. Analysis shows a significant effect of ΔI and also ΔI:percept on the mean durations.

Source	df_{num}	df_{den}	F	p	ges	$p[GG]$
Percept	1	41	3.34	.07		
ΔI	4	164	3.93	.004	.01	.01
ΔI:Percept	4	164	50.01	$< .001$	.32	$< .001$

Table 4.3. One-way repeated measure ANOVA of mean duration of **SIM** perception with respect to intensity difference (ΔI). Analysis shows a significant effect of the intensity difference on the mean durations.

Source	df_{num}	df_{den}	F	p	ges	$p[GG]$
ΔI	4	164	25.04	$< .001$	.03	$< .001$

perceptual alternations. The distribution of mean perceptual dominance time in each trial across both percept types and ΔI conditions is plotted in Figure 4.2A. Mean dominance duration, proportion of time spent in each percept type and alternation rate are plotted against intensity difference (ΔI), respectively in Figure 4.2B-D. Increasing intensity difference (ΔI) (intensity of the H stimulus is fixed, intensity of the L stimulus is decreased), causes the mean dominance of SIM percept to decrease and AM percept to increase (Figure 4.2B). A similar pattern is shown for proportion of perceptual dominance (Figure 4.2C). The alternation rate reaches a maximum at equidominance $\Delta I = 2\,dB$ (the point where each percept approximately dominates half the time), and decreases symmetrically below and above this point (Figure 4.2D). Of the conditions tested $\Delta I = 2\,dB$ is closest to equidominance; from panels B and C in Figure 4.2 it appears $\Delta I = 3\,dB$, if tested, would be closer still to equidominance and have a higher alternation rate. Results from our experiments demonstrate that Levelt's proposition II holds in tactile domain.

A two-way repeated measures ANOVA of mean duration of both percept types (SIM, AM) was performed with Percept type (SIM, AM) and intensity difference ΔI as within-subjects factors. The analysis reported in Table 4.2 shows a significant interaction for ΔI:percept, $F(4, 164) = 50.01$, $p < .001$. As for the individual factor, percept does not reach significance $F(1, 41) = 3.34$, $p = .07$, however for the individual factor ΔI reaches significance, $F(4, 164) = 3.93$, $p = .004$. A one-way repeated measures ANOVA of mean duration of SIM percept was performed with ΔI as the within-subjects factor. The analysis reported in Table 4.3 shows a significant effect of ΔI on mean dominance SIM $F(4, 164) = 25.04$, $p < .001$ (Similar results for AM percept in Table 4.5). Pairwise comparisons with Bonferroni-corrected significance levels revealed that each individual condition has significant differences for all non-adjacent conditions and for the pair $\Delta I = [2, 4]\,dB$ (Table 4.4, Similar results for AM percept in Table 4.6). Taken together, these result demonstrate a significant main effect of varying ΔI on mean dominance duration (Table 4.5 and Table 4.6) and proportion of dominance of each percept (Table A.2 and Table A.3 in supplementary material).

Table 4.4. Pairwise ttest, with Bonferoni corrected p-values, on the mean durations of **SIM** perception with respect to intensity difference (ΔI).

	$\Delta I = .5$	$\Delta I = 1$	$\Delta I = 2$	$\Delta I = 4$
$\Delta I = 1$	.28	-	-	-
$\Delta I = 2$	.001	.45	-	-
$\Delta I = 4$	$< .001$	$< .001$	.004	-
$\Delta I = 6$	$< .001$	$< .001$	.001	1.0

Table 4.5. One-way repeated measure ANOVA of mean duration of **AM** perception with respect to intensity difference (ΔI). Analysis shows a significant effect of the intensity difference on the mean durations.

Source	df_{num}	df_{den}	F	p	ges	$p[GG]$
ΔI	4	164	27.26	$< .001$	.34	$< .001$

4.3.2. Statistics of dominance durations and scaling property

Perceptual phases for bistable stimuli have been shown to be fit well by gamma or log-normal distributions. However, experiments with large numbers of participants found the log-normal distribution to be a better fit across visual and auditory bistable stimuli (Denham et al. 2018). The distributions of normalized perceptual phases for experimental conditions close to equidominance are shown in Figure 4.3A–C. In the temporal analysis of perceptual durations for bistable stimuli, the perceptual phases are normalized by the mean for each percept type (see Figure A.2 in supplementary material for normalization method). The coefficient of variation (c_v), which is the ratio of the standard deviation to the mean, is used as a measure of variability in the perceptual phases. The result of one-way KS tests shows that, except for the gamma standard distributions at $\Delta I = 1\,dB$ ($p(gamma) < .05$), all the other histograms are compatible with the comparison distributions.

To assess how well tactile rivalry conforms to the scaling property reported in (Cao et al. 2014; 2016), we compared observations from three intermediate experimental conditions ($\Delta I = 1, 2, 4\,dB$). The extreme conditions were discarded from further analysis, as they had fewer perceptual phases leading to inaccurate computation of second and third moments. A scaling property obtains if normalized moments, such as the coefficient of variation c_v and ratio of skewness and coefficient of variation γ_1/c_v are constant. Figure 4.3D and E illustrates the results in terms of the coefficient of variation and skewness across different experimental conditions. The coefficient of variation remained consistently near

Table 4.6. Pairwise ttest, with Bonferoni corrected p-values, on the mean durations of **AM** perception with respect to intensity difference (ΔI).

	$\Delta I = .5$	$\Delta I = 1$	$\Delta I = 2$	$\Delta I = 4$
$\Delta I = 1$	1.0	-	-	-
$\Delta I = 2$	1.0	1.0	-	-
$\Delta I = 4$	$< .001$	$< .001$	$< .001$	-
$\Delta I = 6$	$< .001$	$< .001$	$< .001$	.017
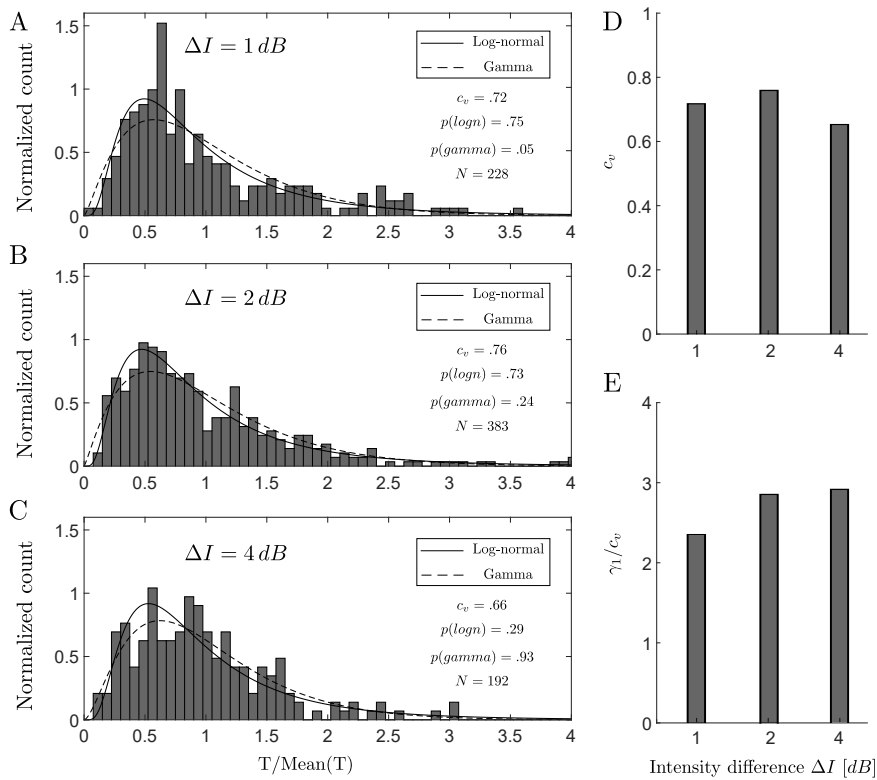
Figure 4.3. Histograms of normalized perceptual phases for experimental conditions close to equidominance, (A) $\Delta I = 1\,dB$, (B) $\Delta I = 2\,dB$ and (C) $\Delta I = 4\,dB$ combined across participants and percept type after normalization by the mean. *Solid* and *dashed curves* show the estimated log-normal and gamma distribution respectively. (D) Coefficient of variation (c_v) and (E) skewness divided by coefficient of variation (γ_1/c_v) for experimental conditions $\Delta I = 1, 2, 4\,dB$.

$c_v = .6$ (Figure 4.3D) and ratio of skewness and coefficient of variation γ_1/c_v remained roughly constant (Figure 4.3E). In other words, a scaling property was maintained over intermediate experimental conditions.

4.3.3. Analysis of correlation

Figure 4.4A–D plots the normalized duration of each perceptual phase against the duration of the next, for the two possible transitions (lag1: SIM→AM and AM→SIM). Importantly, durations were normalized to the average value of each percept type separately within each trial and subject, in order to avoid spurious correlations due to inter-subject and inter-trial differences in switching behaviour (see Methods). For consecutive phase durations (lag 1), the correlation was small but significantly larger than zero (Figure 4.4A and B). For the phase durations that were one phase apart (lag 2: SIM→SIM and AM→AM), the correlation was significantly smaller than zero (Figure 4.4C and D).

We also calculated correlation coefficients separately for each switch type in each individual trial. Figure 4.4E–H shows histograms of the single trial correlations between subsequent phases (lag 1) and between phase durations that are one phase apart (lag 2). Using a t-statistic, we found a significant deviation of the histogram towards positive correlation values for lag 1; SIM→AM transition (Figure 4.4E), and negative correlation values for lag2; SIM→SIM transition (Figure 4.4H). Single trial correlations for lag1; AM→SIM and lag 2; AM→AM were not significantly different from zero.
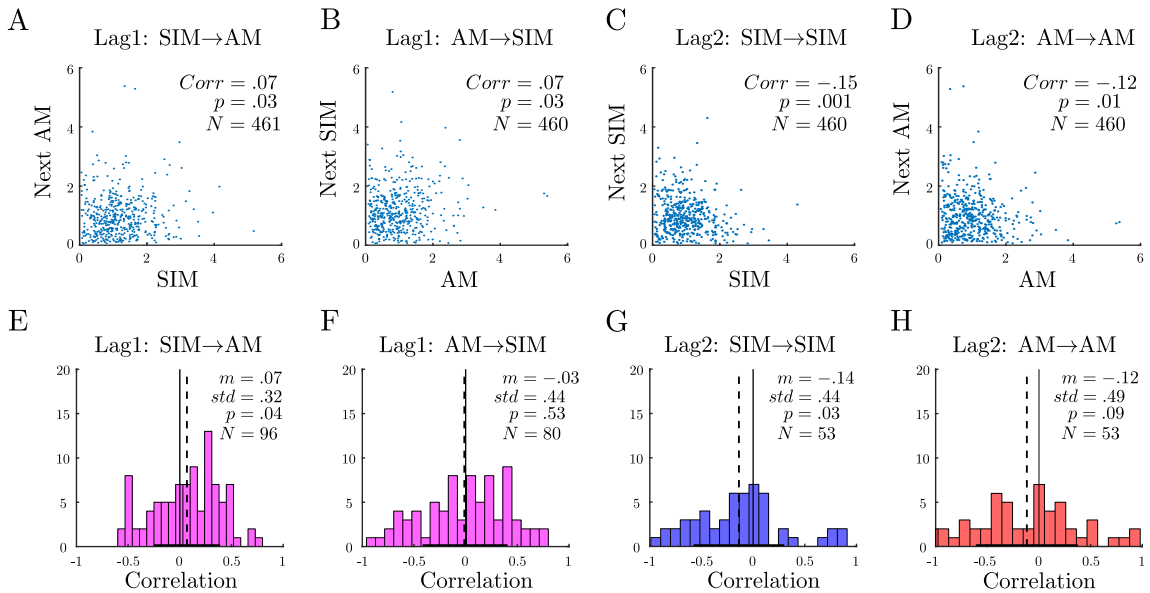
Figure 4.4. (A–D) Scatter plots of normalized durations. The correlation coefficient (*corr*) between perceptual phases for each scatter is indicated in each panel with the corresponding *p*-value and number of pairs (*p* and *N*, respectively). (E–H) Histograms of correlation coefficients between perceptual phases in single trials. The mean (*m*) and standard deviation (*std*) are indicated in each panel, followed by the t-statistic of the fixed effect, its significance (*p*) and the number of trials for which it was possible to calculate the correlation (*N*). The *vertical solid lines* mark zero correlation, and the *vertical dashed lines* mark the mean of each distribution. The transition types are marked above each histogram (A&E) AM following SIM. (B&F) SIM following AM. (C&G) SIM. (D&H) AM.

4.4. Discussion

4.4.1. Summary

Earlier studies with tactile stimuli have identified bistability in somatosensation; these have typically investigated the spatial proximity of stimulation sites as a control parameter. Future studies are needed to characterize the full range of spatial and temporal stimulation parameters capable of inducing bistable tactile apparent motion. Here we introduced a simple tactile stimulus which can evoke bistability through stimulating only two sites (in comparison with four sites in previous studies). We investigated the effect of varying intensity difference (ΔI) asymmetrically on perceptual durations. Our results show that Levelt's proposition II (LVII) and other characteristics of sensory bistability that generalise in vision and auditory sensation extend to the tactile modality.

4.4.2. Novelty of the introduced stimuli and experiment design

In this study, we introduced a new ambiguous tactile stimulus, consisting of anti-phase sequences of high- and low-intensity vibration pulses on the right and left index fingertips. While in similar work on tactile bistability stimuli were presented on at least four sites on the skin (Carter et al. 2008; Liaci et al. 2016), our stimulus is simpler and was only presented at two sites. Our approach probes how motion perception is affected by feature (intensity) differences other than just location. This could be extended to look at other features, e.g., vibration frequency, temporal cues, presentation rate, etc. Another important difference is in the way participants reported their perception and also in the analyses

of perceptual responses. In one study, participants were asked to attend to the stimuli and report their perception at the end of short representations of tactile stimuli (Liaci et al. 2016). In another study, participants reported their perception continuously during long representations of the stimuli, however; the analysis considered temporal evolution of the average responses pooled across all participants (Carter et al. 2008), which does not account for the dynamics of individual perceptual durations and inter-subject variability. In neither study is the intensity difference varied as a control parameter, but the results of our experiment show that it significantly affects the higher-level interpretation of the stimulus. Here, our analysis involves the temporal durations of perceptual phases and investigates the effect of varying the intensity difference (ΔI) asymmetrically on perceptual durations.

4.4.3. Similar properties of perceptual competition across different modalities

Perception of the tactile stimuli showed the following similarities to other sensory modalities. First, visual, auditory and tactile stimuli can induce the perception of apparent motion which can be ambiguous in a certain range of stimulus parameters, for example here with a synchronous percept (SIM). Second, Levelt's proposition generalizes to other visual modalities including ambiguous motion (Moreno-Bote et al. 2010) and to auditory bistability (Rankin et al. 2015). Here our analysis showed Levelt's proposition II extends to include tactile bistability. Third, in the experiments of visual and auditory bistability, the distribution of perceptual phases maintains a characteristic, gamma-like shape (Blake et al. 1980). Denham et al. showed these distributions to be specifically log-normal in experiments with a large number of participants (Denham et al. 2018). Even though mean perceptual phases vary widely between participants and stimulus properties, the variance and skewness of perceptual phases keep a characteristic proportion to the mean (Cao et al. 2014; 2016). Our analysis shows that the scaling property holds in the tactile domain, similar to multistability in other modalities.

Despite these similarities, differences between the other sensory modalities and tactile perception were observed as well. Experiments with an auditory stimulus which utilised sequences of anti-phase high and low tones in each ear showed that the percept can be like a single tone oscillating from ear to ear, which is a form of apparent motion. However, there were other percepts like sensation of either the high tone in the left ear and the low tone in the right ear or vice versa, and the two percepts switching back and forth (Deutsch 1974). While we used a similar stimulus paradigm, the possible perceptual interpretations that we observed in the tactile domain were different. It remains to be determined whether perceptual interpretations equivalent to those reported in audition can be evoked by different ranges of spectrotemporal features in tactile stimuli. On the other hand, we found that perceptual phases in the tactile modality were generally more stable than in the other bistable perception like visual (Conrad et al. 2012) or auditory modality (Rankin et al. 2015) (mean dominance durations were longer in the tactile experiment). Previous studies in vision (van Ee 2009; Cao et al. 2021) and auditory streaming (Barniv and Nelken 2015) suggested that the durations of successive perceptual phases are positively corre-

lated, however, for lag 2 they have been shown to be negatively correlated in auditory streaming (albeit their result did not prove to be statistically significant) (Barniv and Nelken 2015) and to be positively correlated in binocular rivalry (Cao et al. 2021). Our analysis with tactile stimuli shows a significant positive correlation for lag 1 (from one percept type to the other), and a negative correlation for lag 2 (between similar percept types). Existing studies of auditory perception have established that first durations are typically longer than subsequent durations (Pressnitzer and Hupé 2006). However, we found no such trend in our data on vibrotactile bistability (see Table A.3 and Table A.8 in supplementary material). The effects of attentional focus on dominance durations have been widely reported with other bistable modalities (Toppino 2003; Meng and Tong 2004; van Ee et al. 2006; Pressnitzer and Hupé 2006) but this remains to be explored for tactile bistability.

4.4.4. Locus of tactile rivalry and modelling

To the best of our knowledge, there are no models for tactile rivalry. Computational models of perceptual ambiguity have helped significantly with our understanding of other types of bistability. In order to develop a computational model of tactile rivalry, one must consider how inputs from the left and right hands project to primary somatosensory cortex (S1) and how features like amplitude, frequency and timing are encoded there. It is known that information from each half of the body-surface is projected to the opposite side of the brain (Maldjian et al. 1999). Ipsilateral stimuli do not travel directly to the neurons in the primary somatosensory cortex (S1) (Eshel et al. 2010). However, an extensive range of research from invasive studies in monkeys (Clarey et al. 1996), to behavioural or neuroimaging studies of humans (Hlushchuk and Hari 2006) showed that somatosensory processing in the left side of the brain can be modulated by the right side and vice versa. For instance, during unilateral touch, contralateral activation can be observed as well as ipsilateral deactivation in S1 (Hlushchuk and Hari 2006; Kastrup et al. 2008).

In contrast, intracranial recording (Noachtar et al. 1997), functional magnetic resonance imaging (fMRI) (Hämäläinen et al. 2002; Nihashi et al. 2005) and magnetoencephalography (MEG) (Korvenoja et al. 1995; Schnitzler et al. 1995) in humans, demonstrated that unilateral tactile stimulation activates bilateral S1 response. Moreover, single-cell recording in monkeys showed that some neurons in S1 display bilateral hand receptive fields (Iwamura et al. 2001). These results suggest that interhemispheric connections may not be purely inhibitory for somatosensation and they are likely to have excitatory effects as well (Eshel et al. 2010). We might use modelling to check whether purely inhibitory interactions can account for observed behavioural responses, or whether other types of interhemispheric interplay might explain the results instead.

The experiments presented here used tactile pulses at 200 Hz lasting 400 ms. The neural encoding of location and of spectro-temporal properties of tactile stimuli is relatively well documented. There exist quite a lot of discussions in the literature about the cortical representation of flutter frequencies (less than 80 Hz) (Talbot et al. 1968; Romo and Salinas 2003), however, it is under debate whether the somatosensory cortices process high

frequencies. There is some evidence to suggest that the temporal patterning of the neural activities in primary and secondary somatosensory cortex does not contain information about the frequency of the stimuli in the vibration range (greater than 80 Hz) (Ferrington and Rowe 1980). The perception of flutter and high frequency vibration may be processed through distinct processing streams (Tommerdahl et al. 2005). Auditory cortex undoubtedly plays a main role in the spectro-temporal representation of acoustic stimuli. There are some hypotheses that the putative neural populations are independently stimulated by tactile and auditory sensory modalities (Yau et al. 2009). The cutaneous vibration frequency can be distinguished at a significantly lower resolution (with Weber fractions around .2 for tactile versus .003 for auditory), and over a narrower range than auditory tone pitch (up to 1 kHz for tactile versus 20 kHz for auditory stimuli) (Saal et al. 2016). The resolution of perception is likely hierarchical as supported by modelling work in visual (Wilson 2003) and auditory bistability (Rankin et al. 2015).

There is a need for a tactile rivalry model that accounts for both well-established results on the timing of dominance intervals and is also compatible with the physiological evidence and structure of somatosensation. General models of rivalry usually incorporate a slow process together with reciprocal inhibition to produce perceptual alternations. Perceptual bistability results from a competition between units representing neural populations associated with different percepts (e.g. units driven by inputs from the left and right eyes in binocular rivalry) (Wilson 2003; Rankin et al. 2015; Cao et al. 2021). A possible model of tactile rivalry could be based on competition between neural populations in primary somatosensory cortex associated with the right and the left hands. For the development of a model, an important aspect of tactile rivalry is that information is integrated across locations and over time to form the SIM and AM percepts. Dynamical analysis of models with different architecture and connectivity can help us to find a model that induces observed percept types with the specific characteristics and intrinsic dynamics. Our result show that Levelt's proposition II (LVII) holds in the tactile modality. This provides a new avenue to test and expand the computational and neurobiological models for bistability currently dominated by vision science. The correlation structure and statistical distribution properties can be used as an important constraint on models of tactile rivalry, and could reveal mechanistic differences with other modalities.

4.4.5. Conclusions

We presented a new, simple form of tactile rivalry and explored generalisations with respect to perceptual rivalry in other sensory modalities. First, the results of our study show that Levelt's proposition II which describes the relation between stimulus features and mean perceptual dominance extends to tactile bistability. Second, the stochastic characteristics of irregular perceptual alternations were shown to follow similar distribution shapes across different experimental conditions and with different mean perceptual dominance (known as a scaling property). Third, we found negative correlations for durations that were one phase apart (lag 2) which is opposite to the effect found in vision (Cao et al. 2021). In auditory bistability no significant correlation was found, though it trended in the same direction as the tactile modality results (Barniv and Nelken 2015). The paradigm intro-

duced here and the methods of analysis provide a basis to further explore how similar processes generate changes in perception across different senses. This opens up a new avenue for a range of experiments to explore the role of e.g., adaptation and cross-inhibition in somatosensation, voluntary control (attention), perceptual memory and the integration of tactile cues with the other senses. This approach will allow for insights gained in previous work from a substantial literature on auditory and visual perception to deepen our understanding of tactile perception.

5. Model of tactile rivalry

5.1. Introduction

Perceptual rivalry occurs when sensory information is ambiguous and the brain cannot commit to a single percept; instead, it switches between mutually exclusive interpretations every few seconds (Sterzer et al. 2009). Examples of perceptual rivalry span across different sensory modalities including vision (Hupé and Rubin 2003; Meso et al. 2016; Blake 1989), audition (Pressnitzer and Hupé 2006) and olfaction (Zhou and Chen 2009). In the tactile domain, perceptual rivalry was introduced with a tactile illusion based on the apparent-motion quartet (Carter et al. 2008; Conrad et al. 2012; Liaci et al. 2016; Haladjian et al. 2020). Recent experiments with vibrotactile stimuli have shown that several of the general characteristics of perceptual rivalry extend to tactile domain (Darki and Rankin 2021) (see Chapter 4). In these experiments, vibrotactile stimuli consisted of anti-phase sequences of 400 ms high and low intensity high frequency pulses (200 Hz), each followed by a 400 ms silent interval, delivered to the right and left index fingers. Participants perceived the stimulus as either one simultaneous pattern of vibration on both hands (SIM), or patterns of vibration that jumped from one hand to the other hand, giving a sensation of apparent movement (AM), and for long presentations of the stimulus ($> 30\,s$), perception switches back and forth between these two percepts.

The spatio-temporal characteristics of tactile perception have been investigated with a range of experimental approaches. At the somatosensory periphery, the firing rate response of tactile fibres to a vibration is dependent not only on its amplitude but also on its frequency. Therefore, the amplitude information carried in the firing rates of any population of tactile fibres is ambiguous. Rather, the intensity of skin vibrations is encoded in the firing rate evoked in all tactile nerve fibres, weighted by fibre type (Muniak et al. 2007). So it is unclear how these two stimulus dimensions can be independently decoded by downstream structures (Harvey et al. 2013).

The different types of tactile receptors differ in their frequency sensitivity profiles. Slowly adapting fibres (SA1) tend to be more sensitive at low frequencies (below about 10 Hz), PC fibres (RA2) peak in sensitivity at around 250 Hz (40-400 Hz), and rapidly adapting fibers (RA1) prefer intermediate frequencies (5-50 Hz) (Talbot et al. 1968). Neural signals from a single class of receptors can convey ambiguous information. Afferent signals from different types of mechanoreceptors are combined to give rise to tactile percepts. A striking aspect of afferent responses to skin vibrations is that they exhibit phase locked response to periodic vibratory stimuli (that is, they produce one spike or burst of spikes within a restricted portion of each stimulus cycle) as do their counterparts in the auditory nerve (Freeman

and Johnson 1982a;b). This temporal patterning in afferent responses carries information about the frequency composition of vibratory stimuli applied to the skin (Birznieks and Vickery 2017). However, how afferent spiking activity translates into the perception of frequency is still unknown. Neurons in somatosensory cortex also exhibit phase locking to low-frequency vibrations, but the constancy of the phase locking decreases rapidly as vibratory frequency increases.

There are numerous stimulus examples for perceptual ambiguity across different sensory modalities and across different paradigms within the same sensory modality. In spite of this diversity, general characteristics of this phenomenon appear to be quasiuniversal. Firstly, Levelt's propositions have been widely used to describe perceptual rivalry in the visual (Moreno-Bote et al. 2010; Brascamp et al. 2015), auditory (Rankin et al. 2015) and recently in tactile domains (Darki and Rankin 2021). For example, the generalization of Levelt's proposition II states that increasing the difference between percept strengths increases the mean perceptual dominance of the stronger percepts (Levelt 1965). Secondly, despite mean dominance times varying widely in multistable experiments, across different observers and stimulus contrasts (Zhou et al., 2004; Brascamp et al., 2005), the statistical distribution of perceptual phases maintains a constant shape, resembling a lognormal or gamma distribution with similar parameters (Cao et al. 2016; Denham et al. 2018; Darki and Rankin 2021). Thirdly, the durations of successive perceptual phases are correlated positively for perceptual phases that were one phase apart (between different percepts) (van Ee 2009; Barniv and Nelken 2015; **?**; Darki and Rankin 2021). These similar properties in multistable phenomena suggest that the underlying mechanisms may be general.

Computational models of perceptual alternations have helped significantly with our understanding of sensory processing across visual and auditory domains. These models focus on the neural processing of sensory information, the dependence of average switching times on stimulus parameters and the statistical distribution of times between switches (Laing and Chow 2002; Shpiro et al. 2007; Wilson 2003; Brascamp et al. 2005; Moreno-Bote et al. 2007; Rankin et al. 2015). General models of rivalry usually incorporate a slow process together with reciprocal inhibition to produce perceptual alternations. Perceptual bistability results from a competition between units representing neural populations associated with different percepts (e.g. units driven by inputs from the left and right eyes in binocular rivalry) (Wilson 2003; Rankin et al. 2015; **?**). To the best of my knowledge, there are no mathematical models that capture perceptual alternations for tactile rivalry. The research in this chapter addresses a need for tactile rivalry model that accounts for both well-established results on the timing of dominance intervals and is also compatible with the physiological evidence and structure of somatosensation.

In this study, I develop a mathematical model of tactile rivalry that focuses on accurately reproducing the dynamics of the perceptual alternations. This formulation is directly motivated from physiological studies of tactile perception (Noachtar et al. 1997; Maldjian et al. 1999; Nihashi et al. 2005) and general models of perceptual bistability (Ferrario and Rankin 2021). The model of tactile rivalry presented here consists of two processing stages; first stage for producing perceptual alternations; and a second stage for encoding

the percept types (SIM and AM). The powerful combination of bifurcation analysis along with optimisation tools have been used to tune certain features of the model. The model presented here is able to produce common characteristics of tactile rivalry, as observed in tactile rivalry experiments.

5.2. Model overview, design and analysis

In the experiments of tactile rivalry, stimuli consist of sequences of high (H) and low (L) intensity vibratory pulses, with duration TD that followed by a silent interval with duration $TR-TD$ (sequences of $H-L-H-L$ for the right hand and $L-H-L-H$ for the left hand, "$-$" indicates the silent gap) (Figure 5.1A). The intensity of the L stimulus was ΔI below the intensity of the H stimulus on a logarithmic scale (dB). During experimental trials of tactile rivalry, these stimuli are perceived as either one simultaneous pattern of vibration on both hands (SIM), or patterns of vibration that jumped from one hand to the other hand, giving a sensation of apparent movement (AM) (Figure 5.1B).

Here I want to introduce a computational model of tactile rivalry to capture the characteristics of this phenomenon as observed in the experiments. To this end, we consider how inputs from the left and right hands project to primary somatosensory cortex (S1) and how features like amplitude, frequency and timing are encoded there. The model presented here consist of two processing stages (Figure 5.1C); first stage which is responsible for generating perceptual alternations, and a second stage which is encoding the percepts (SIM and AM).

Inputs presented to the model are illustrated in Equation 5.8, and Equation 5.9 (and also sketched in Figure 5.1A). In addition to contra-lateral excitation, ipsi-lateral inhibition has been observed during unilateral touch in S1 (Hlushchuk and Hari 2006; Kastrup et al. 2008). These effects are shown in Figure 5.1C, as inputs i_R and i_L have excitatory effect on the opposite sides (units ν_L and ν_R, respectively), and inhibitory effects on the same sides (units ν_R and ν_L, respectively). Thus, units ν_R and ν_L effectively receive $i_L - i_R$, and $i_R - i_L$, respectively, which are antiphase pulses with amplitude equal to ΔI (Figure 5.6A). Units ν_R and ν_L are adapting recurrent models which can produce UP/DOWN alternations. The dynamics and parameters of the model are further described in subsection 5.2.1.

The second stage in Figure 5.1C shows units u_R and u_L that receive direct ipsi-lateral excitatory inputs from the right and the left side (i_R and i_L, respectively), and also inhibitory ipsi- and contra-lateral connections through the earlier stage (units ν_R and ν_L). Existence of these direct ipsi-lateral excitation motivated by the fact that some neurons in S1 display bilateral hand receptive fields (Iwamura et al. 2001; Nihashi et al. 2005). Interhemispheric connections at the second stage are assumed to exist between units u_R and u_L through direct fast excitation with strength a, and the delayed, slowly decaying inhibition with strength b. Dynamics of units u_R and u_L are described with a system of ODEs in Equation 5.11.
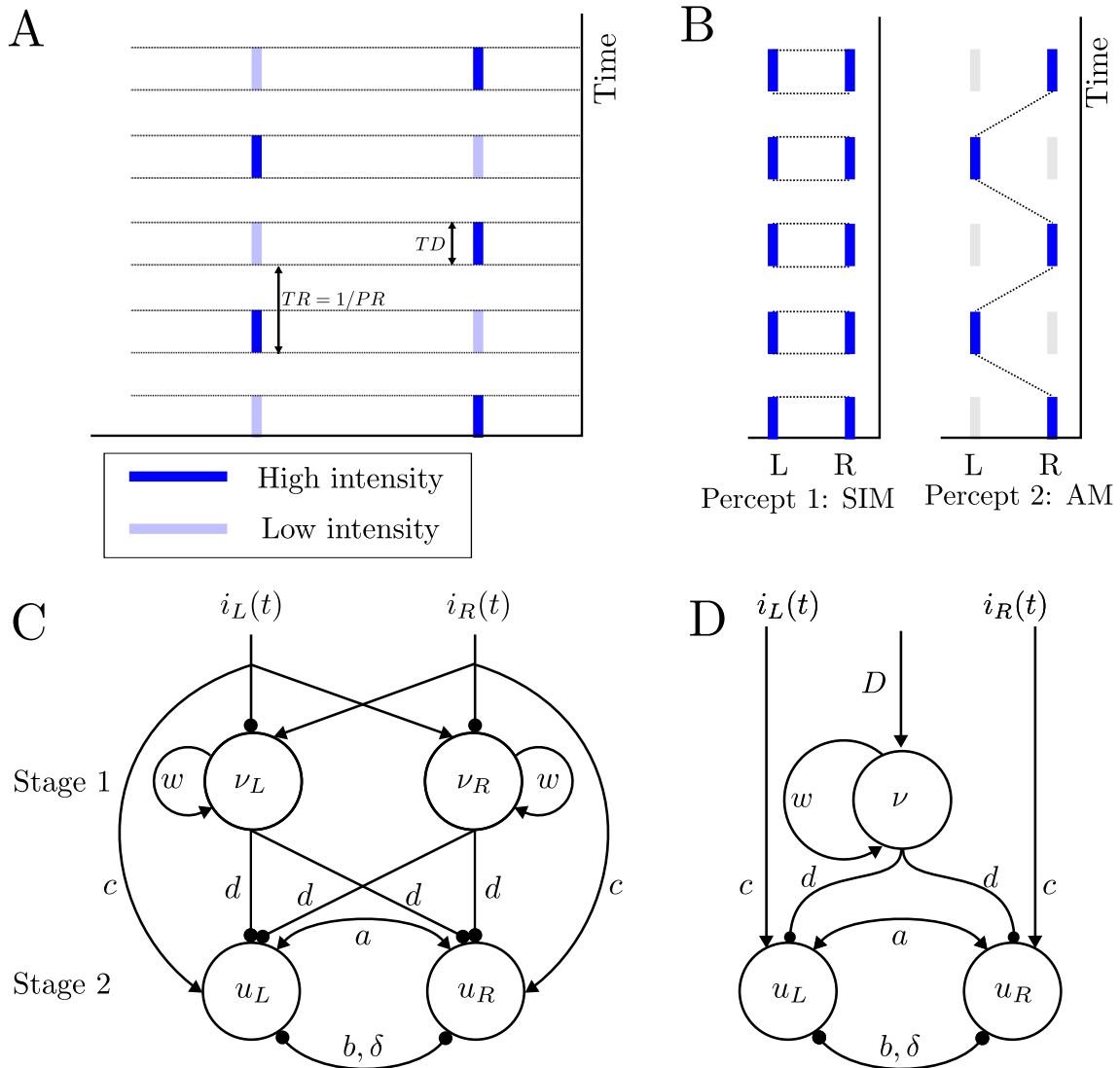
Figure 5.1. **(A) Vibrotactile stimuli.** Vibrotactile stimuli consist of anti-phase sequences of high (dark blue) and low-intensity (light blue) of 200 KHz vibrations to the right and left index finger ($TD = 0.4\,s$, $TR = 0.8\,s$). **(B) Percept types.** During a trial subject's perception of the stimuli changes. When the patterns are played with equal intensity, they can be perceived as one simultaneous vibration (SIM). With a fixed intensity difference ($\Delta I > 0\,dB$) between the high- and low-intensity tactile pulses, perception switches back and forth between two percepts: SIM (perceived as a fixed intensity on each hand, even though the intensity is changing) and AM (perceived as pulses of vibrations jumping from one hand to the other hand). **(C) Schematic of the model of tactile rivalry.** Inhibitory connections are shown with filled circles, and excitatory connections with black arrows. **(D) Schematic of the simplified model.**

5.2.1. Stage 1 - encoding perceptual alternations

Here I introduce adapting recurrent model from (Levenstein et al. 2019) which can produce UP/DOWN alternations. Previously, this model has been used to study the state of hippocampal and neocortical populations during NREM sleep (UP/DOWN states observed as spontaneous transitions during sleep). The analysis in their study provides a useful reference to tune model parameters. The population activity of this model is used at the first stage to modify the net inputs to the u_R and u_L units at the second stage and produce alternations between different dynamical states of the model encoding the percepts (switches between SIM and AM percepts). When the first stage units are in the DOWN state, inputs drive the second stage in its default setting where typically SIM is encoded, unless ΔI is very large. If the first stage units are in the UP state, inputs driving the second stage are less excitatory, leading to AM, unless ΔI is very small (see subsubsection 5.2.4).

The dynamics of this model is described in terms of the mean firing rate ν, and activity-driven adaptation a (Figure 5.7A):

$$\begin{cases} \tau_\nu \dot{\nu} = -\nu + N_\infty \left(w\nu - ga + D + \zeta(t) \right), \\ \tau_a \dot{a} = -a + A_\infty \left(\nu \right). \end{cases} \tag{5.1}$$

Where w is the strength of recurrent excitation, g is the strength of adaptation, D is the level of input and $\zeta(t)$ is noisy fluctuations. $N_\infty(x)$ and $A_\infty(r)$ are assumed to be sigmoidal functions.

$$N_\infty(x) = \frac{1}{1 + e^{-(x-x_0)}} \tag{5.2}$$

$$A_\infty(\nu) = \frac{1}{1 + e^{-k(\nu-\nu_0)}} \tag{5.3}$$

Unless otherwise specified, I use $x_0 = 5$, $\nu_0 = 0.5$ and $k = 15$ to parametrize the activation functions. Noise $\zeta(t)$ was implemented using Ornstein-Uhlenbeck model described with;

$$d\zeta = -\theta\zeta dt + \sigma\sqrt{2\theta dt}W_t, \tag{5.4}$$

where W_t is a Weiner process. Time scale $\theta = 0.05$ and standard deviation $\sigma = 0.25$ were used unless otherwise specified.

We used two of these adapting excitatory units (Figure 5.1C), one for the right and one for the left side (similar equations for variables ν_R, a_R for the left side, and variables ν_L, a_L for the left side). Where inputs D_R and D_L to these models are the stimulus differences from the right and left as follow;

$$\begin{aligned} D_R &= f(i_L - i_R), \\ D_L &= f(i_R - i_L). \end{aligned} \tag{5.5}$$

Function f is a nonlinearity which will be determined later.
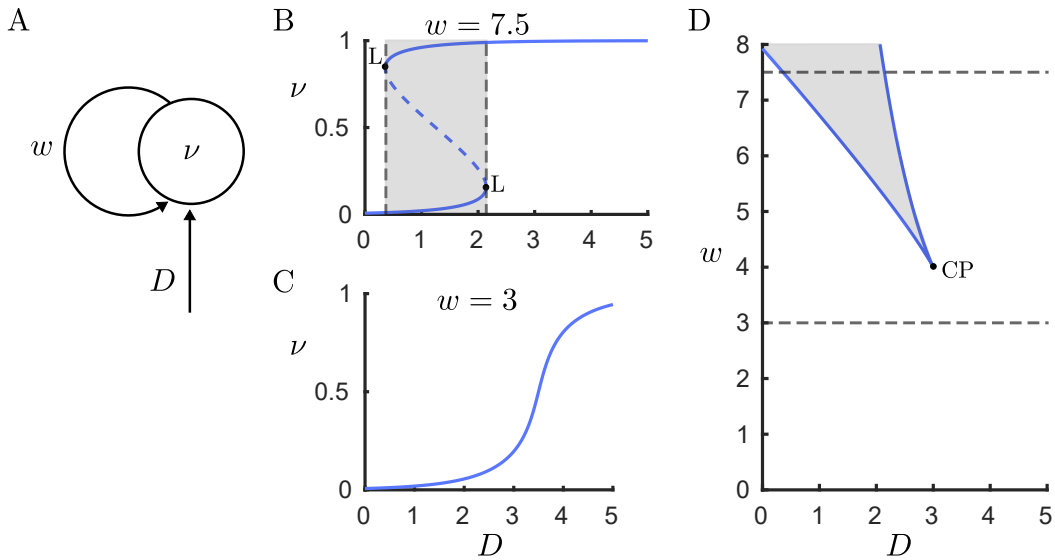
Figure 5.2. **Bifurcation analysis of the adapting recurrent model (without adaptation $g = 0$).** Mechanism of bistability with sufficient levels of recurrent excitation and input (high levels of recurrent excitation and low levels of input). **(A) Adapting recurrent model.** Population firing rate ν driven by D and recurrent excitation with strength w. **(B & C) One parameter bifurcation diagram.** Population rate steady state as a function of input D, for a population with low ($w = 3$), and high ($w = 7.5$) level of recurrent excitation. Stable and unstable fixed points are indicated with solid and dashed curves, respectively. **(D) Two parameter bifurcation diagram.** $w - D$ parameter space, bistable region (grey shaded area) surrounded by two fold bifurcations (L) which merge together and disappear through a cusp bifurcation (CP).

Stage 1 - Bifurcation analysis

In the adapting recurrent model, UP/DOWN alternations are possible only if the population activity can potentially exist in an UP or a DOWN state. This requires adequate strength of recurrent excitation w, to self-maintain the UP state under conditions of low drive. I show this first for a reduced case without adaptation dynamics ($g = 0$ in Equation 5.1).

Bifurcation analysis of the model in the absence of noise was implemented in `Auto07p`. For the statistical analysis of dominance duration distributions, similar codes was implemented in `MATLAB` for simulations of the model with noisy input.
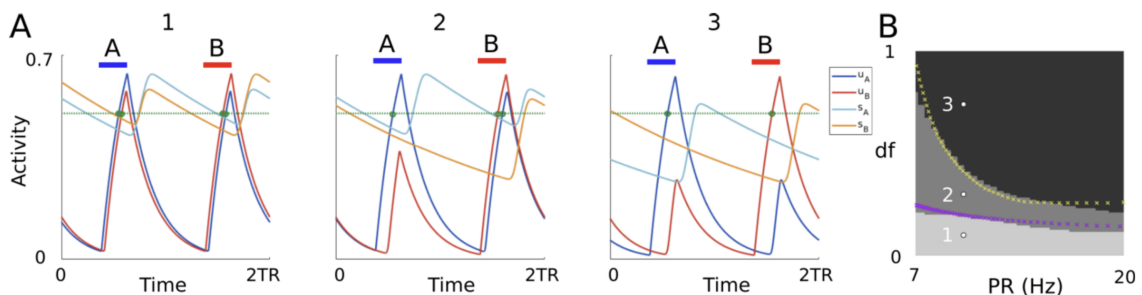
Figure 5.3. **(A)** Time histories of the 2TR-periodic states in system Equation 5.6. Units' threshold crossings are shown by green dots. **(B)** The total number of threshold crossings for both units is shown in greyscale for simulated trajectories at varying PR and df (black = 2, gray =3, lightest gray = 4 crossings). Parameters PR and df in panel (A) are shown by white dots in panel (B). The remaining parameters are $a = 2$, $b = 2.8$, $c = 5.5$, $\delta = 0.015$, $TD = 0.022$, $\tau_i = 0.25$, $\tau = 0.025$, $\theta = 0.5$. Adapted from (Ferrario and Rankin 2021)

The steady states of firing rate variable ν, depend on the level of drive D, and the strength of recurrent excitation w. If recurrent excitation is weak ($w = 0$), the right-hand side of Equation 5.1 increases monotonically with D, and has only one root which is a stable fixed point (Figure 5.2C). As recurrent excitation increases, the right-hand side of Equation 5.1 shows a region of bistability between a low-rate bifurcation point at weak drive and a high-rate bifurcation point at strong drive (Figure 5.2B). In the $w - D$ parameter space, the bistable region (grey shaded area) has borders that correspond to saddle-node bifurcations (Figure 5.2D). UP/DOWN bistability emerges at a critical value of recurrent excitation ($w = 4$), and a critical level of drive ($D = 3$). Consequently, a first general insight of adapting recurrent models is that UP/DOWN bistability will emerge in neuronal populations with sufficiently strong recurrent excitation, during conditions of low drive.

5.2.2. Stage 2 - encoding perceptual interpretation

The starting point for the model is a periodically driven competition network of two localised Wilson–Cowan units previously used for the encoding of different perceptual interpretations of the auditory streaming paradigm (Ferrario and Rankin 2021). The model is described by the following system of DDEs:

$$
\begin{aligned}
\tau \dot{u}_R &= -u_R(t) + H(au_L(t) - bs_L(t - \delta) + ci_R(t)), \\
\dot{s}_R &= \frac{H(u_R(t) - \theta)(1 - s_R(t))}{\tau} - \frac{s_R(t)}{\tau_i}, \\
\tau \dot{u}_L &= -u_L(t) + H(au_R(t) - bs_R(t - \delta) + ci_L(t)), \\
\dot{s}_L &= \frac{H(u_L(t) - \theta)(1 - s_L(t))}{\tau} - \frac{s_L(t)}{\tau_i},
\end{aligned}
\tag{5.6}
$$

where units u_R and u_L represent the average firing rate of two neural populations encoding sequences of tone inputs with timescale τ. The Heaviside gain function $H(x)$ with activity threshold θ is described in Equation 5.7. Mutual coupling through direct fast excitation has strength a. The delayed, slowly decaying inhibition has timescale τ_i, strength b and delay δ. The model is driven by excitatory inputs $i_R(t)$ and $i_L(t)$ (described below) with strength c. The synaptic variables s_R and s_L describe the time-evolution of the inhibitory dynamics.

$$
H(x) = \begin{cases} 1 & x >= \theta, \\ 0 & otherwise. \end{cases}
\tag{5.7}
$$

The input functions $i_R(t)$ and $i_L(t)$ as defined by Equation 5.8 and Equation 5.9, respectively, are anti-phase periodic square waves (Ferrario and Rankin 2021) (Figure 5.1A).

$$
\begin{aligned}
i_R(t) &= \sum_{k=0}^{\infty} \chi_{I_{high}^k}(t) + (1 - \Delta I) \sum_{k=0}^{\infty} \chi_{I_{low}^k}(t), \\
I_{high}^k &= [2kTR, 2kTR + TD], \\
I_{low}^k &= [(2k + 1)TR, (2k + 1)TR + TD].
\end{aligned}
\tag{5.8}
$$

$$
\begin{aligned}
i_L(t) &= (1 - \Delta I) \sum_{k=0}^{\infty} \chi_{I_{low}^k}(t) + \sum_{k=0}^{\infty} \chi_{I_{high}^k}(t), \\
I_{low}^k &= [2kTR, 2kTR + TD], \\
I_{high}^k &= [(2k+1)TR, (2k+1)TR + TD].
\end{aligned}
\tag{5.9}
$$

Where ΔI represents the intensity difference between high and low amplitude vibratory pulses. χ_I is the standard indicator function over the set I, defined as $\chi_I(t) = 1$ for $t \in I$ and 0 otherwise. The intervals when high and low intensity vibrations are on are respectively given by I_{high}^k and I_{low}^k (see Figure 5.1A). The parameter TD represents the duration of each tone's presentation, and TR is the time between tone onsets (called repetition time; $PR = 1/TR$ is the presentation rate).

Transformation to continuous model for bifurcation analysis

As shown in (Ferrario and Rankin 2021), this system exhibits three different dynamical states relevant to perceptual interpretations of alternating stimuli (Figure 5.3A). The states are distinguishable by the number of threshold crossings per $2TR$ period: (1) both units (u_L and u_R) cross threshold in response to both input pulses (low and high) (total of 4 crossings, corresponds to integration in auditory streaming), (2) the R unit crosses threshold twice and the L unit once (total of 3 crossings, corresponds to bistability in auditory streaming), and (3) both units cross threshold once (total of 2 crossings, corresponds to segregation in auditory streaming).

The states (1) and (3) match the percepts observed in the experiments of tactile rivalry (SIM, AM). However, the state (2) does not have any specific meaning in the tactile domain (Figure 5.3B). So, I am looking for a region in the parameter space that the state (2) does not exist.

The model in Equation 5.6 has been described using a system of DDEs. To be able to perform bifurcation analysis (using `Auto07p`), I need to transform it to a system of ODEs. For this reason, the dynamics of direct inhibitory synapses $s_R(t)$ and $s_L(t)$ is replaced with the dynamics of an indirect synapse (to describe the dynamics of $s_R(t - \delta)$ and $s_L(t - \delta)$). These indirect synapses are modelled by introducing two other synaptic variables $x_R(t)$ and $x_L(t)$ (Rubin and Terman 2000) which their dynamics described with following equations:

$$
\begin{aligned}
\dot{s}_i &= \alpha_s H(u_i - \theta_u)(1 - s_i) - \beta_s s_i, \\
\dot{x}_i &= \epsilon \alpha_x H(s_i - \theta_s)(1 - x_i) - \epsilon \beta_x x_i.
\end{aligned}
\tag{5.10}
$$

Here, α_i and β_i ($i = s, x$) are positive constants and ϵ is small relative to 1. These indirect synapses have the effect of introducing a delay in the synaptic action, and this delay takes place on the slow timescale. Once u_i crosses the threshold θ_u, then s_i will activate. The activation of x_i must wait until s_i crosses the second threshold θ_s, thus introducing a delay.

We can choose $\alpha_s = \frac{1}{\tau}$, $\beta_s = \frac{1}{\tau_i}$, and $\theta_u = \theta$, and fit parameters ϵ, α_x, β_x, and θ_s, so
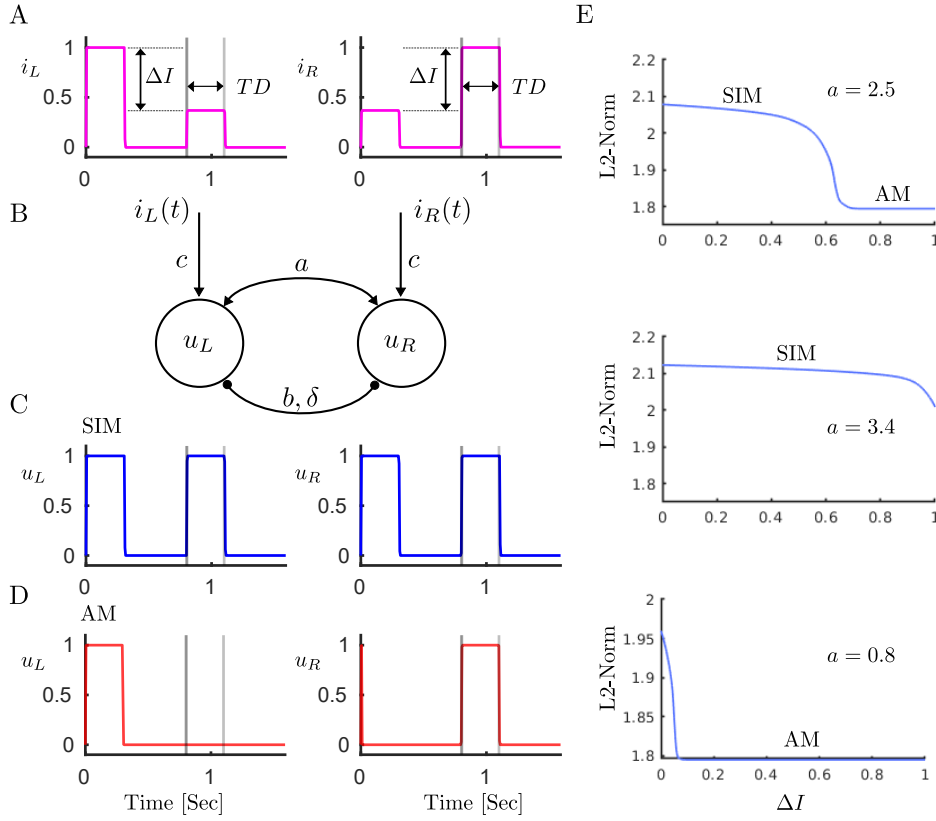
Figure 5.4. **Mechanism of encoding percepts. (A) Stimuli.** One period (length $2TR = 1.6\,s$) of the stimuli to the left and right units consists of one full amplitude pulse (length $TD = 0.3\,s$), and one pulse that its amplitude is ΔI below the intensity of the full amplitude pulse on a logarithmic scale (dB). **(B) Model encoding percepts.** Schematic of the model consisting of mutual fast excitation with strengths a and delayed inhibition with strength b. Inhibition is delayed of the amount D. **(C) SIM percept.** Model can encode percept SIM, when u_L and u_R have full respond to both pulses. **(D) AM percept** is encoded when they only respond to the full amplitude pulse and no response to the low intensity pulse. **(E) Bifurcation analysis with respect to intensity difference** ΔI. One parameter bifurcation diagram sketched at three different values of a, with other parameters fixed at, $b = 2.8$, $c = 5.5$, $\tau = 0.001\,s$, $\tau_i = 0.25\,s$, $\delta = 0.005\,s$, $\epsilon\alpha_x = 50$, $\epsilon\beta_x = 8$, and $\theta_s = 0.22$. Blue curve shows the branch of periodic orbit, in which there is a sharp transition between periodic respond encodes SIM and AM percepts (top panel). For higher values of excitation (middle panel) this boundary moves to the right, and for lower values of excitation (bottom panel) moves to the left.

that the dynamics of $x_R(t)$ and $x_L(t)$ can generate delays equal to δ. Then $s_R(t - \delta)$ and $s_L(t - \delta)$ in Equation 5.6 can be replaced with $x_R(t)$ and $x_L(t)$, respectively. Now the dynamics of the model can be described by the following system of ODEs:

$$
\begin{aligned}
\tau\dot{u}_R &= -u_R + H(au_L - bx_L + ci_R - \theta), \\
\dot{s}_R &= \frac{H(u_R - \theta)(1 - s_R)}{\tau} - \frac{s_R}{\tau_i}, \\
\dot{x}_R &= \epsilon\alpha_x H(s_R - \theta_s)(1 - x_R) - \epsilon\beta_x x_R, \\
\tau\dot{u}_L &= -u_L + H(au_R - bx_R + ci_L - \theta), \\
\dot{s}_L &= \frac{H(u_L - \theta)(1 - s_L)}{\tau} - \frac{s_L}{\tau_i}, \\
\dot{x}_L &= \epsilon\alpha_x H(s_L - \theta_s)(1 - x_L) - \epsilon\beta_x x_L.
\end{aligned}
\tag{5.11}
$$

Stage 2 - Bifurcation analysis

Bifurcation analysis of the second stage with respect to intensity difference ΔI have been shown in Figure 5.4. The left and the right units receive inputs i_L and i_R, which are antiphase sequences of high and low amplitude pulses (ΔI below the full amplitude pulse) with duration TD (Figure 5.4A). There are reciprocal excitatory (with strength a) and inhibitory (with strength b) connections between the two units (Figure 5.4B). Population activities u_L and u_R can encode percept SIM, when u_L and u_R have full respond to both pulses (Figure 5.4C). AM percept is encoded when they only respond to the full amplitude pulse and no response to the low intensity pulse (Figure 5.4D). One parameter bifurcation diagram sketched at three different values of mutual excitation a, with other parameters fixed ($b = 2.8$, $c = 5.5$). Blue curve shows the branch of periodic orbit, in which there is a sharp transition between periodic responses encoding the SIM and AM percepts (top panel in Figure 5.4E). The boundary between these two dynamical behaviours moves to the right with higher values of excitation (middle panel), and to the left with lower values of excitation (bottom panel).

5.2.3. Full tactile rivalry model

To present the model of tactile rivalry, the model described for encoding the alternations at the first stage is incorporated with the model described for encoding the percepts at the second stage (Figure 5.1C). The unites ν_R and ν_L in the first stage make inter- and intra-hemispheric inhibitory connections with the units u_R and u_L in the second stage.

$$
\begin{aligned}
\tau_\nu \dot{\nu}_R &= -\nu_R + N_\infty \left(w\nu_R - ga_R + f(i_L - i_R) + \zeta(t) \right), \\
\tau_a \dot{a}_R &= -a_R + A_\infty \left(\nu_R \right), \\
\tau_\nu \dot{\nu}_L &= -\nu_L + N_\infty \left(w\nu_L - ga_L + f(i_R - i_L) + \zeta(t) \right), \\
\tau_a \dot{a}_L &= -a_L + A_\infty \left(\nu_L \right), \\
\tau \dot{u}_R &= -u_R + H(au_L - bx_L - d(\nu_R + \nu_L) + ci_R - \theta), \\
\dot{s}_R &= \frac{H(u_R - \theta)(1 - s_R)}{\tau} - \frac{s_R}{\tau_i}, \\
\dot{x}_R &= \epsilon \alpha_x H(s_R - \theta_s)(1 - x_R) - \epsilon \beta_x x_R, \\
\tau \dot{u}_L &= -u_L + H(au_R - bx_R - d(\nu_R + \nu_L) + ci_L - \theta), \\
\dot{s}_L &= \frac{H(u_L - \theta)(1 - s_L)}{\tau} - \frac{s_L}{\tau_i}, \\
\dot{x}_L &= \epsilon \alpha_x H(s_L - \theta_s)(1 - x_L) - \epsilon \beta_x x_L.
\end{aligned}
\tag{5.12}
$$

Where d is the strength of inhibitory connections between the first and the second stage.

5.2.4. Simplified tactile rivalry model

As the inputs (D_R and D_L) are anti-phase and there is also symmetry in the first stage of the tactile rivalry, the model can be simplified, and units ν_R and ν_L can be replaced by
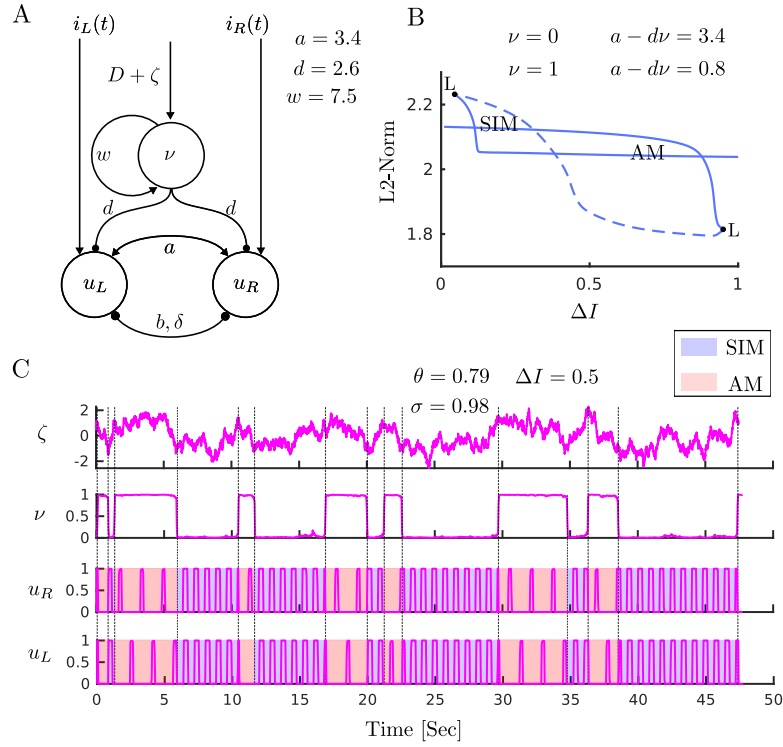
Figure 5.5. **Mechanism of perceptual alternations. (A) Simplified model of tactile rivalry.** The adapting recurrent model (Figure 5.2) makes inhibitory connections with strength d to the model encoding the percepts (Figure 5.4). **(B) Bifurcation analysis with respect to intensity difference ΔI.** There is a region of bistability between two fold of limit cycle bifurcation points (L). Branches of periodic orbits associated with SIM and AM percepts coexist at this interval. **(C) Time histories of model responses.** Population activities are simulated for 50 s at $\Delta I = 0.5$. Noise realization (top panel), UP/DOWN alternations of the first stage unit driven by noise (second panel, $g = 0$), firing activities of the second stage unit (two bottom panels). Perceptual switching times are shown between SIM (blue) and AM (red) with dashed lines. Other parameters are $d = 0.8$, $\tau_\nu = 0.9\,s$

one adapting recurrent model with input D (Figure 5.7D).

$$D = f(\Delta I). \tag{5.13}$$

Where ΔI is a positive constant, and f is a nonlinearity which should be determined. The simplified tactile rivalry model is described by;

$$
\begin{aligned}
\tau_\nu \dot{\nu} &= -\nu + N_\infty \left(w\nu - ga + D + \zeta(t) \right), \\
\tau_a \dot{a} &= -a + A_\infty \left(\nu \right), \\
\tau \dot{u}_R &= -u_R + H(au_L - bx_L + ci_R - d\nu - \theta), \\
\dot{s}_R &= \frac{H(u_R - \theta)(1 - s_R)}{\tau} - \frac{s_R}{\tau_i}, \\
\dot{x}_R &= \epsilon\alpha_x H(s_R - \theta_s)(1 - x_R) - \epsilon\beta_x x_R, \\
\tau \dot{u}_L &= -u_L + H(au_R - bx_R + ci_L - d\nu - \theta), \\
\dot{s}_L &= \frac{H(u_L - \theta)(1 - s_L)}{\tau} - \frac{s_L}{\tau_i}, \\
\dot{x}_L &= \epsilon\alpha_x H(s_L - \theta_s)(1 - x_L) - \epsilon\beta_x x_L.
\end{aligned}
\tag{5.14}
$$

95
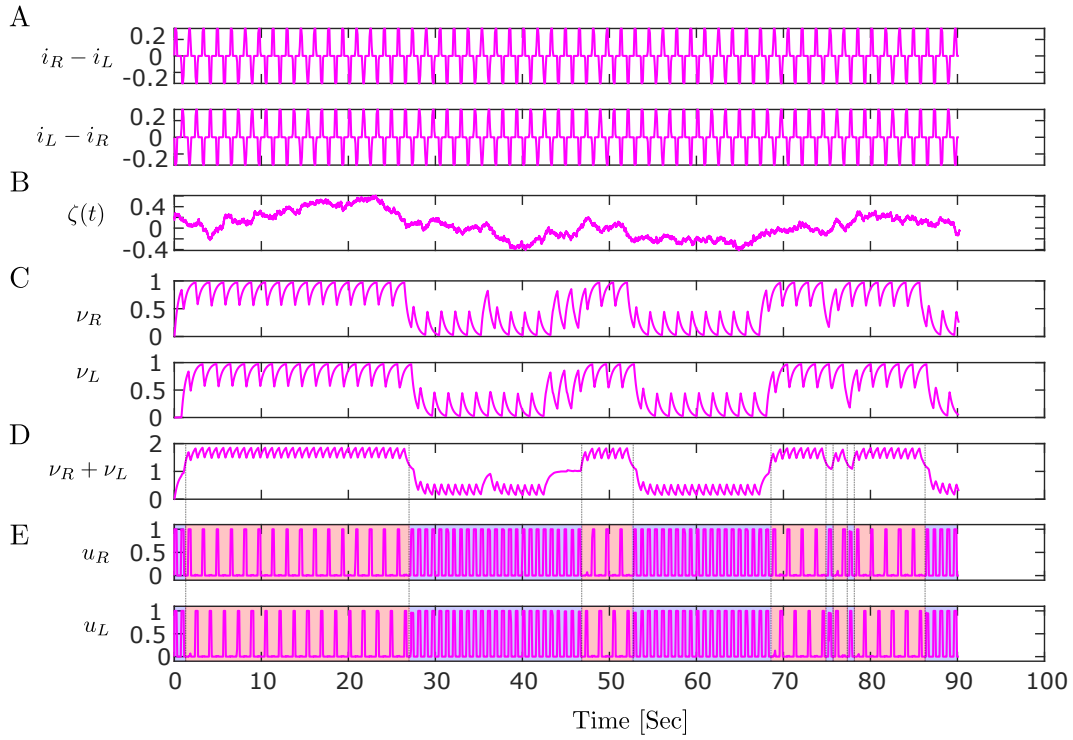
Figure 5.6. **Time histories of tactile rivalry model.** Population firing time responses at $\Delta I = 2\,dB$ for 90 s simulation. **(A)** Net inputs to the left (top panel) and right (bottom units of the first stage. **(B)** Noise with parameters $\sigma = 0.3$ and $\theta = 0.05$ which is added to the first stage inputs. **(C)** Firing activities of the first stage units to the inputs in panel A and noise in panel B. **D** Sum of firing activities of the first stage units, which will be the inhibitory input to the both units of second stage. **E** Firing activities of the second stage units to the inputs in panel D. Perceptual alternation between SIM and AM percepts are seen as transition occurs between DOWN and UP states in panel D. Other parameters are $g = 1.2$, $\tau_\nu = 0.9\,s$

Simplified tactile rivalry model - Bifurcation analysis

Bifurcation analysis of the simplified model of tactile rivalry with respect to intensity difference ΔI is shown in Figure 5.5. The adapting recurrent model in the first stage makes inhibitory connections with strength d to the model encoding the percepts in the second stage (Figure 5.5A). As seen in (Figure 5.2) unit ν has a region of bistability where ν can be either zero or one (when input D lies between two fold bifurcation points). As this unit inhibits u_L and u_R with strength d, this will modify the excitatory net inputs to u_L and u_R units and thus shift the branch of periodic orbits to the right and and to the left (when $\nu = 1$, second stage receives less level of excitation $a_{effective} = a - d\nu$, see Figure 5.7E). This results in bistability between SIM and AM dynamical states shown in the the bifurcation diagram of the whole model (Figure 5.5B). Time histories of this model responses are shown in Figure 5.5C. Population activities are simulated for 50 s at $\Delta I = 0.5$. Top panel shows the noise realization with parameters $\sigma = 0.79$ and $\theta = 0.98$. Perceptual switches between SIM (blue) and AM (red) are seen as ν transition occurs from zero to one or vice versa.

5.3. Results

In this section, I go through a qualitative description of the model presented in subsection 5.2.3, which shows that activity matches perceptual interpretations and alternations observed in tactile rivalry experiment. Later in this section, I will look at the dependence of mean dominance durations on stimulus parameter, and variability of perceptual durations.

5.3.1. Time history simulations of full tactile rivalry model

We first discuss the output from individual simulations of the model and illustrate how the model's firing rate variables can encode the competing percepts and perceptual alternations. The bifurcation analysis for the simplified model (Figure 5.1D) has been investigated in subsubsection 5.2.4, which further explains how the vibrotactile model is designed to encode percepts and generates perceptual alternations.

A time simulation over 90 s of the full tactile rivalry model is shown in Figure 5.6. The units in the first stage are excited by the contra-lateral stimulus and inhibited by the ipsilateral stimulus. Thus, the net inputs to the left and right units of the first stage will be the contra-lateral stimuli minus ipsi-lateral stimuli. These inputs are antiphse pulses with amplitude equal to $\Delta I = 2\,dB$ as shown in Figure 5.6A. Noise is added to these inputs with parameters $\sigma = 0.3$ and $\theta = 0.05$ (Figure 5.6B). Firing activities of these units in first stage in response to the stimuli and noise are shown in Figure 5.6C. In the absent of noise, these adapting recurrent units could oscillate between the UP and DOWN states regularly. However, as seen these oscillations are now driven by both the adaptation and the noise process. Figure 5.6D shows sum of firing activities of the first stage, which is received as an inhibitory input to the both units of second stage. Firing activities of the second stage units to these inputs are shown in Figure 5.6E. Units of the second stage encode the SIM percept (both units fully respond to the high and low intensity pulses in the inputs) when there is low levels of inhibitions from the first stage. When the level of inhibition crosses a threshold, the units in the second stage encode AM percept (both units only fully respond to the high intensity pulses in the inputs). Perceptual alternation between the SIM and AM percepts are seen as transitions between DOWN and UP states occur in the inhibitory inputs (Figure 5.6D&E).

5.3.2. Stimulus parameter dependence

Results from experiments with vibrotactile stimuli demonstrate that Levelt's proposition II holds in tactile domain (Darki and Rankin 2021). Increasing intensity difference, causes the mean dominance of SIM percept to decrease and AM percept to increase. Mean dominance duration for both the perceptual durations from the model and the experiment (Experimental data from (Darki and Rankin 2021)) are plotted against intensity difference (ΔI) in Figure 5.7. The parameters of the noise (σ, θ), time constant of adaptation (τ_a), and nonlinearity in the inputs of the first stage ($D = f(\Delta I)$) must be determined using a genetic algorithm in order to minimise a cost function, and as a result the curves
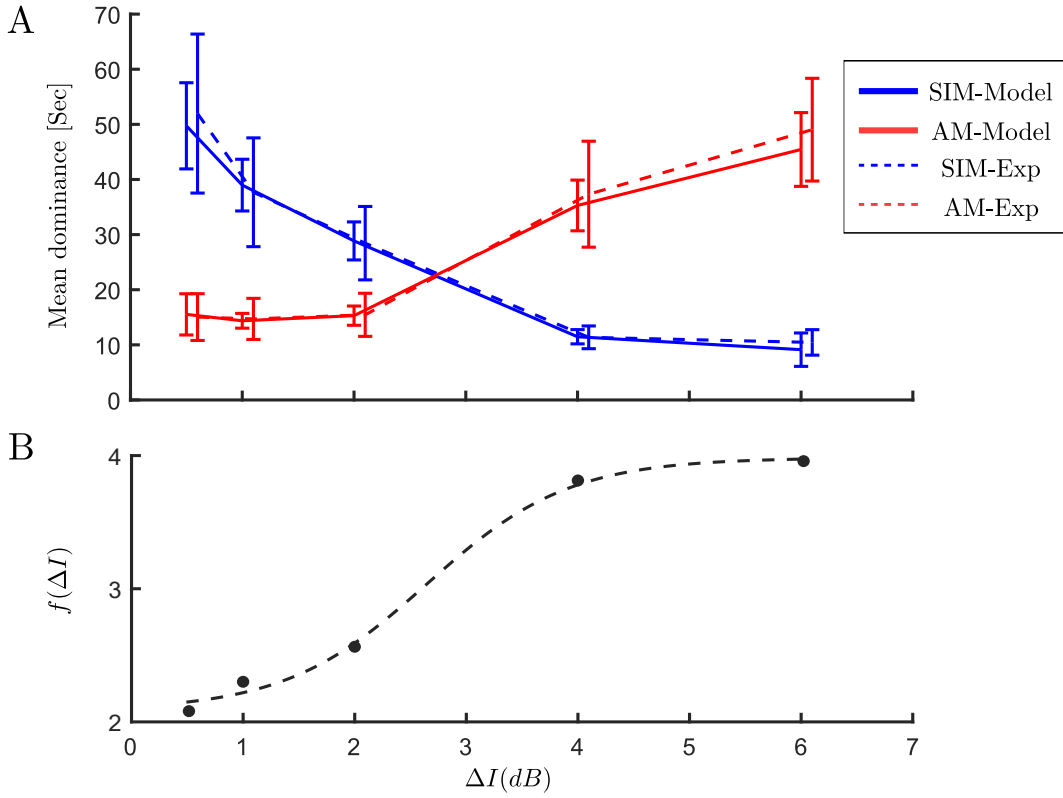
Figure 5.7. **Levelt's proposition II. (A)** Experimental data are dashed curves and computational data from the model are solid curves with data points at different values of intensity difference $\Delta I = 0.5, 1, 2, 4, 6$ on the x-axis, error bars show standard error of the mean. Mean dominance duration of the SIM percept (blue) increase as the intensity difference increase, while opposite effect is observed for the AM percept (red). **(B)** Nonlinearity in the inputs of the first stage $(D = f(\Delta I))$ are determined using a algorithm optimisation method. Dashed black curve is the best fit for an offset and scaled sigmoid nonlinearity.

from the model simulations fit to the curves from the experimental data. To find the nonlinear function $f(\Delta I)$, I first estimated some points of it at the experimental conditions $(\Delta I = 0.5, 1, 2, 4, 6)$ using a genetic algorithm $(f(0.5) = 2.16, f(1) = 2.3, f(2) = 2.6, f(4) = 3.75, f(6) = 3.92$ with $\theta = 0.05, \sigma = 0.3, \tau_a = 5\,s)$. Having these points, I showed an offset and scaled sigmoid function like;

$$f(x) = f_0 + \frac{f_1}{1 + \exp(-r(x - x_0))}, \tag{5.15}$$

with parameters: $f_0 = 1.25$ (offset), $f_1 = 1.80$ (scale), $r = 1.57$ (slope), $x_0 = 2.64$ (threshold), fits best to these points.

5.3.3. Variability of perceptual durations

The distributions of normalized perceptual durations from the model and from the experiment are shown in Figure 5.8A&B. These distributions were compared with the gamma and log-normal distributions using a one-way Kolmogorov-Smirnov (KS) test. The null hypothesis is that the test data are drawn from the standard distribution and a significant result $(p < .05)$ indicates that the test data are not drawn from the comparison distribution. The result of one-way KS tests shows that the results produced by simulation of the tactile rivalry model best fit by a log-normal distribution, however, these results are not
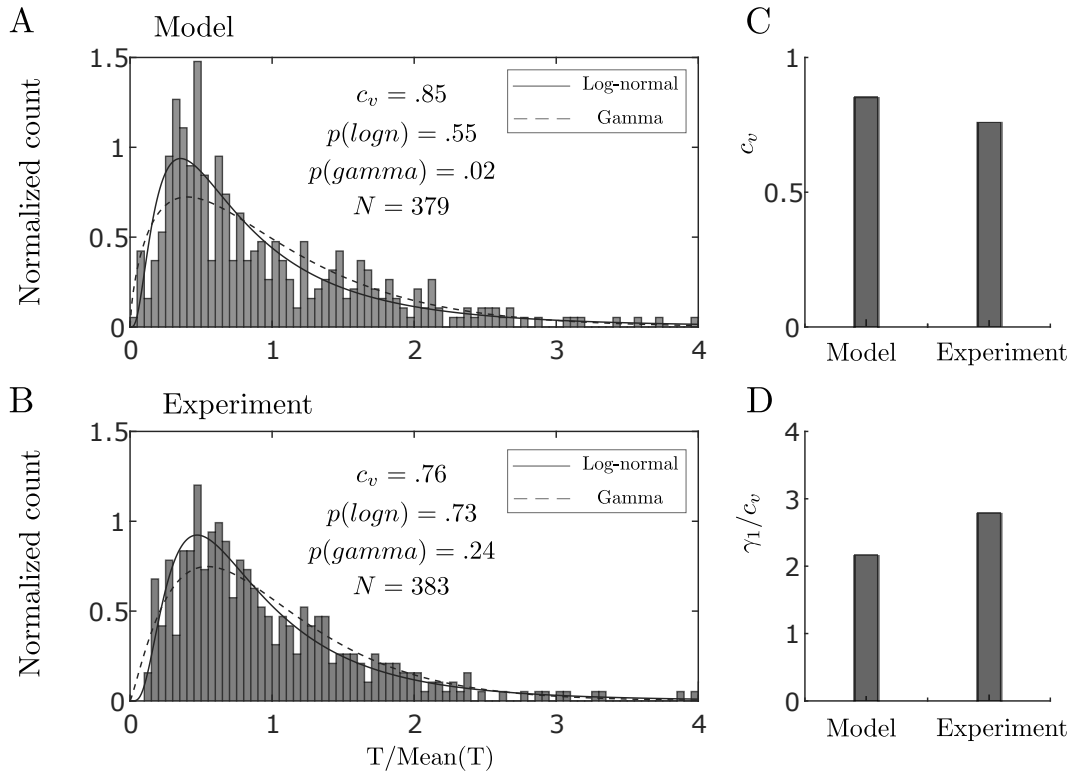
Figure 5.8. **Statistics of dominance durations. (A) Model.** Histogram of 379 durations from model simulations at $\Delta I = 2\,dB$ combined across perceptual type after normalising by the mean. Solid and dashed curves show the estimated log-normal and gamma distribution, respectively. P-values are from one-way KS test. **(B) Experiment.** Histogram of normalized perceptual durations combined across participants and percept type after normalization by the mean, for experimental conditions close to equidominance ($\Delta I = 2\,dB$). **(C) Scaling property.** Coefficient of variation (c_v) and **(D)** skewness divided by coefficient of variation ($\gamma 1/c_v$) computed for distributions from the model and the experiment at intensity difference $\Delta I = 2\,dB$.

comparable with gamma distribution ($p(gamma) < .05$).

To assess how well tactile rivalry model conforms to the scaling property, the statistical characteristics are compared across the model and the experiments. A scaling property obtains if the coefficient of variation c_v and ratio of skewness and coefficient of variation γ_1/c_v are constant. As Figure 5.8C&D shows coefficient of variation for the distribution from the model is $c_v = .85$, and the ratio of skewness and coefficient of variation is $\gamma_1/c_v = 2.17$, which are comparable to the corresponding values from experiment ($c_v = .76$, $\gamma_1/c_v = 2.79$), see subsection 5.4.3.

5.4. Discussion

5.4.1. Summary

Here, a two-stage model of tactile rivalry is introduced that is able to produce perceptual alternations and encodes two percepts observed in tactile rivalry experiments. Bifurcation analysis was used to tune model parameters for the first stage to operate within bistable or oscillatory regime. And the second stage model parameters are tuned to operate within a range where direct transitions between SIM and AM are possible. Other model parameters have been estimated through a genetic algorithm with a cost function to minimise the

differences between the experimental and computational mean dominance curves with respect to intensity difference. The powerful combination of bifurcation analysis to tune certain features of the model, along with optimisation tools allows for the design of a model that captures many features from the experiments of tactile rivalry.

5.4.2. Physiological basis of tactile rivalry model

The somatosensory cortex consists of several neighbouring, functionally distinct areas whose interconnections are complex and only partially understood. S1 and S2 are two major areas of the somatosensory cortex. The most anterior (forward) of S1's four strips is known as area 3a, the most posterior (rear) strip is known as area 2, areas 3b and 1 lay in between (Figure 1.6). The model at the first stage receives contra-lateral excitation and ipsi-lateral inhibition, assumed to be tactile nerve fibre responses to the right and left hand stimuli. Neural populations in the first stage could be located somewhere in somatosensory pathway between the brainstem nuclei (where the right and left afferent fibres cross over) and area 3b of primary somatosensory cortex (see Figure 1.5).

In the model, neural populations in the first stage make inter- and intra-hemispheric inhibitory connections with the neural populations in the second stage. Several studies have reported evidence for interhemispheric interactions in anterior parietal cortex during bimanual stimulation in humans (Krubitzer and Kaas 1990; Reed et al. 2011). In area 3b of monkeys, interhemispheric interactions have been described as primarily suppressive, in that simultaneous tactile stimulation of both hands suppresses neural activity in area 3b measured on one side through optical imaging (Tommerdahl et al. 2006).

Neurons in area 3b of primary somatosensory cortex have been characterized using linear spatial receptive fields with spatially separated excitatory and inhibitory regions (Delhaye et al. 2011). In addition to inhibitory component flanking the excitatory one, receptive fields tend to also comprise an inhibitory component co-localized with the excitatory field but delayed by 20 to 30 ms (Gardner and Costanzo 1980; DiCarlo and Johnson 2000). This receptive field structure results in an initial excitatory drive that is followed by an inhibitory one, rendering the neuron less excitable for a period of time (Delhaye et al. 2011). Considering these facts, the existence of intra-cortical fast excitation and delayed inhibition in the model (a delay of 5 ms is considered in the model, which is comparable to the delays observed in area 3b) can account for these excitatory and lagged inhibitory components of receptive fields which suggest the neural populations at the second stage are probably located within area 3b of the primary somatosensory cortex. Neurons in areas 1 and 2 (higher processing areas within S1), in contrast to their counterparts in area 3b, tend to have larger and more complex receptive fields and also exhibit more complex feature selectivity (Iwamura and Tanaka 1978; Bensmaia et al. 2008).

5.4.3. Stochastic influences on perceptual switching

In neural competition models, noise and adaptation processes are two possible switching mechanisms that describe the alternating behaviours (Moreno-Bote et al. 2007; Chholak

et al. 2020). In consideration of the experimental constraints on the statistics of alternations (mean of the dominance durations and their coefficient of variation and correlations between successive durations), the models must operate within a balance between the noise and adaptation strength (Shpiro et al. 2009). In several competition models, alternations are possible over large regions of parameter space, but the experimental constraints are satisfied in only a restricted domain, the region of relevance. In order to produce the statistical characteristics consistent with bistable perception experiments, precise tuning of the system's parameters is necessary (Shpiro et al. 2009).

Choice of stochastic process to reproduce stochastic characteristics of perceptual rivalry including the scaling property and the short-tailed skewness of reversal time distributions has recently been under investigation (Cao et al. 2014). It has also been shown that a generalized Ehrenfest stochastic process can reproduce both the scaling property and the short-tailed skewness of reversal time distributions (Cao et al. 2016). In this study, I used Ornstein-Uhlenbeck process, and the results produced by simulation of the tactile rivalry model best fit by a log-normal distribution, but not with a gamma distribution. On the other hand, the coefficient of variation and the ratio of skewness and coefficient of variation for the distribution from the model are comparable to the corresponding values from experiment. Other choices of the stochastic process can lead to different results than what was observed here. Further investigation of the stochastic processes in the model should also look at correlations between successive durations.

5.4.4. Future work, Levelt's proposition IV

In this study, I only investigated Levelt's proposition II, which consider the relation between dominant perceptual durations and asymmetric variation of intensity difference. Further experimental work needs to be done to prove Levelt's proposition IV also extents to tactile rivalry. Once I have the experimental results, I can improve the model to also produce consistent results with Levelt's proposition IV.

There was also lack of experimental work that investigate the effects of other features of the stimuli such as presentation rate (PR) and tone durations (TD). However, the bifurcation analysis with periodic forcing framework that presented here can be used to predict how the experimental result may be affected by the variation of these stimulus parameters.

The model presented here works with the simple tactile rivalry stimuli which was presented on two locations on both hands. This model can be further developed to look at more complex stimuli such as tactile motion quartet which is presented at four locations on the skin.

5.4.5. Conclusion

Earlier experimental work showed that perceptual rivalry extends to the tactile domain and common characteristics of multistable phenomenon also persist with vibrotactile stimuli. This study presents a mathematical model for tactile rivalry based on physiological facts

of somatosensory processing. By accurately tuning the parameters, this model produces the general characteristics of perceptual rivalry including Levelt's proposition, short-tailed skewness of reversal time distributions and the scaling property. As I discussed, putative neural populations of the first stage could be located early in the somatosensory pathway at brainstem nuclei, and the neural populations of the second stage could be located within area 3b of the primary somatosensory cortex.

6. Conclusions and future work

Our brain receives only a restricted amount of information about the world around us which are often fragmentary, conflicting or even ambiguous. In such conditions, our perceptual system cannot produce a stable unambiguous percept, especially if the sensory information is equally compatible with different perceptual interpretations. With no additional cues are available to allow perception to converge to a unique interpretation, perception alternates spontaneously every few seconds between two (bistable) or more (multistable) interpretations of the same sensory input.

Multistable perception can help us understand the intrinsic neural processes that generate a unified and coherent experience of the world. For decades, the neural mechanisms of perceptual rivalry, and where the ambiguity resolve in sensory processing hierarchy have been under intense investigation. Two explanatory approaches argue if multistable perception arises from interactions between low-level (sensory) or high-level (cognitive) processes. Experimental studies together with powerful tools such as mathematical modelling and bifurcation analysis have been utilized to describe the neural dynamics and structures for this phenomenon. However, a theory explaining all empirical findings is still missing to date.

6.1. Mathematical analysis of binocular rivalry models

Most theoretical and empirical studies have investigated visual multistability. However, there are striking similarities with comparable phenomena in other sensory domains (e.g. auditory streaming and tactile multistability). Thus the same or similar mechanisms involved in visual multistable perception might also have a role in other sensory domains. Considering this fact, I have started my analysis with models of binocular rivalry (see Chapter 2 for analysis of Adaptation-LC model and Chapter 3 for analysis of the Wilson model).

Earlier work with models of bistable perception has identified parameter ranges with winner-take-all dynamics (WTA), rivalry oscillations (RIV) and simultaneous activity (SIM) (Shpiro et al. 2009; Seely and Chow 2011). Analysis of the Wilson model with fixed inputs showed that the transition from rivalry alternation to the WTA regime is much more complicated than previously thought, and includes complex dynamical behaviours such as MMOs and LAWTA oscillations which was not reported before.

6.2. Perceptual rivalry with periodic stimuli

Several competition models have been proposed to describe binocular rivalry with periodic stimuli, however, interpretation of results from these models are based on a specific set of parameters. Using numerical continuation, I introduced a method to assess whether the existing models of binocular rivalry are valid or not in a specific parameter regime and, more generally, to find the parameter regions where these models work. This research provides a framework for either assessing binocular rivalry models for consistency with empirical results, or for better understanding neural dynamics and the mechanisms necessary to implement a minimal binocular rivalry model.

Using this framework with the Wilson model in Chapter 3, the results show that periodic forcing with high frequency (e.g. 18 Hz, known as flicker) modulates the three main types of behaviours that occur with fixed inputs by the forcing frequency (WTA-Mod, RIV-Mod, SIM-Mod). However, the dynamical behaviour will be different with low frequency periodic forcing (around 1.5Hz, so-called swap), and in addition to WTA-Mod and SIM-Mod, cycle skipping and multi-cycle skipping behaviour exist which can lead to chaotic dynamics. Results of this analysis provides a deeper explanation of how the Wilson model produces slow alternations with the F&S (but not Swap only stimulus).

As discussed in (Brascamp et al. 2013; Li et al. 2017), the Wilson model is only capable of generating slow perceptual alternations with the F&S stimulus, and it fails to do so with blank intervals inserted before each swap, so-called Blank & Swap (B&S) (van Boxtel et al. 2008; Denison and Silver 2012). This reported limitation of the Wilson model could simply be avoided if the parameters had been set in a way that the model operated in a specific regime. These results cast a new light on binocular rivalry with periodic forcing and it is now clear that these two limitations of the Wilson model could be fixed by tuning model parameters.

Our approach for studying perceptual bistability with periodic stimuli is applicable for a range of other stimuli including auditory streaming (Rankin et al. 2015), motion illusions (Vattikuti et al. 2016) and haptic bistability (Carter et al. 2013).

6.3. Tactile rivalry experiments

Earlier studies with tactile stimuli have identified bistability in somatosensation; however the range of spatial and temporal stimulation parameters capable of inducing bistable tactile perception which provides context for comparison across modalities have not been studied so far. In Chapter 4, a simple tactile stimulus is introduced which investigates the effect of varying intensity difference asymmetrically on perceptual durations. The results show that Levelt's proposition II (LVII) and other characteristics of sensory bistability that generalise in vision and auditory sensation extend to the tactile modality. This could be extended to look at other features, e.g., vibration frequency, temporal cues, presentation rate, etc. The dynamics of perceptual bistability are characterised by very similar properties across a wide range of qualitatively different paradigms. This suggests that perceptual

switching may be triggered by some common source across different modalities.

6.4. Tactile rivalry modelling

To the best of my knowledge, there are no models for tactile rivalry. Computational models of perceptual ambiguity have helped significantly with our understanding of other types of bistability. With understanding mechanisms from mathematical analysis of binocular rivalry models, and the tools developed for bifurcation analysis with periodic stimuli, I could present the first model of tactile rivalry. The model presented is able to produce perceptual alternations between two types of perception observed in the experiments with tactile stimuli, and is also compatible with the physiological evidence and structure of somatosensation. By accurately tuning the model parameters through combination of bifurcation analysis and optimisation tools, this model produces the general characteristics of perceptual rivalry including Levelt's proposition, short-tailed skewness of reversal time distributions and scaling property. As discussed in subsection 5.4.2, neural populations associated with the first stage are possibly located early in the somatosensory pathway at brainstem nuclei, and the neural populations associated with the second stage are possibly located within area 3b of the primary somatosensory cortex.

6.5. Suggesting future work

The deterministic and stochastic factors can both influence the timing of perceptual decisions, as the gradual accumulation of sensory evidence (deterministic) is modulated by sensory and/or internal noise (stochastic) (Cao et al. 2016). Astonishingly, the distribution of reversal times maintains a characteristic, gamma-like shape, even though mean reversal times vary widely between observers, displays, and input levels. Moreover, the distribution in question is considerably more variable (wider) and less skewed (shorter-tailed) than typical choice-time distributions) (Cao et al. 2016; Shpiro et al. 2009). The constancy of distribution shape constitutes a scaling property, as it implies that higher moments scale as appropriate powers of the mean. Despite a long tradition of perceptual competition research there are still questions about the neuro-computational basis and the underlying mechanisms of this phenomenon.

Mathematical models of these phenomena focus on the neural processing of sensory information, the dependence of average switching times on stimulus parameters and the statistical distribution of times between switches. In neuronal competition models, noise and adaptation processes are two possible switching mechanisms that describe the alternating behaviours. In consideration of the experimental constraints on the statistics of the alternations (mean of the dominance durations and their coefficient of variation and correlations between successive durations), the models must operate within a balance between the noise and adaptation strength (Shpiro et al. 2009). It has also been shown that a generalized Ehrenfest stochastic process can reproduce both the scaling property and the short-tailed skewness of reversal time distributions (Cao et al. 2016). However, there

is currently no presented modelling approach that can assess the role of stochasticity in deterministic dynamical systems models for perceptual competition.

Noise plays an important role in perceptual competition, and this is often considered in models (Li et al. 2017). The introduction of noise to timescale-separated dynamical systems (like competition models) can introduce dynamics that are not present in the deterministic case, especially local to bifurcations (Berglund and Gentz 2008). In my earlier study, I found exotic dynamics including relaxation oscillations and mixed mode oscillations in a deterministic model of rivalry (Darki and Rankin 2021). Interactions between noise and the dynamics may modify the exotic dynamics in the deterministic model in an interesting way and could either expand the parameter regions where these states persist or wash out the complex dynamics.

It would be of interest to see how these complex dynamics (MMOs & LAWTA) will interact with noise. Further analysis is needed to check whether these dynamical regimes persist or are modified in the presence of noise.

Appendices

A. Appendix1

Table A.1. Two-way repeated measure ANOVA of proportion of **both percept types (AM, SIM)** with respect to intensity difference (ΔI) and percept type. Analysis shows a significant effect of ΔI:percept on the proportion

Source	df_{num}	df_{den}	F	p	ges	$p[GG]$
Percept	1	41	0.09	.76	.001	
ΔI	4	164	0.91	.46	.01	
ΔI:Percept	4	164	201.85	$< .001$	.71	$< .001$

Table A.2. One-way repeated measure ANOVA of proportion of **SIM** perception with respect to intensity difference (ΔI). Analysis shows a significant effect of the intensity difference on the proportion

Source	df_{num}	df_{den}	F	p	ges	p[GG]
ΔI	4	164	114.01	$< .001$	.07	$< .001$

Table A.3. Pairwise ttest, with Bonferoni corrected p-values, on the proportion of **SIM** perception with respect to intensity difference (ΔI)

	$\Delta I = 0.5$	$\Delta I = 1$	$\Delta I = 2$	$\Delta I = 4$
$\Delta I = 1$	.23	-	-	-
$\Delta I = 2$	.001	.45	-	-
$\Delta I = 4$	$< .001$	$< .001$	$< .001$	-
$\Delta I = 6$	$< .001$	$< .001$	$< .001$	.06

Table A.4. One-way repeated measure ANOVA of proportion of **AM** perception with respect to intensity difference (ΔI). Analysis shows a significant effect of the intensity difference on the proportion

Source	df_{num}	df_{den}	F	p	ges	p[GG]
ΔI	4	164	146.10	$< .001$	.07	

Table A.5. Pairwise ttest, with Bonferoni corrected p-values, on the proportions of **AM** perception with respect to intensity difference (ΔI)

	$\Delta I = 0.5$	$\Delta I = 1$	$\Delta I = 2$	$\Delta I = 4$
$\Delta I = 1$	.08	-	-	-
$\Delta I = 2$	.01	1.00	-	-
$\Delta I = 4$	$< .001$	$< .001$	$< .001$	-
$\Delta I = 6$	$< .001$	$< .001$	$< .001$	$< .001$

Table A.6. One-way repeated measure ANOVA of frequency of **both percept types (AM, SIM)** with respect to intensity difference (ΔI). Analysis shows a significant effect of ΔI on the frequency

Source	df_{num}	df_{den}	F	p	ges	p[GG]
ΔI	4	176	15.98	$< .001$	.12	$< .001$

Table A.7. Pairwise ttest, with Bonferoni corrected p-values, on the frequency of **both percept types (AM, SIM)** with respect to intensity difference (ΔI)

	$\Delta I = 0.5$	$\Delta I = 1$	$\Delta I = 2$	$\Delta I = 4$
$\Delta I = 1$	1.00	-	-	-
$\Delta I = 2$	$< .001$	.02	-	-
$\Delta I = 4$	1.00	1.00	.003	-
$\Delta I = 6$	.82	.82	$< .001$	1.00

Table A.8. One-way repeated measure ANOVA of the first five phase with respect to phase number. Analysis shows there is no significant effect of phase number on the duration of phases

Source	df_{num}	df_{den}	F	p	ges	p[GG]
phase	4	420	.71	.59	.005	.58
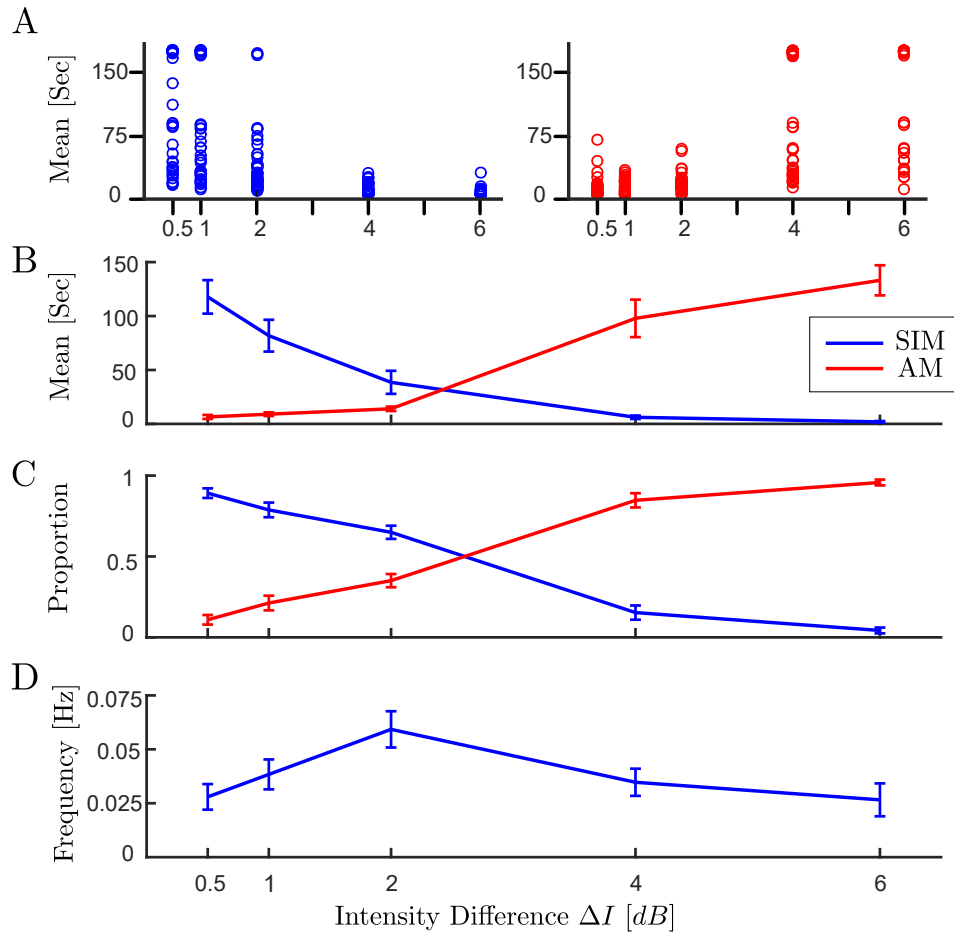
Figure A.1. Levelt's proposition II (A) The distribution of dominance durations at each trial with different experimental conditions (45 observation per experimental condition). (B) Mean dominance duration, (C) proportion of dominance for each percept type, (D) alternation rate, as a function of intensity difference (ΔI)
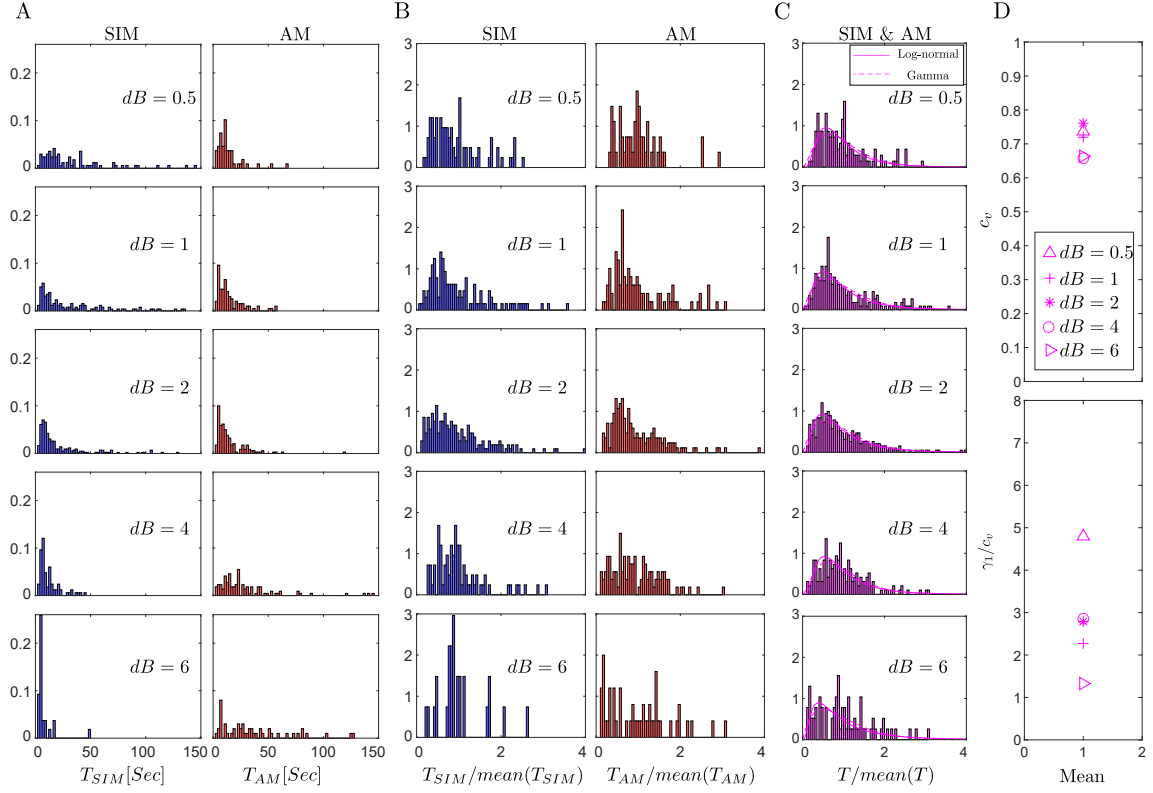
Figure A.2. **(A)** Histograms of perceptual phases for SIM (blue) and AM (red) percepts for each experimental condition. **(B)** Histograms of normalized perceptual phases. For normalization all samples of each histogram in panel (A) divided by its mean. **(C)** Normalized phase durations combined across the two percepts for each experimental condition. Solid and dashed curves show the estimated log-normal and gamma distribution respectively. **(D)** Coefficient of variation (c_v) and skewness divided by coefficient of variation (γ_1/c_v) for histograms in panel (C) with different experimental conditions ($\Delta I = 0.5, 1, 2, 4, 6\, dB$)
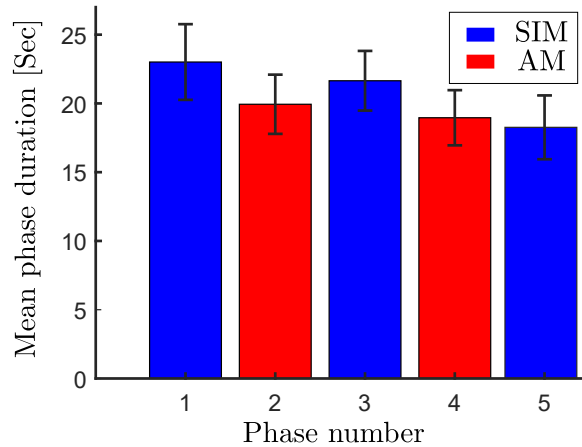
Figure A.3. Comparing the first five perceptual phases. As the result of one-way ANOVA analysis shows (Table 8), there is no significant difference between means of consecutive phase durations. Durations were averaged across all the trials in which participants had experienced five or more successive phases ($N = 106$)

Bibliography

Baker, D. H., Meese, T. S., and Summers, R. J. (2007). Psychophysical evidence for two routes to suppression before binocular summation of signals in human vision. *Neuroscience*, 146(1):435–448.

Barniv, D. and Nelken, I. (2015). Auditory streaming as an online classification process with evidence accumulation. *PloS one*, 10(12).

Bensmaia, S. J., Denchev, P. V., Dammann, J. F., Craig, J. C., and Hsiao, S. S. (2008). The representation of stimulus orientation in the early stages of somatosensory processing. *Journal of Neuroscience*, 28(3):776–786.

Berglund, N. and Gentz, B. (2008). Stochastic dynamic bifurcations and excitability. *Stochastic methods in Neuroscience*, pages 64–93.

Birznieks, I. and Vickery, R. M. (2017). Spike timing matters in novel neuronal code involved in vibrotactile frequency perception. *Current Biology*, 27(10):1485–1490.

Blake, R. (1989). A neural theory of binocular rivalry. *Psychological review*, 96(1):145.

Blake, R. and Logothetis, N. K. (2002). Visual competition. *Nature Reviews Neuroscience*, 3(1):13.

Blake, R. and Sekuler, R. (2006). *Perception*. McGraw-Hill higher education. McGraw-Hill Companies,Incorporated.

Blake, R., Westendorf, D. H., and Overton, R. (1980). What is suppressed during binocular rivalry? *Perception*, 9(2):223–231.

Boring, E. G. (1942). Sensation and perception in the history of experimental psychology.

Brascamp, J., Klink, P., and Levelt, W. J. (2015). The 'laws' of binocular rivalry: 50 years of levelt's propositions. *Vision research*, 109:20–37.

Brascamp, J., Sohn, H., Lee, S.-H., and Blake, R. (2013). A monocular contribution to stimulus rivalry. *Proceedings of the National Academy of Sciences*, 110(21):8337–8344.

Brascamp, J. W., Van Ee, R., Pestman, W. R., and Van Den Berg, A. V. (2005). Distributions of alternation rates in various forms of bistable perception. *Journal of Vision*, 5(4):1–1.

Bruce, V., Green, P. R., and Georgeson, M. A. (2003). *Visual perception: Physiology, psychology, & ecology*. Psychology Press.

Burtt, H. E. (1917). Tactual illusions of movement. *Journal of Experimental Psychology*, 2(5):371.

Byrne, Á., Rinzel, J., and Rankin, J. (2019). Auditory streaming and bistability paradigm extended to a dynamic environment. *Hearing research*, 383:107807.

Cao, R., Braun, J., and Mattia, M. (2014). Stochastic accumulation by cortical columns may explain the scalar property of multistable perception. *Physical review letters*, 113(9):098103.

Cao, R., Pastukhov, A., Aleshin, S., Mattia, M., and Braun, J. (2021). Binocular rivalry reveals an out-of-equilibrium neural dynamics suited for decision-making. *Elife*, 10:e61581.

Cao, R., Pastukhov, A., Mattia, M., and Braun, J. (2016). Collective activity of many bistable assemblies reproduces characteristic dynamics of multistable perception. *Journal of Neuroscience*, 36(26):6957–6972.

Carter, O., Konkle, T., Wang, Q., Hayward, V., and Moore, C. (2008). Tactile rivalry demonstrated with an ambiguous apparent-motion quartet. *Current Biology*, 18(14):1050–1054.

Carter, T., Seah, S. A., Long, B., Drinkwater, B., and Subramanian, S. (2013). Ultrahaptics: multi-point mid-air haptic feedback for touch surfaces. In *Proceedings of the 26th annual ACM symposium on User interface software and technology*, pages 505–514. ACM.

Chholak, P., Hramov, A. E., and Pisarchik, A. N. (2020). An advanced perception model combining brain noise and adaptation. *Nonlinear Dynamics*, 100(4):3695–3709.

Clarey, J. C., Tweedale, R., and Calford, M. B. (1996). Interhemispheric modulation of somatosensory receptive fields: evidence for plasticity in primary somatosensory cortex. *Cerebral Cortex*, 6(2):196–206.

Conrad, V., Vitello, M. P., and Noppeney, U. (2012). Interactions between apparent motion rivalry in vision and touch. *Psychological science*, 23(8):940–948.

Curtu, R. (2010). Singular hopf bifurcations and mixed-mode oscillations in a two-cell inhibitory neural network. *Physica D: Nonlinear Phenomena*, 239(9):504–514.

Curtu, R. and Rubin, J. (2011). Interaction of canard and singular hopf mechanisms in a neural model. *SIAM Journal on Applied Dynamical Systems*, 10(4):1443–1479.

Curtu, R., Shpiro, A., Rubin, N., and Rinzel, J. (2008). Mechanisms for frequency control in neuronal competition models. *SIAM journal on applied dynamical systems*, 7(2):609–649.

Darki, F. and Rankin, J. (2021). Perceptual rivalry with vibrotactile stimuli. *Attention, Perception, & Psychophysics*, pages 1–12.

Delhaye, B. P., Long, K. H., and Bensmaia, S. J. (2011). Neural basis of touch and proprioception in primate cortex. *Comprehensive Physiology*, 8(4):1575–1602.

Denham, S. L., Farkas, D., Van Ee, R., Taranu, M., Kocsis, Z., Wimmer, M., Carmel, D., and Winkler, I. (2018). Similar but separate systems underlie perceptual bistability in vision and audition. *Scientific reports*, 8(1):1–10.

Denison, R. N. and Silver, M. A. (2012). Distinct contributions of the magnocellular and parvocellular visual streams to perceptual selection. *Journal of Cognitive Neuroscience*, 24(1):246–259.

Deutsch, D. (1974). An auditory illusion. *Nature*, 251(5473):307–309.

DiCarlo, J. J. and Johnson, K. O. (2000). Spatial and temporal structure of receptive fields in primate somatosensory area 3b: effects of stimulus scanning direction and orientation. *Journal of Neuroscience*, 20(1):495–510.

Doedel, E. J., Fairgrieve, T. F., Sandstede, B., Champneys, A. R., Kuznetsov, Y. A., and Wang, X. (2007). Auto-07p: Continuation and bifurcation software for ordinary differential equations (software package). *(software package)*.

Dragoi, V. and Tsuchitani, C. (2016). Chapter 15: visual processing: cortical pathways. *Neuroscience Online, UTHealth, accessed Jun*, 29.

Ermentrout, B. and Wechselberger, M. (2009). Canards, clusters, and synchronization in a weakly coupled interneuron model. *SIAM Journal on Applied Dynamical Systems*, 8(1):253–278.

Eshel, N., Ruff, C. C., Spitzer, B., Blankenburg, F., and Driver, J. (2010). Effects of parietal tms on somatosensory judgments challenge interhemispheric rivalry accounts. *Neuropsychologia*, 48(12):3470–3481.

Faul, F., Erdfelder, E., Lang, A., and Buchner, A. A flexible statistical power analysis program for the social, behavioral and biomedical sciences. *Behavior Research Methods*.

Ferrario, A. and Rankin, J. (2021). Auditory streaming emerges from fast excitation and slow delayed inhibition. *The Journal of Mathematical Neuroscience*, 11(1):1–32.

Ferrington, D. and Rowe, M. (1980). Differential contributions to coding of cutaneous vibratory information by cortical somatosensory areas i and ii. *Journal of Neurophysiology*, 43(2):310–331.

Fox, R. and Herrmann, J. (1967). Stochastic properties of binocular rivalry alternations. *Perception & psychophysics*, 2(9):432–436.

Freeman, A. W. (2005). Multistage model for binocular rivalry. *Journal of Neurophysiology*, 94(6):4412–4420.

Freeman, A. W. and Johnson, K. O. (1982a). Cutaneous mechanoreceptors in macaque

monkey: temporal discharge patterns evoked by vibration, and a receptor model. *The Journal of physiology*, 323(1):21–41.

Freeman, A. W. and Johnson, K. O. (1982b). A model accounting for effects of vibratory amplitude on responses of cutaneous mechanoreceptors in macaque monkey. *The Journal of physiology*, 323(1):43–64.

Gardner, E. P. and Costanzo, R. M. (1980). Temporal integration of multiple-point stimuli in primary somatosensory cortical receptive fields of alert monkeys. *Journal of Neurophysiology*, 43(2):444–468.

Gegenfurtner, K. R., Kiper, D. C., and Fenstemaker, S. B. (1996). Processing of color, form, and motion in macaque area v2. *Visual neuroscience*, 13(1):161–172.

Gengerelli, J. (1948). Apparent movement in relation to homonymous and heteronymous stimulation of the cerebral hemispheres. *Journal of Experimental Psychology*, 38(5):592.

Haladjian, H. H., Anstis, S., Wexler, M., and Cavanagh, P. (2020). The tactile quartet: Comparing ambiguous apparent motion in tactile and visual stimuli. *Perception*, 49(1):61–80.

Hämäläinen, H., Hiltunen, J., and Titievskaja, I. (2002). Activation of somatosensory cortical areas varies with attentional state: an fmri study. *Behavioural brain research*, 135(1-2):159–165.

Harvey, M. A., Saal, H. P., Dammann III, J. F., and Bensmaia, S. J. (2013). Multiplexing stimulus information through rate and temporal codes in primate somatosensory cortex. *PLoS Biol*, 11(5):e1001558.

Hlushchuk, Y. and Hari, R. (2006). Transient suppression of ipsilateral primary somatosensory cortex during tactile finger stimulation. *Journal of Neuroscience*, 26(21):5819–5824.

Horton, J. C. and Hocking, D. R. (1996). Intrinsic variability of ocular dominance column periodicity in normal macaque monkeys. *Journal of Neuroscience*, 16(22):7228–7339.

Hupé, J.-M. and Rubin, N. (2003). The dynamics of bi-stable alternation in ambiguous motion displays: a fresh look at plaids. *Vision research*, 43(5):531–548.

Iwamura, Y. and Tanaka, M. (1978). Postcentral neurons in hand region of area 2: their possible role in the form discrimination of tactile objects. *Brain research*.

Iwamura, Y., Taoka, M., and Iriki, A. (2001). Book review: Bilateral activity and callosal connections in the somatosensory cortex. *The Neuroscientist*, 7(5):419–429.

Jayasuriya, S. and Kilpatrick, Z. P. (2012). Effects of time-dependent stimuli in a competitive neural network model of perceptual rivalry. *Bulletin of mathematical biology*, 74(6):1396–1426.

Kastrup, A., Baudewig, J., Schnaudigel, S., Huonker, R., Becker, L., Sohns, J. M.,

Dechent, P., Klingner, C., and Witte, O. W. (2008). Behavioral correlates of negative bold signal changes in the primary somatosensory cortex. *Neuroimage*, 41(4):1364–1371.

Kim, Y.-J., Grabowecky, M., and Suzuki, S. (2006). Stochastic resonance in binocular rivalry. *Vision research*, 46(3):392–406.

Kirman, J. H. (1974). Tactile apparent movement: The effects of interstimulus onset interval and stimulus duration. *Perception & Psychophysics*, 15(1):1–6.

Korvenoja, A., Wikstrom, H., Huttunen, J., Virtanan, J., Laine, P., Aronen, H. J., Seppalainen, A.-M., and Ilmoniemi, R. J. (1995). Activation of ipsilateral primary sensorimotor cortex by median nerve stimulation. *Neuroreport*, 6(18):2589–2593.

Krubitzer, L. A. and Kaas, J. H. (1990). The organization and connections of somatosensory cortex in marmosets. *Journal of Neuroscience*, 10(3):952–974.

Laing, C. R. and Chow, C. C. (2002). A spiking neuron model for binocular rivalry. *Journal of computational neuroscience*, 12(1):39–53.

Lathrop, R. G. (1966). First-order response dependencies at a differential brightness threshold. *Journal of Experimental Psychology*, 72(1):120.

Lederman, S. J. and Jones, L. A. (2011). Tactile and haptic illusions. *IEEE Transactions on Haptics*, 4(4):273–294.

Lederman, S. J. and Klatzky, R. L. (2009). Haptic perception: A tutorial. *Attention, Perception, & Psychophysics*, 71(7):1439–1459.

Lee, S.-H. and Blake, R. (1999). Rival ideas about binocular rivalry. *Vision research*, 39(8):1447–1454.

Lehky, S. R. (1988). An astable multivibrator model of binocular rivalry. *Perception*, 17(2):215–228.

Leopold, D. A. and Logothetis, N. K. (1996). Activity changes in early visual cortex reflect monkeys' percepts during binocular rivalry. *Nature*, 379(6565):549.

Leopold, D. A. and Logothetis, N. K. (1999). Multistable phenomena: changing views in perception. *Trends in cognitive sciences*, 3(7):254–264.

Levelt, W. J. (1965). *On binocular rivalry*. PhD thesis, Van Gorcum Assen.

Levenstein, D., Buzsáki, G., and Rinzel, J. (2019). Nrem sleep in the rodent neocortex and hippocampus reflects excitable dynamics. *Nature communications*, 10(1):1–12.

Li, B., Peterson, M. R., Thompson, J. K., Duong, T., and Freeman, R. D. (2005). Cross-orientation suppression: monoptic and dichoptic mechanisms are different. *Journal of neurophysiology*, 94(2):1645–1650.

Li, H.-H., Rankin, J., Rinzel, J., Carrasco, M., and Heeger, D. J. (2017). Attention model

of binocular rivalry. *Proceedings of the National Academy of Sciences*, 114(30):E6192–E6201.

Liaci, E., Bach, M., van Elst, L. T., Heinrich, S. P., and Kornmeier, J. (2016). Ambiguity in tactile apparent motion perception. *PLoS One*, 11(5).

Logothetis, N. K., Leopold, D. A., and Sheinberg, D. L. (1996). What is rivalling during binocular rivalry? *Nature*, 380(6575):621.

Logothetis, N. K. and Schall, J. D. (1989). Neuronal correlates of subjective visual perception. *Science*, 245(4919):761–763.

Maldjian, J. A., Gottschalk, A., Patel, R. S., Detre, J. A., and Alsop, D. C. (1999). The sensory somatotopic map of the human hand demonstrated at 4 tesla. *Neuroimage*, 10(1):55–62.

Meng, M. and Tong, F. (2004). Can attention selectively bias bistable perception? differences between binocular rivalry and ambiguous figures. *Journal of vision*, 4(7):2–2.

Meso, A. I., Rankin, J., Faugeras, O., Kornprobst, P., and Masson, G. S. (2016). The relative contribution of noise and adaptation to competition during tri-stable motion perception. *Journal of vision*, 16(15):6–6.

Moradi, F. and Heeger, D. J. (2009). Inter-ocular contrast normalization in human visual cortex. *Journal of Vision*, 9(3):13–13.

Moreno-Bote, R., Rinzel, J., and Rubin, N. (2007). Noise-induced alternations in an attractor network model of perceptual bistability. *Journal of Neurophysiology*, 98(3):1125–1139.

Moreno-Bote, R., Shpiro, A., Rinzel, J., and Rubin, N. (2010). Alternation rate in perceptual bistability is maximal at and symmetric around equi-dominance. *Journal of vision*, 10(11):1–1.

Muniak, M. A., Ray, S., Hsiao, S. S., Dammann, J. F., and Bensmaia, S. J. (2007). The neural coding of stimulus intensity: linking the population response of mechanoreceptive afferents with psychophysical behavior. *Journal of Neuroscience*, 27(43):11687–11699.

Najafian, S., Jin, J., and Alonso, J.-M. (2019). Diversity of ocular dominance patterns in visual cortex originates from variations in local cortical retinotopy. *Journal of Neuroscience*, 39(46):9145–9163.

Nihashi, T., Naganawa, S., Sato, C., Kawai, H., Nakamura, T., Fukatsu, H., Ishigaki, T., and Aoki, I. (2005). Contralateral and ipsilateral responses in primary somatosensory cortex following electrical median nerve stimulation—an fmri study. *Clinical Neurophysiology*, 116(4):842–848.

Noachtar, S., Lüders, H. O., Dinner, D. S., and Klem, G. (1997). Ipsilateral median somatosensory evoked potentials recorded from human somatosensory cortex. *Electroencephalography and Clinical Neurophysiology/Evoked Potentials Section*, 104(3):189–198.

Nowacki, J., Osinga, H. M., and Tsaneva-Atanasova, K. (2012). Dynamical systems analysis of spike-adding mechanisms in transient bursts. *The Journal of Mathematical Neuroscience*, 2(1):7.

Polonsky, A., Blake, R., Braun, J., and Heeger, D. J. (2000). Neuronal activity in human primary visual cortex correlates with perception during binocular rivalry. *Nature neuroscience*, 3(11):1153.

Pressnitzer, D. and Hupé, J.-M. (2006). Temporal dynamics of auditory and visual bistability reveal common principles of perceptual organization. *Current biology*, 16(13):1351–1357.

Ramachandran, V. S. and Anstis, S. M. (1983). Perceptual organization in moving patterns. *Nature*, 304(5926):529–531.

Rankin, J., Sussman, E., and Rinzel, J. (2015). Neuromechanistic model of auditory bistability. *PLoS computational biology*, 11(11):e1004555.

Reed, J. L., Qi, H.-X., and Kaas, J. H. (2011). Spatiotemporal properties of neuron response suppression in owl monkey primary somatosensory cortex when stimuli are presented to both hands. *Journal of Neuroscience*, 31(10):3589–3601.

Romo, R. and Salinas, E. (2003). Flutter discrimination: neural codes, perception, memory and decision making. *Nature Reviews Neuroscience*, 4(3):203–218.

Rubin, J. and Terman, D. (2000). Geometric analysis of population rhythms in synaptically coupled neuronal networks. *Neural computation*, 12(3):597–645.

Saal, H. P., Wang, X., and Bensmaia, S. J. (2016). Importance of spike timing in touch: an analogy with hearing? *Current opinion in neurobiology*, 40:142–149.

Salinas, E. (2003). Background synaptic activity as a switch between dynamical states in a network. *Neural computation*, 15(7):1439–1475.

Schnitzler, A., Salmelin, R., Salenius, S., Jousmäki, V., and Hari, R. (1995). Tactile information from the human hand reaches the ipsilateral primary somatosensory cortex. *Neuroscience letters*, 200(1):25–28.

Seely, J. and Chow, C. C. (2011). Role of mutual inhibition in binocular rivalry. *Journal of neurophysiology*, 106(5):2136–2150.

Sengpiel, F., Blakemore, C., and Harrad, R. (1995a). Interocular suppression in the primary visual cortex: a possible neural basis of binocular rivalry. *Vision research*, 35(2):179–195.

Sengpiel, F., Freeman, T., and Blakemore, C. (1995b). Interocular suppression in cat striate cortex is not orientation selective. *Neuroreport*, 6(16):2235–2239.

Sherrick, C. E. (1968). Bilateral apparent haptic movement. *Perception & Psychophysics*, 4(3):159–160.

Sherrick, C. E. and Rogers, R. (1966). Apparent haptic movement. *Perception & Psychophysics*, 1(3):175–180.

Shpiro, A., Curtu, R., Rinzel, J., and Rubin, N. (2007). Dynamical characteristics common to neuronal competition models. *Journal of neurophysiology*, 97(1):462–473.

Shpiro, A., Moreno-Bote, R., Rubin, N., and Rinzel, J. (2009). Balance between noise and adaptation in competition models of perceptual bistability. *Journal of computational neuroscience*, 27(1):37.

Smith, A. T. (2015). Binocular vision: joining up the eyes. *Current Biology*, 25(15):R661–R663.

Sterzer, P., Kleinschmidt, A., and Rees, G. (2009). The neural bases of multistable perception. *Trends in cognitive sciences*, 13(7):310–318.

Talbot, W. H., Darian-Smith, I., Kornhuber, H. H., and Mountcastle, V. B. (1968). The sense of flutter-vibration: comparison of the human capacity with response patterns of mechanoreceptive afferents from the monkey hand. *Journal of neurophysiology*, 31(2):301–334.

Tommerdahl, M., Hester, K., Felix, E., Hollins, M., Favorov, O., Quibrera, P., and Whitsel, B. (2005). Human vibrotactile frequency discriminative capacity after adaptation to 25 hz or 200 hz stimulation. *Brain research*, 1057(1-2):1–9.

Tommerdahl, M., Simons, S. B., Chiu, J. S., Favorov, O., and Whitsel, B. L. (2006). Ipsilateral input modifies the primary somatosensory cortex response to contralateral skin flutter. *Journal of Neuroscience*, 26(22):5970–5977.

Tong, F. and Engel, S. A. (2001). Interocular rivalry revealed in the human cortical blind-spot representation. *Nature*, 411(6834):195.

Toppino, T. C. (2003). Reversible-figure perception: Mechanisms of intentional control. *Perception & psychophysics*, 65(8):1285–1295.

van Boxtel, J. J., Knapen, T., Erkelens, C. J., and van Ee, R. (2008). Removal of monocular interactions equates rivalry behavior for monocular, binocular, and stimulus rivalries. *Journal of Vision*, 8(15):13–13.

van Ee, R. (2009). Stochastic variations in sensory awareness are driven by noisy neuronal adaptation: evidence from serial correlations in perceptual bistability. *JOSA A*, 26(12):2612–2622.

van Ee, R., Noest, A., Brascamp, J., and van den Berg, A. (2006). Attentional control over either of the two competing percepts of ambiguous stimuli revealed by a two-parameter analysis: Means do not make the difference. *Vision research*, 46(19):3129–3141.

Vattikuti, S., Thangaraj, P., Xie, H. W., Gotts, S. J., Martin, A., and Chow, C. C. (2016). Canonical cortical circuit model explains rivalry, intermittent rivalry, and rivalry memory. *PLoS computational biology*, 12(5):e1004903.

Wilke, M., Logothetis, N. K., and Leopold, D. A. (2003). Generalized flash suppression of salient visual targets. *Neuron*, 39(6):1043–1052.

Wilson, H. R. (2003). Computational evidence for a rivalry hierarchy in vision. *Proceedings of the National Academy of Sciences*, 100(24):14499–14503.

Wilson, H. R. (2007). Minimal physiological conditions for binocular rivalry and rivalry memory. *Vision research*, 47(21):2741–2750.

Wolfe, J. M. (1996). Resolving perceptual ambiguity. *Nature*, 380(6575):587–588.

Wuerger, S., Shapley, R., and Rubin, N. (1996). "on the visually perceived direction of motion" by hans wallach: 60 years later. *Perception*, 25(11):1317–1367.

Yau, J. M., Olenczak, J. B., Dammann, J. F., and Bensmaia, S. J. (2009). Temporal frequency channels are linked across audition and touch. *Current biology*, 19(7):561–566.

You, H., Meng, Y., Huan, D., and Wang, D.-H. (2011). The neural dynamics for hysteresis in visual perception. *Neurocomputing*, 74(17):3502–3508.

Zhang, P., Jamison, K., Engel, S., He, B., and He, S. (2011). Binocular rivalry requires visual attention. *Neuron*, 71(2):362–369.

Zhou, W. and Chen, D. (2009). Binaral rivalry between the nostrils and in the cortex. *Current Biology*, 19(18):1561–1565.

Zhou, Y., Gao, J., White, K. D., Merk, I., and Yao, K. (2004). Perceptual dominance time distributions in multistable visual perception. *Biological cybernetics*, 90(4):256–263.